# Activity-Dependent Regulation of Neuronal Ion Channel Expression During Epileptogenesis

Dissertation

zur

Erlangung des Doktorgrades (Dr. rer. nat.)

der

Mathematisch-Naturwissenschaftlichen Fakultät

der

Rheinischen Friedrich-Wilhelms-Universität

Bonn

vorgelegt von

Jian Chen

Bonn 2004

Diese Arbeit wurde mit der Genehmigung der Mathematisch-Naturwissenschaftlichen Fakultät an der Klinik für Epileptologie und der Institut für Neuropathologie der Medizinischen Fakultät der Rheinischen-Friedrich-Wilhelms-Universität in Bonn angefertigt.

Referent: Prof. Dr. Thomas Magin
Koreferent: Prof. Dr. Heinz Beck

Tag der mündlichen Prüfung, Hauptfach: 8.12.2004

Tag der mündlichen Prüfung, Nebenfach: 10.12.2004

For my wife Hong Lu

my daughter Sijia Chen

and my parents

# Table of Contents

# 1 Introduction

## 1.1 Basic structure and function of neurons

The immense number of neurons in the brain, and the multitude of synaptic and nonsynaptic connections they form between each other result in an incredibly complex information processing network. The complexity of this network is contrasted by the fact that the elementary units of this network, single neurons, display a number of very basic properties common to all neurons. Two of these basic properties are polarity and excitability.

Polarity designates the fact that neuronal processes are not uniform in their properties and the tasks they perform. A neuron typically consists of dendrites, a cell body (or soma), and the axon and presynaptic terminals. The dendrites and the soma are the main areas upon which synaptic input from other neurons converges, and may thus be considered mainly an input structure. Excitatory and inhibitory synaptic input propagates to the soma, where it is converted into an output signal consisting of a sequence of all-or-nothing membrane depolarizations termed action potentials. Action potentials propagate down the axon, and may induce neurotransmitter release at associated presynaptic terminals onto postsynaptic neurons. Thus, as a rough approximation, the dendrites and soma contribute to the integration of synaptic input, while the axon may be considered the output structure of neurons.

Clearly, how neurons process synaptic input to generate an output in which information is encoded as frequency and pattern of action potentials is crucial to understand the input-output properties of neurons. The input-output properties of neurons are dependent on their intrinsic membrane properties, which in turn are largely determined by the expression of a large number of different ion selective channels within the neuronal cell membrane.

## 1.2 Basic properties of neuronal membranes: resting membrane potential

Among the most important ions found on either side of the neuron membrane, $Na^+$ and $Cl^-$ are more concentrated outside the neuron, while $K^+$ are more concentrated inside. Table1.1 summarizes the concentrations of different ions inside and outside a typical mammalian cell.

**Table 1.1**: Ion concentration across a typical mammalian cell membrane at rest:

| Species of ion | Concentration in cytoplasm (mM) | Concentration in extracellular fluid (mM) |
|---|---|---|
| $K^+$ | 140 | 5 |
| $Na^+$ | 5 - 15 | 145 |
| $Ca^{2+}$ [a] | $10^{-4}$ | 1 - 2 |
| $Cl^-$ [b] | 5-15 | 110 |

a. The concentrations of $Ca^{2+}$ given are for the free ions. There is total about 1 – 2mM $Ca^{2+}$in cells, mostly bound to proteins, stored in various organelles.

b. The cell contains many other charged substances, such as $HCO_3^-$, $PO_4^{3-}$, proteins, nucleic acid.

The unequal distribution of ions causes a diffusive force driving the ion from the membrane side with the higher concentration to that with the lower concentration through the resting membrane ion channels. Conversely, an electrostatic force results in a driving force in the opposite direction. At some point, the diffusion force created by concentration gradient is exactly balanced by the electrostatic force resulted from potential difference. At this, point, ionic flux for that particular ion is zero, a voltage termed the equilibrium potential. The relation between the equilibrium potential and the ionic gradient is given by the Nernst Equation:

$$E_X = \frac{RT}{zF} \ln \frac{[X]_0}{[X]_i}$$

R = the gas constant (2 cal / mol K)

T = the absolute temperature in Kelvin degree (K)

z = the valence of the ion

F = the Faraday's constant (2.3 X 104 cal / V mol)

$[X]_0$ and $[X]_i$ = outside and inside concentrations of the ion

Since RT/F is 26.7 mV at 37°C (physiology temperature), and the constant for converting from natural logarithms to base 10 logarithms is 2.3, the Nernst Equation can be written as:

$$E_X = \frac{61.5\ mV}{z} \log \frac{[X]_0}{[X]_i}$$

As an example, for $K^+$, z equals one, given that the concentrations inside and outside a neuron are 140 and 5 mM:

$$E_K = \frac{61.5\ mV}{1} \log \frac{5\ mM}{140\ mM} = -90mV$$

Similarly, the equilibrium potential for $Na^+$, would be derived as:

$$E_{Na} = \frac{61.5\ mV}{1} \log \frac{145\ mM}{15\ mM} = +60mV$$

Generally, because the membrane in its resting state is mainly permeable to $K^+$, the membrane potential is close to the Nernst potential for $K^+$. The membrane is also

somewhat permeable to other ions such as $Na^+$, $Cl^-$ or $K^+$. In summary, the resting conductances cause the resting membrane potential to be somewhat more positive that the $K^+$ equilibrium potential. Most neurons maintain a resting membrane potential around –65 mV to –75 mV. As this potential is different from the $K^+$ equilibrium potential, a small outward flux of $K^+$ occurs through resting conductances. The gradual flow of $K^+$ out of the cell would eventually result in reduction of the ionic gradients, finally reducing the resting membrane potential. To prevent this from happening, the ionic gradient is maintained by the $Na^+$ - $K^+$ pump. It is a large membrane-spanning protein with catalytic binding sites for $Na^+$, $K^+$ ions and ATP. The sites for $Na^+$ and ATP are located in its intracellular surface and the sites for $K^+$ on its extracellular surface. With each cycle the pump extrudes three $Na^+$ ions and allows two $K^+$ ions to enter the neuron, simultaneously hydrolyzing one molecule of ATP.

## 1.3 Basic properties of neuronal membranes: excitability

Excitability is one of the main characteristics of neurons. Generally, excitability designates non-ohmic properties of the neuronal membrane, such that an imposed current flux over the membrane leads to either smaller or larger voltage excursions than would be expected from Ohm's law. A crucial example of excitable properties of neuronal, but not glial cell membranes is the generation of action potentials. Action potentials are generated when the neuronal membrane is depolarized from resting membrane potential to a threshold, and consist of a steep depolarization followed by a repolarization phase. The duration of action potentials is in the millisecond range.

The mechanisms governing the generation of action potentials are well understood. The ground-breaking early work of Hodgkin and Huxley (Hodgkin AL, Huxley AF. 1952) demonstrated, using both physiological measurements on the squid giant axon and neuronal modeling approaches, that just two types of ion channels are sufficient to endow membranes with the capacity to generate action potentials: a fast $Na^+$ inward current, and a delayed $K^+$ outward current. Both of these currents are activated by depolarization.

In this model, membrane depolarization beyond a threshold potential causes $Na^+$ channels to open, permitting $Na^+$ ions to flow into the neuron causing further depolarization. This $Na^+$ influx causes the fast upstroke of the action potential, the depolarization phase and subsequently inactivate rapidly. In addition to $Na^+$ current, $K^+$ currents are also activated by depolarization. However, due to the slower activation time course of the delayed outward rectifying voltage-gated $K^+$ channels, the efflux of $K^+$ is greatest after the fast upstroke of the action potential, and then causes the repolarization of the neuronal membrane. The duration of an action potential is around 1-2 ms in neuronal somata and axons.

Even though just these two ionic conductances are required for action potentials, neurons contain a great diversity of voltage-gated ion channels that modulate the shape of action potentials, generate depolarizing or hyperpolarizing afterpotentials, and modulate the repetitive firing properties of neurons. The properties of different ion channels will be explored in more detail below.

## 1.4 Ion channels in neuronal cell membranes

In the past decade, significant advances in molecular biology have led to an increasing understanding of the molecular basis for the diversity of different classes of ion channels.

All voltage-gated ion channels are large transmembrane glycoproteins. The principal subunit ($\alpha$ subunit) of voltage-gated $Na^+$ channels contains four highly homologous domains (I-IV). Each domain has six highly hydrophobic transmembrane segments (S1-S6) and a membrane re-entrant loop (P-loop) between S5 and S6 (Numa S, 1986; Noda M, 1984). S4 segments serve as the voltage sensors. P-loops form the pore, and the short intracellular loop between domain III and IV forms the inactivation gate (Catterral WA, 2000). Each individual $Na^+$ channel subunit is capable of forming a functional channel. Pore-forming voltage-gated $Ca^{2+}$ channel $\alpha$ subunits have a similar

fundamental structure. In contrast, voltage-gated $K^+$ channels have a different structure, depending on the different families. A large family of $K^+$ channel subunits are composed of 6 transmembrane domains with one reentrant loop forming a pore region. This structure thus corresponds to a single domain of voltage-gated $Na^+$ or $Ca^{2+}$ channels. Voltage-gated $K^+$ channel subunits with 6 transmembrane domains coassemble to form homo- or heteromultimeric channels composed of 4 subunits. Inward-rectifier $K^+$ channels and "leak" $K^+$ channels have a quite different structure. As these channels have not been examined in the current thesis, their structure and function will not be further discussed.

### 1.4.1 Voltage-gated sodium channels

There are nine principal subunits ($\alpha$ subunits) forming functional voltage-gated $Na^+$ channels. They belong to one family, and have been named $Na_V1.1$ to $Na_V1.9$ (Goldin AL et al., 2000; 2001). Some of the main fundamental properties and distribution of the voltage-gated $Na^+$ channel $\alpha$ subunits are summarized in Table 1.2.

**Table 1.2:** Properties of voltage-gated $Na^+$ channels in rats

| Functional subunit | GenBank accession number | TTX-sensitivity | Predominant Localization |
|---|---|---|---|
| $Na_V1.1$ | X03638 | Sensitive | CNS, PNS |
| $Na_V1.2$ | X03639 | Sensitive | CNS |
| $Na_V1.3$ | Y00766 | Sensitive | CNS (embryonic) |
| $Na_V1.4$ | M26643 | Sensitive | skeletal muscle |
| $Na_V1.5$ | NM_013125 | Resistant | heart muscle, CNS |
| $Na_V1.6$ | L39018 | Sensitive | CNS, PNS, glia, nodes of ranvier |
| $Na_V1.7$ | U79568 | Sensitive | PNS, Schwann cells |
| $Na_V1.8$ | X92184 | Resistant | PNS (sensory neurons), DRG |
| $Na_V1.9$ | AF059030 | Resistant | PNS |

Besides the channel pore formed by an $\alpha$ subunit, accessory subunits $\beta_1$, $\beta_2$ and $\beta_3$ are also important for modifying the kinetic properties of voltage-gated $Na^+$ channel, such as the activation and inactivation properties (Isom LL et al., 1992; Isom LL et al., 1995a; Isom LL et al., 1995b; Morgan K et al., 2000).

$Na_V1.1$, $Na_V1.2$ and $Na_V1.3$ are mainly expressed in the central nervous system (CNS), $Na_V1.4$ in skeletal muscle, $Na_V1.5$ in heart and CNS, $Na_V1.6$ in CNS and peripheral nervous system (PNS), and $Na_V1.7$ mainly in PNS. $Na_V1.8$ and $Na_V1.9$ are only expressed in peripheral nervous system (PNS), predominantly in dorsal root ganglion neurons (Waxman SG et al., 1999). Both of them are thought to have special roles in pain sensation (Amaya F et al., 2000). $Na_V1.5$, $Na_V1.8$ and $Na_V1.9$ are resistant to tetrodotoxin (TTX), all of the other subunits are sensitive to TTX.

Most voltage-gated $Na^+$ channel $\alpha$ subunits give rise to transient, fast inactivating $Na^+$ currents ($I_{Na}$). Fast, transient channels underlie the action potential upstroke in excitable cells. Persistent (noninactivating) $Na^+$ currents, $I_{NaP}$, which contributes only a small fraction (1-3%) to the total $Na^+$ currents, can also be recorded in various tissues (Cummins TR et al., 1994; Crill WE et al., 1996; Raman IM et al., 1997). They inactivate slowly and have low threshold of activation. Recent studies indicate that, in some cell types, $I_{NaP}$ plays a pivotal role in regulating the repetitive bursting firing (Azouz R et al., 1996; 1997; Alkadhi KA et al., 1996; Su H et al., 2002). The channels underlying $I_{NaP}$ are still a matter of debate. It might be due to alternate gating of the same channels that mediate transient $Na^+$ currents (Alzheimer C et al., 1993; Crill WE et al., 1996;). Alternatively $I_{NaP}$ may be mediated by $Na_V1.6$, which is expressed in central and peripheral neurons (Raman IM et al., 1997).

### 1.4.2 Voltage-gated potassium channels

The diversity of the voltage-gated $K^+$ channels is impressive. Over 100 different types of $K^+$ channel subunits have been identified to date, and this number will probably

increase. The $K^+$ channel principal $\alpha$ subunits are divided into three groups based on structural properties — those with six transmembrane domains (TMDs), those with four TMDs and those with two TMDs.

The first group, consisting of six TMD channels, includes voltage-gated $K^+$ channels and $Ca^{2+}$-activated $K^+$ channels. A single subunit of this family resembles a single domain of the voltage-gated $Na^+$ or $Ca^{2+}$ channels. A functional $K^+$ channel consists of four subunits arranged around a central pore. The second group, consisting of proteins with two TMDs, gives rise to inward rectifier $K^+$ channels. The third group, known as two-pore channels, has four TMDs, and underlie “leak” $K^+$ currents. Table 1.3 shows the most important properties of these $K^+$ channel families.

Voltage-gated $K^+$ channel subfamily 1 (Shak) consists of seven characterized subunits ($K_V1.1$ to $K_V1.7$). They are 4-aminopyridine (4-AP) sensitive and include both delayed rectifier and transient A-type $K^+$ channels. Delayed rectifiers have high $K^+$ permeability and display slow activation upon depolarization. They play an important role in action potential generation and propagation. $K_V1$ channels may underlie fast A-type $K^+$ currents in terminals and axons (Debanne D et al., 1997, Geiger JR et al., 2000) as they are highly expressed in presynaptic terminals (Veh RW et al., 1995). Besides these, various combinations of $K_V1.2$ with other $K_V1$ proteins and $K_V$ $\beta$ subunits may contribute to transient dendrotoxin-sensitive $K^+$ currents, termed $I_D$, which activate rapidly and show intermediate time-dependent inactivation (Wu RL et al., 1992).

Voltage-gated $K^+$ channel subfamily 2 (Shab) consists of three characterized subunits ($K_V2.1$ to $K_V2.3$). These subunits also give rise to 4-AP-sensitive delayed rectifier $K^+$ currents that share many properties of delayed rectifier currents mediated by the Kv1 family of subunits. Most of the subunits mediate slowly activating and slowly inactivating currents. Kv2 channels show a characteristic pattern of expression. While $K_V2.1$ is expressed in a relatively restricted fashion in neuronal somata and dendrites, but not axons and glial cells, $K_V2.2$ appears to be present in axons of some neuron types (Trimmer JS et al., 1991; Antonucci DE et al., 2001). $K_V2.3$ is a silent $K^+$ channel alpha-

**Table 1.3:** Properties of voltage-gated $K^+$ channels in rats

| Functional subunits | Current type | | Characteristic | Function |
|---|---|---|---|---|
| $K_V$1.1-1.7 (Shak) | Delayed rectifier<br>A-type | 6 TMD | • 4-AP sensitive, voltage-gated<br>• delayed rectifiers: slow activating and inactivating or no inactivating<br>• Kv1.4 A-types: fast inactivating<br>• Kv1.2: combined with other Kv1, dendrotoxin-sensitive current | Action potential repolarization in axons (delayed rectifier)<br>Contributes to fast afterhyperpolarization, controls repetitive firing and the latency to first spike (A-type currents) |
| $K_V$2.1-2.3 (Shab) | Delayed rectifier | | • 4-AP sensitive, voltage-gated<br>• slow activation, slow inactivation<br>• in combination with others e.g. Kv6 | Contribution to action potential repolarization and after-hyperpolarizations |
| $K_V$3.1-3.4 (Shaw) | Delayed rectifier<br>A-type | | • TEA and 4-AP sensitive, voltage-gated<br>• High voltage activating<br>• Fast deactivating delayed rectifier (Kv3.1, 3.2)<br>• Fast inactivating, oxidation sensitive (Kv3.3, 3.4)<br>• Might exist as homo and heteromultimeric channels | Contribute to fast action potential repolarization (Kv3.1, 3.2), may couple excitability to metabolism (Kv3.3, 3.4) |
| $K_V$4.1-4.3 (Shal) | A-type | | • Blocked by high millimolar 4-AP, voltage-gated<br>• Low voltage activating and fast inactivating | Underlie fast action potential afterhyperpolarizations, control frequency of repetitive firing and the latency to first spike. Contribute to dendritic integration of EPSPs. |
| KCNQ1-5 | M-current | | • blocked by acetylcholine, voltage-gated<br>• slowly activated, non-inactivating | Prevention of repetitive action potential firing, potentially underlie medium afterhyperpolarizations. |

**Table 1.3:** Properties of voltage-gated $K^+$ channels (continued)

| Functional subunits | Current type | | Characteristic | Function |
|---|---|---|---|---|
| SK1-4<br>Slo1-3 | $Ca^{2+}$-activated | 6 TMD | Activated by depolarization and increase in cytoplasmic $Ca^{2+}$ ion concentration | Underlie $Ca^{2+}$-dependent action potential afterhyperpolarizations |
| Kir | Inward rectifier | 2 TMD | activated by hyperpolarization | $K^+$ uptake in glial cells |
| TWIK TREK TASK TRAAK | "leak" | 4 TMD | Relatively voltage-independent 'leak' channels, modulated by pH, arachidonic acid, anandamide, depending on subtype. | $K^+$ uptake in glial cells, resting potential regulation |

subunit, but it is capable of forming heterotetramers with other pore-forming subunits to form transient $K^+$ currents (Chiara MD et al., 1999). The coexpression with $K_V5.1$, $K_V6.1$, $K_V8.1$, $K_V9.1$-9.3 gives rise to currents with variable kinetics (Ottschytsch N et al., 2002; Sano Y et al., 2002).

The Kv channel subfamily 3 (Shaw) consists of four subunits ($K_V3.1$ to $K_V3.4$). currents through the corresponding channels are sensitive to 1 mM tetraethylammonium (TEA) and 4-AP, and require relatively strong depolarization in order to activate (Rettig J et al., 1992). The $K_V3.1$ and $K_V3.2$ subunits mediate slowly activating delayed rectifier currents which display a particularly fast deactivation (Rettig J et al., 1992). $K_V3.3$ and 3.4, on the other hand, give rise to fast-inactivating $K^+$ channels (Ruppersberg JP et al., 1991). In contrast to channels, these channels display a more depolarized threshold of activation. Kv3.2 with its fast deactivation characteristics appears to be specialized for mediating the repolarization of action potentials in fast spiking neurons (Rudy B et al., 1999). Interestingly, both Kv3.3 and 3.4 are highly oxidation sensitive, and thus link the cell metabolism to membrane excitability (Ruppersberg JP et al., 1991)

Voltage-gated $K^+$ channel subfamily 4 (Shal) consists of three subunits ($K_V4.1$ to $K_V4.3$). Currents through $K_V4$ subunits are blocked by 4-AP and are characteristically low voltage activating, rapidly inactivating A-type $K^+$ channels. $K_V4.1$ is expressed in heart (Brahmajothi MV et al., 1996), while $K_V4.2$ and $K_V4.3$ are widely distributed in brain, with high levels of expression in dendrites of hippocampal CA1 pyramidal neurons (Sheng M et al., 1992). These channels prevent initiation of an action potential in the dendrites, limit the back-propagation of action potentials into the dendrites, and inhibit the propagation of excitatory synaptic events occurring in the dendrites to the soma (Hoffman DA et al., 1997).

KCNQ channels are a group of slowly activating, non-inactivating $K^+$ channels. KCNQ channels are thought to underlie the so-called M-current in native cells (Brown DA.1980 Halliwell JV. 1986; Wang HS et al., 1995). M-currents can be blocked by activation of muscarinic receptors (therefore the designation M-current), but also by a large number

of other neurotransmitter receptors (Brown DA et al., 1980, Simmons MA et al., 1990; Chen H et al., 2001). The KCNQ channels play a critical role in determining the sub-threshold electrical excitability of neurons. Therefore the inhibition of this current leads to enhanced neuronal excitability (Jentsch TJ, 2000). There are five subunits in this group (KCNQ1 to KCNQ5). KCNQ1 is expressed in heart and epithelial cells of gut and exocrine pancreas (Robbins J, 2001). KCNQ4 is largely restricted to the central auditory system and the hair cells of the inner ear (Kharkovets T et al., 2000). KCNQ2, 3 and 5 are widely distributed in the central nervous system (Tinel N et al., 1998; Schroeder BC et al., 2000; Cooper EC et al., 2000; 2001). Recent evidence suggests the M-channels are composed of a heteromeric assembly of KCNQ2, KCNQ3 and KCNQ5 gene products (Wang HS et al., 1998; Shah MM et al., 2002).

$Ca^{2+}$-activated $K^+$ channel opening requires both depolarization and increase in the cytoplasmic $Ca^{2+}$ ion concentration. The relative importance of voltage- and $Ca^{2+}$-dependent activation can vary from channel subunit to channel subunit. A family of $K^+$ channel subunits termed SK1-4 give rise to $Ca^{2+}$-dependent $K^+$ channels. These channels require repetitive action potentials for activation, and are thought to mediate long-lasting hyperpolarizations following high-frequency action potential series. The BK channel, another type of $Ca^{2+}$-activated $K^+$ channel, activates following single action potentials, and may give rise to fast action potential afterhyperpolarizations. The molecular basis of this current subtype appears to be the slo subunit. In general, $Ca^{2+}$-dependent $K^+$ currents hyperpolarize the neuronal membrane upon influx of $Ca^{2+}$ via voltage-gated $Ca^{2+}$ channels. This hyperpolarization, in turn, closes voltage-gated $Ca^{2+}$ channels, thereby providing a powerful feedback mechanism that limits $Ca^{2+}$ influx into neurons.

A further two groups of $K^+$ channel subunits contain less than six TMDs. The family of inward-rectifying $K^+$ (Kir) channel subunits contain two TMDs in each subunit. There are currently seven members of this family (Kir1-Kir7). The other group is referred to as “Leak” $K^+$ channels which contain four TMDs. These channels are distinct from the above mentioned $K^+$ channels because they have two pore-forming domains (P-loop) per subunit, in contrast to all other subunits containing only one P-loop. There are at

least four members in this family. This group of "Leak" $K^+$ channels is thought to be very important in the regulation of the resting membrane potential (Goldstein SAN et al., 1998).

### 1.4.3 Voltage-gated Calcium Channels

The principal subunits ($\alpha_1$ subunits) of voltage-gated $Ca^{2+}$ channels constitute the channel pore and structurally resemble those of voltage-gated $Na^+$ channels. Up to date, ten distinct $\alpha_1$ subunits have been identified (Ertel EA et al., 2000). Accessory subunits, including $\alpha_2\delta$, $\gamma$, $\beta_1$, $\beta_2$, $\beta_3$ and $\beta_4$, play an important role in modifying channel properties (Hofmann F et al., 1999).

The $\alpha_1$ subunits of voltage-gated $Ca^{2+}$ channels are classified by their electro-physiological properties, and their sensitivity to drugs or toxins. The distinctive pharmacology of most subunits, as well as the availability of knockout models for some subunits have allowed to dissect the contribution of specific subunits to $Ca^{2+}$ currents in native neurons. Table 1.4 summarizes the most important properties of voltage-gated $Ca^{2+}$ channels.

L-type currents are generated by the $Ca_V1$ family which includes four $\alpha_1$ subunits ($Ca_V1.1$, $Ca_V1.2$, $Ca_V1.3$ and $Ca_V1.4$). These subunits all give rise to high voltage activated $Ca^{2+}$ channels i.e. they require strong depolarization in order to activate. L-type $Ca^{2+}$ channels are highly sensitive to dihydropyridine, some of which block currents through these channels, while others enhance channel opening. $Ca_V1.1$ is expressed in skeletal muscle. $Ca_V1.2$ and $Ca_V1.3$ are expressed in heart, smooth muscle and neurons in CNS. Recently $Ca_V1.4$ has also been found to be expressed in retina (Morgans CW et al., 2001). L-type $Ca^{2+}$ channels play a critical role in excitation-contraction coupling in cardiac, skeletal and smooth muscle (Bers DM, 1999; Rios E, 1991). In the CNS, L-type $Ca^{2+}$ channels are present in most neuronal somata and dendrites.

**Table 1.4:** properties of voltage-gated $Ca^{2+}$ channels

| Subunit | Current type | Activation | Inactivation | Drugs or toxins | Function | Localization |
|---|---|---|---|---|---|---|
| $Ca_V1.1$ | L-type | Depolarized threshold of activation: high voltage activated, HVA | Slow, voltage-gated, $Ca^{2+}$-dependent | Dihydropyridines (nicardipine, nifedipine), BAY K | Voltage sensor, $Ca^{2+}$ release from SR | Skeletal muscle |
| $Ca_V1.2$ | L-type | | | | $Ca^{2+}$ influx in soma and dendrites, coupling to $Ca^{2+}$-activated $K^+$ channels | Heart, neurons, smooth muscle |
| $Ca_V1.3$ | L-type | | | | | |
| $Ca_V1.4$ | L-type | | | | | retimna |
| $Ca_V2.1$ | P/Q-type | | Slow, voltage-gated, $Ca^{2+}$-dependent | ω-conotoxin MVIIC, ω-agatoxin IVa | Mediation of presynaptic $Ca^{2+}$ transients triggering synchronized transmitter release, postsynaptic $Ca^{2+}$ influx | Presynaptic terminals, neuronal cell body, dendrites |
| $Ca_V2.2$ | N-type | | | ω-conotoxin GVIA, ω-conotoxin MVIIC | | |
| $Ca_V2.3$ | R-type | | Intermediate voltage-gated inactivation | SNX-482, $Ni^{2+}$ ($IC_{50}$=15-23μM) | Presynaptic $Ca^{2+}$ influx mediating transmitter release and plasticity, postsynaptic $Ca^{2+}$ influx | Neuronal cell body, dendrites, some presynaptic termimals |
| $Ca_V3.1$ | T-type | Hyperpolarized threshold of activation: low voltage activated, LVA | Rapid voltage-gated inactivation, slow deactivation | $Ni^{2+}$ ( $IC_{50}$=250μM) | Pacemaker in thalamic neurons, generation of burst firing, boosting of dendritic EPSPs and backpropagating action potentials. | Cardiac muscle, neurons (in particular dendrites), endocrine cells |
| $Ca_V3.2$ | | | | $Ni^{2+}$ ( $IC_{50}$=12μM), Kurtoxin, anandamide | | |
| $Ca_V3.3$ | | | | $Ni^{2+}$ ( $IC_{50}$=216μM) | | |

The $Ca_V2$ family includes three subunits that give rise to high voltage-activated $Ca^{2+}$ currents, $Ca_V2.1$, $Ca_V2.2$ and $Ca_V2.3$. $Ca_V2.1$ subunits are thought to underlie P-/Q-type $Ca^{2+}$ currents in native neurons. Differential splicing results in channel isoforms that differ in their sensitivity to the spider toxin ω-Aga-IVA, and have been differentiated as P or Q-type channels (Bourinet E et al., 1999). $Ca_V2.1$ channels are widely distributed in the CNS (Mintz IM et al., 1992a; 1992b; Randall A et al., 1995), $Ca_V2.2$ most probably is the molecular correlate for N-type currents in native neurons. Both $Ca_V2.2$ currents as well as N-type currents are blocked by low concentrations of the marine snail toxin ω-conotoxin GVIA. As is $Ca_V2.1$, $Ca_V2.2$ subunits are prominently expressed in presynaptic terminals (Ino M et al., 2001). Both $Ca_V2.1$ and $Ca_V2.2$ are the main channel subunits that mediate the highly localized presynaptic $Ca^{2+}$ transients that cause neurotransmitter release from presynaptic terminals (Takahashi T et al., 1993; Wheeler DB et al., 1994; Qian J et al., 1999; Bischofberger J et al., 2002). Thus, they play a prominent role in the release of most neurotransmitters in the CNS including GABA and glutamate (Luebke JI et al., 1993; Woodward JJ et al., 1988; Ino M et al., 2001). $Ca_V2.3$ subunits have been shown to underlie R-type currents in CNS neurons. $Ca_v2.3$ also give rise to high-voltage activated $Ca^{2+}$ currents. However, different from $Ca_V2.1$ and $Ca_V2.2$, the inactivation of $Ca_V2.3$ is rapid and voltage-gated. The absence of any $Ca^{2+}$ dependent inactivation also sets these channels apart from other channels such as L-type channels. $Ca_V2.3$ is blocked by low concentrations of $Ni^{2+}$, as well as a more selective toxin obtained from the tarantula, SNX-482 (Newcomb R et al., 1998).

$Ca_V3.1$, $Ca_V3.2$ and $Ca_V3.3$ subunits give rise to so-called T-type $Ca^{2+}$ currents (Perez-Reyes E. 2003). These currents show a number of distinctive properties. In contrast to all other types of $Ca^{2+}$ channels, $Ca_V3$ subunits require only subtle depolarizations from resting membrane potential to open, with thresholds for activation around –60 to –50 mV. Thus, they have been termed low voltage activated (LVA) $Ca^{2+}$ channels (Fishman MC et al., 1981; Nowycky MC et al., 1985; Yaari Y et al., 1987; Perez-Reyes E, 2003). A further distinguishing property of $Ca_V3$ channels is their rapid and voltage-gated inactivation, resulting in transient currents. Finally, $Ca_V3$ channels display a slow deactivation upon repolarization of the membrane, and consequently are capable of generating slow tail currents (Carbone E et al., 1984; Amstrong CM et al., 1985; Kozlov

AS et al., 1999). The T-type channel subunits are not sensitive to any of the abovementioned organic $Ca^{2+}$ channel blockers. They are, however, sensitive to $Ni^{2+}$, in particular $Ca_V3.2$. Furthermore, anandamide and a peptide toxin (kurtoxin) have been shown to preferentially block $Ca_V3.2$.

T-type $Ca^{2+}$ channels are expressed throughout the body, including nervous tissue, heart, kidney, smooth muscle, sperm and many endocrine organs. These channels have been implicated in variety of physiological processes. T-type $Ca^{2+}$ channels are particularly important in the generation of low-threshold spikes that lead to burst firing through activating other voltage-gated ion channels (Huguenard JR 1996; Su H et al., 2002). This activity is especially important in the thalamus, where it plays a critical role in sensory gating, sleep and arousal (McCormick DA et al., 1997). The dysfunction of these channels has been implicated in wide range of neurological disorders including epilepsy (McCormick DA et al., 2001; Llinas R et al., 2001).

### 1.4.4 Hyperpolarization-activated and cyclic nucleotide-gated channels

**H**yperpolarization-activated and **C**yclic **N**ucleotide-gated channels (therefore HCN channels) are activated by hyperpolarization and powerfully regulated by cyclic nucleotides (cAMP) on the cytoplasmic side. They are known to underlie a so-called H-current or $I_H$ in native neurons (Ludwig A et al., 1998; Chen S et al., 2001). HCN channels are permeable to both $Na^+$ and $K^+$ ions. They activate slowly upon hyperpolarization, and do not inactivate. All HCN channels are blocked by low concentrations of $Cs^+$, as well as by more specific blockers such as ZD7288. Due to the depolarized reversal potential of HCN channels, opening of these channels depolarizes the neuronal membrane. Thus, when hyperpolarization opens HCN channels, these have a tendency to oppose this hyperpolarization and produce a prolonged inward current. This property of HCN channels/$I_H$ renders them very appropriate to contribute to pacemaking. Indeed, the HCN channels constitute pacemaker channels in the heart (DiFrancesco D. 1993), and are also involved in the generation of rhythmic activity in the thalamus (Luethi A et al 1998; Ludwig A et al., 2003). Additionally, $I_H$ appears to contribute to the resting membrane potential and membrane conductance in many

neurons. There may be a particular role for dendritic $I_H$ channels in the integration of synaptic input (Pape HC. 1996; Magee JC. 1999a; 1999b).

HCN channels have a structure and proposed topology similar to voltage-gated $K^+$ channels with a cyclic nucleotide-binding domain in the C-terminal (Kaupp UB et al., 2001). Until now four isoforms (HCN1-4) have been identified (Chen J et al., 2002). All four HCN isoforms are expressed in brain and HCN2 and HCN4 are present at high levels in the heart (Ludwig A et al., 1998; Santoro B et al., 1998). Generally HCN1 has the fastest kinetics, followed by HCN2 and HCN4 (Santoro B et al., 2000; Altomare C et al., 2001). All HCN subunits are modulated by intracellular cAMP, which causes a shift in the voltage-dependence of activation. However, HCN1 is far less sensitive to cAMP than HCN2 and HCN4.

## 1.5 Structure and function of the hippocampal formation

The hippocampal formation usually designates a group of histoarchitectonically defined fields that include the dentate gyrus, the hippocampus proper or Ammon's horn (composed of the CA1-CA4 subfields), the subicular complex, and the entorhinal cortex. The reason for grouping these diverse subfields under a single heading is that the principal cells in this area show a highly specific and largely unidirectional projection that interconnects them to one functional entity. Most of the hippocampal formation is situated on the floor of the temporal horn of the lateral ventricle.

Within the dentate gyrus and Ammon's horn, a characteristic three-layered histoarchitecture is observed. The principal cells in the dentate gyrus are termed granule neurons, and their cell bodies are densely packed within the granule cell layer. Granule neurons send their dendrites into the molecular layer (Fig 1.1), where they receive glutamatergic input from the entorhinal cortex via the perforant path. Granule neurons project with their unmyelinated axons (mossy fibers) to the hilar region and to CA3 pyramidal neurons and interneurons and form excitatory glutamatergic synapses onto these targets.

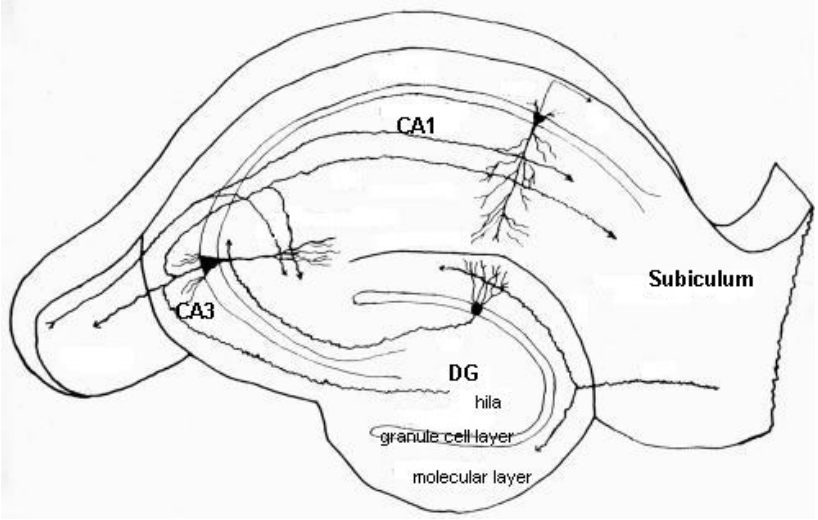


**Fig 1.1** Diagram of the structure and connections of the hippocampus.

CA3 cells, in turn, give rise to a strong glutamatergic projection to CA1 neurons (and in humans CA2) that is termed Schaffer collateral pathway. As in CA3, the principal neuron type in the CA1 region is the pyramidal neuron. The somata of these neurons are found densely packed in the pyramidal cell layer. The CA1 axons then project to the subicular complex. The excitation in all these regions is modulated by powerful feed-forward and feed-back inhibition mediated by a far smaller number of inhibitory interneurons.

Thus, the hippocampus displays a strongly unidirectional propagation of information. The dentate gyrus receives its major input from entorhinal cortex (perforant pathway Andersen P et al., 1966; Witter MP et al., 1989). The dentate granule cells project via the distinctive mossy fibers upon the proximal dendrites of the pyramidal neurons of the CA3 region (Blackstad TW et al., 1970; Gaarskjaer FB, 1978). CA3 pyramidal neurons project to CA1 (the Schaffer collateral Ishizuka N et al., 1990) and to other layer CA3 pyramidal neurons (recurrent collaterals). CA1 pyramidal neurons are not as strongly interconnected to other CA1 neurons (Amaral DG et al., 1991), rather, they project predominantly to the subiculum (Finch DM et al., 1983). The subiculum, in turn, projects to the pre- and parasubiculum (Köhler C, 1985). In this study, we have focused on CA1

pyramidal neurons within the hippocampus. This neuron type is particularly vulnerable to injury during ischemia and seizures.

## 1.6 Human and experimental temporal lobe epilepsy

Epilepsy, which affects about 1% of the population worldwide, is a common neurological disorder characterized by recurrent spontaneous seizures, showing abnormal, synchronized firing of large populations of neurons. Although there are several rare types of epilepsy linked to mutations of some ion channels, most of the epilepsy cases are idiopathic. The factors leading to development of the epileptic condition are unsolved so far.

In a large fraction of epilepsy patients, seizures originate in the mesial temporal lobe that includes the hippocampal formation. Many of these patients (~30%) do not respond to antiepileptic drug therapy (Elger CE et al., 1993). Several lines of evidence suggest the hippocampal formation to be critically involved in temporal lobe epilepsy (TLE): Recordings from intracerebrally implanted electrodes demonstrate that the first electrographic abnormalities in temporal lobe seizures often appear within the hippocampus (Van Roost D et al., 1998). In addition, surgical removal of the amygdala and hippocampal formation considerably diminishes or abolishes seizures in most TLE patients (Zentner J et al., 1995). TLE pathogenesis involves a variety of developmental, metabolic and/or hypoxic alterations, while it lacks significant genetic inheritance (Jackson DG et al., 1998).

Neuropathological evaluation of surgical specimens suggests the majority of resected mesial temporal lobe structures can be classified in two groups: focal lesions versus Ammon's horn sclerosis. The first group, approx. 30-40% of TLE patients, exhibits focal lesions within the temporal lobe, which usually do not involve the hippocampus. The second group, representing approx. 60-70% of TLE patients, presents with severe unilateral atrophy of either the right or left hippocampus (Blümcke I et al., 1999a). Histopathologically, the hippocampal formation shows segmental neuronal loss in CA1,

CA3, whereas dentate gyrus granule cells appear more resistant (Coulter DA et al., 1999; Sloviter RS, 1999; Blümcke I et al., 1999a).

There are several animal models with chronic brain dysfunctions which reflect the processes underlying human TLE. Such chronic models of epilepsy include the kindling model, the pilocarpine model and kainate model. The latter two are models of TLE in which epilepsy develops after a sustained status epilepticus. These three models are the most widely used models for studies on TLE and on drug targets (Loscher W 2002).

In the present experiments, we have used the pilocarpine model of epilepsy. In this models, the muscarinic agonist pilocarpine is given to induce acute status epilepticus in rats following intraperitoneal or subcutaneous injection. This acute status epilepticus is termined by diazepam after 40 minutes. In the following ‘silent’ period, the rats are behaviorally normal, and display no overt signs of seizures. However, in later ‘chronic’ stages, the animals develop a chronic epileptic condition characterized by recurrent seizures. The initial status epilepticus initiates profound damage within different areas of the hippocampus. Characteristically, pyramidal neurons within the CA1, CA3 and CA4 area undergo prominent neuronal cell loss, while the dentate granule cells are relatively preserved. Furthermore, axonal sprouting of surviving neurons, i.e. the granule cells is observed, with mossy fibers aberrantly contacting granule neuron apical dendrites (mossy fiber sprouting). Finally, pronounced gliosis is observed throughout the hippocampus. Collectively, this picture strongly resembles the neuropathological characteristics seen in TLE patients with Ammon’s horn sclerosis. Owing to the presence of spontaneous seizures and the many similarities to human TLE, the pilocarpine model has become one of the most widely used animal model for studies on TLE (Turski WA et al., 1983; Mello LE et al., 1993).

## 1.7 Plasticity of discharge behavior in epilepsy

Both in humans and in experimental animals, continuous seizure activity as occurs during status epilepticus (SE), results in a large number of plastic changes within the hippocampus and adjacent brain areas (Coulter DA et al., 1999; Ben-Ari Y, 2001; Sloviter RS, 1999; Blümcke I et al., 1999a). The SE-induced modifications in neuronal function may consist either of altered synaptic function or of changes in the intrinsic membrane properties of neurons. A large body of data indicates multiple changes in inhibitory and excitatory synaptic transmission, both on the pre- and on the postsynaptic level (McNamara JO, 1999). These synaptic changes may certainly be of great importance in mediating an increase in neuronal input-output properties that ultimately results in augmented neuronal synchronization and hyperexcitability.

However, an increase in neuronal input-output relation can also be caused by changes in the intrinsic neuronal properties that affect how synaptic input is converted to an output signal. Intrinsic properties rely – as set out in more detail above – on the expression of a large number of voltage-gated membrane conductances. These may also be substantially altered in chronic epilepsy, causing huge changes in intrinsic neuronal membrane properties (Sanabria ER et al., 2001). Nevertheless, compared to synaptic changes, much less is known about epilepsy-related changes in intrinsic neuronal properties.

### 1.7.1 Changes in intrinsic neuronal properties in genetic epilepsy syndromes

The importance of voltage-gated membrane conductances in modulating neuronal excitability is exemplified by a number of genetic syndromes in which a mutation in an ion channel gene leads to a phenotype that includes hyperexcitability and seizures.

For instance, benign familial neonatal convulsions (BFNC) is a rare dominantly inherited epileptic syndrome characterized by frequent brief seizures within the first days of life that typically disappear spontaneously after weeks to months. The mutations that give

rise to this disorder are loss-of-function mutations in the voltage-gated $K^+$ channel genes KCNQ2 (Biervert C et al., 1998; Singh NA et al., 1998; Biervert C et al., 1999; Lerche H et al., 1999, Miraglia del Giudice E et al., 2000) and KCNQ3 (Charlier C et al., 1998, Hirose S et al., 2000). As explained above, these two genes are highly expressed in CNS neurons and underlie M-currents.

Generalized epilepsy with febrile seizures plus ($GEFS^+$) is an autosomal dominant disease and identified a point mutation within the SCN1B gene, encoding the $\beta_1$ subunit of the voltage-gated sodium channel (Wallace RH et al., 1998). And recently, several more SCN1A mutations have been described (Escayg A, et al., 2000, 2001, Wallace RH et al., 2001).

Although these and other rare types of epilepsy are linked to mutations of ion channels and provide us interesting models to study the molecular basis and intrinsic properties of epilepsy, most of the epilepsy cases, including TLE, have complex rather than simple inheritance patterns. In these epilepsies, the pathogenesis of the condition relies not on a mutation in an ion channel (genetic channelopathy), but rather constitutes an acquired channelopathy, with multiple transcriptional and posttranscriptional changes in diverse voltage- and neurotransmitter-activated ion channels.

### 1.7.2. Changes in intrinsic neuronal properties in chronic temporal lobe epilepsy

Do changes in intrinsic neuronal properties occur in chronic TLE? A recent study in the pilocarpine model of epilepsy suggests that such alterations occur and may be highly significant. In this model, Sanabria ER et al. (2001) examined the intrinsic discharge behavior of CA1 pyramidal neurons. Normally, virtually all pyramidal neurons in the hippocampal CA1 area are regular firing neurons, i.e. they fire a series of independent action potentials upon prolonged depolarization. Brief threshold stimulation elicits just one action potential. In pilocarpine-treated rats, a high fraction of CA1 neurons generated a high-frequency burst of spikes upon brief threshold stimulation (low-threshold bursters). Thus, there was a dramatic up-regulation of intrinsic neuronal burst firing associated with the development of TLE (Sanabria ER et al., 2001). Interestingly,

spontaneously bursting neurons were observed in epileptic hippocampus that were never seen in normal hippocampus, and that initiated epileptiform discharges in-vitro. Thus, augmented bursting and the appearance of spontaneously bursting neurons may well be of paramount importance for seizure initiation.

The ionic mechanism of the aberrant bursting in pilocarpine-treated animals was $Ca^{2+}$-dependent, because burst discharges were blocked in the presence of the $Ca^{2+}$ channel blocker $Ni^{2+}$ (1 mM), or by deleting $Ca^{2+}$ ions from the extracellular solution. The availability of selective $Ca^{2+}$ channel antagonists (see above) allowed dissecting which types of $Ca^{2+}$ channels are important in mediating burst discharges. Pharmacological evidence indicated that blockers of L-, N- and P-/Q-type $Ca^{2+}$ channels did not affect aberrant intrinsic burst firing. In contrast, low-threshold intrinsic burst firing was suppressed in most neurons by application of 30 to 100 µM $Ni^{2+}$, which blocks R-type and T-type $Ca^{2+}$ channels. Further experiments indicated that a genuine up-regulation of T-type $Ca^{2+}$ channels occurs in CA1 pyramidal neurons, while R-type $Ca^{2+}$ currents remained unchanged (Su H et al., 2002). These results suggested up-regulation of a $Ni^{2+}$-sensitive T-type $Ca^{2+}$ channel underlies the emergence of pathological burst firing in CA1 pyramidal neurons. Preliminary data from the same group indicates that at very late stages following status epilepticus (> 60 days), persistent $Na^{+}$ channels may also become important in mediating low-threshold bursting.

These data show that T-type $Ca^{2+}$ current regulation, and perhaps augmented persistent $Na^{+}$ currents may be important in the increased excitability seen following status epilepticus. However, these data do not imply that other voltage-gated currents do not contribute to altered intrinsic excitability. Even though the depolarizing drive for the burst discharge is mediated by inward $Ca^{2+}$ and/or $Na^{+}$ currents, a reduction in repolarizing $K^{+}$ conductances might contribute greatly to enhanced excitability. Thus, we have undertaken to systematically analyze the expression of different families of voltage-gated ion channels following SE in the pilocarpine model of epilepsy.

# 2 Materials and Methods

## 2.1 Materials

### 2.1.1 Animal Model

Male Wistar rats (150-200 g) approximately 30 days after birth.

### 2.1.2 Instruments

| instrument | Model | Company |
|---|---|---|
| ABI Prism Sequence Detection System | ABI Prism 7700 | Applied Biosystems |
| Ultraviolet laser-microdissection and -harvesting system | | PALM |
| Semiautomated sequencer | 373 | PE Biosystems |
| GeneChip Fluidics Station | | Affymetrix |
| HP GenArray™ scanner | | Affymetrix |
| UV-Spectrophotometer | GeneQuant II | Pharmacia |
| Ultra-pure water system | Milli Q UF Plus | Millipore |
| Vapor pressure osmometer | Wescor 5520 | Wescor |
| Vibrating microslicer | | Leica |
| Cryostat | Cryo-Star HM 560 | Microm |
| Inverted microscope | Axiovert | Zeiss |
| Stereomicroscope | | |
| Centrifuge | Sigma 1-15K | Sigma |
| Centrifuge | 5415 C | Eppendorf |
| Magnetic particle concentrator | Dynal MPC-E | Dynal |
| PCR-Thermocycler | Uno-Thermoblock | Biometra |
| Pipetten | P10, P20, P200, P1000 | Gilson |
| Oven | | Heraeus |
| Shaker | EL-2 | Edmund Bühler |

### 2.1.3 Chemicals

| Substances | Manufacturer |
|---|---|
| Acetic anhydride | Sigma |
| Aceton | Merck |
| Acrylamide | Serva |
| Agarose | Peqlab |
| Ammoniumpersulfate | Sigma |
| Bis-acrylamide | Serva |
| Bromchlorindolyphosphate | Roche |
| Bromphenolblue | Merck |
| Bovine serum albumin (BSA) | Sigma |
| Calcium chloride ($CaCl_2$) | Merk |
| Diazepam | Roch |
| Diethylpyrocarbonat (DEPC) | Sigma |
| Dimethylformamide | Merck |
| d´NTPs | Peqlab |
| Ethylenediaminetetraacetic acid (EDTA) | Sigma |
| Eosin | Merck |
| Acetic acid | Merck |
| Ethanol | Sigma |
| Ether | Merck |
| Ethidiumbromid | Sigma |
| Ficoll | Merck |
| Formamide | Merck |
| Gelatine | Sigma |
| Glucose | Merck |
| Glycerin | Sigma |
| Hydrochloric acid ( HCl) | Merck |
| Haematoxylin | Merck |
| Hydroxyethylpiperazine-1-ethanesulfonic acid (HEPES) | Sigma |

| Substances | Manufacturer |
|---|---|
| Isopropanol | Riedel de Haen |
| Magnesium chloride ($MgCl_2$) | Sigma |
| Maleic acid | Sigma |
| Methanol | Merck |
| NitroBlu-Tetrazolium | Roche |
| Pilocarpine hydrochloride | Sigma |
| Phosphate buffer saline (PBS) | GibcoBRL |
| Paraformaldehyde (PFA) | Merck |
| Polyvinylpyrolidone 40 | Merck |
| Potassium chloride (KCl) | Sigma |
| Scopolamine methylnitrate | Sigma |
| Sodiumacetate | Merck |
| Sodium bicarbonate ($NaHCO_3$) | Sigma |
| Sodium chloride (NaCl) | Merck |
| Sodium citrate | Sigma |
| Sodium phosphate ($Na_2HPO_4$) | Sigma |
| Sodium methanesulfonate ($NaCH_3SO_3$) | Aldrich |
| Sodium dihydrogen phosphate ($NaH_2PO_4$) | Merk |
| Sodium hydroxide (NaOH) | Sigma |
| N,N,N',N'-Tetramethyl-ethylenediamine (TEMED) | BioRad |
| Triethalnolamine | Sigma |
| Tris | Roth |
| Triton X-100 | Roth |
| Xylol | Riedel de Haen |

### 2.1.4 Enzymes and antibodies

| | |
|---|---|
| Protease type XIV | Sigma |
| Taq Polymerase (5 U/µl) | Life Technologies |
| DNase-I (RNase-frei; 10 U/µl) | Boehringer Mannheim |
| Anti-Digoxigenin-AP Fab Fragments (1093274) | Roche |

### 2.1.5 Kits and Reagents

| | |
|---|---|
| Dynabeads mRNA Direct Micro Kit<br>(mRNA isolation Kit) | Dynal |
| RNeasy Mini Kit (Cat Nr. 74104) | Qiagen |
| QIAquick PCR Purification Kit (Cat Nr. 28104) | Qiagen |
| Taq Cycle Sequencing Kit | PE Biosystems |
| DIG RNA Labeling Kit (Cat Nr. 1175025)<br>(*in situ* hybridization cRNA labelling) | Roche |
| SuperScript Preamplification System (Cat. No. 8089-11)<br>(First strand and second strand cDNA synthesis) | GibcoBRL |
| BioArray *HighYield*™ RNA Transcript Labeling Kit<br>(microarray cRNA labeling and synthesis) | Enzo |
| rat U34A microarray | Affymetrix |
| EZ RT-PCR Core Reagents(Part. No. 808-0236)<br>(Reverse Transcription and Amplification Kit) | AppliedBiosystems |
| Salmon Testes DNA (Cat. Nr. D7656) | Sigma |
| Phenol:Chloroform:Isoamyl Alcohol (25:24:1)<br>( Cat. Nr. 101K2001) | Sigma |
| Mounting Medium (Cat. Nr. S3023) | Dako |

### 2.1.6 Others

| | |
|---|---|
| Primer Express<br>(software for PCR primer, real-time RT-PCR<br>primer/fluorescent oligonucleotide design) | Applied Biosystems |
| Sequence Detection System, version1.6.3<br>(software for real-time RT-PCR data collection and analysis ) | Applied Biosystems |
| LPC-Membrane (Laser microdissection, 1.35µm) | PEN foil |
| pUC19/MspI (DNA-Marker) | MBI |
| Tissue-Tek (Brain fixation) | Sakura |
| Liquid Nitrogen | |
| Carbogen | |

## 2.2 Methods

### 2.2.1 Induction of Status Epilepticus and Brain Preparation

Male Wistar rats (150-200g, approximal 30 days of age) were kept on a 12 : 12 hour light : dark cycle. Rats were injected with a single high dose of the muscarinic agonist pilocarpine (340 mg/kg i.p.), which induced status epilepticus (SE) in most animals (~80%). Peripheral muscarinic effects were reduced by prior administration of methyl-scopolamine (1 mg/kg s.c.; 30 min) before injecting pilocarpine. Diazepam (0.1 mg/kg s.c.) was administered to all animals 40 minutes after status SE. It terminated the convulsions in the responsive rats and sedated all animals. At various time points following pilocarpine treatment, rats were sacrificed by decapitation under ether anesthesia. The brains were rapidly removed for later experiments at different time points. Age-matched rats served as controls. All animals sacrificed ≥ two weeks after pilocarpine injection were under video monitoring to detect onset and severity of seizure activity. All animal experiments were carried out according to the University of Bonn Animal Care Guidelines with permission of the local administration.

### 2.2.2 RNA Isolation

#### 2.2.2.1 Tissue Preparation

Three complementary methods were used to isolate neurons from subregions of the individual hippocampus for later mRNA or total RNA isolation: 1) dissociated individual neurons, 2) microdissected hippocampal subregions and 3) laser-microdissected neurons.

ACSF (artificial cerebrospinal fluid):

| | |
|---|---|
| NaCl | 125 mM |
| KCl | 3 mM |
| $NaH_2PO_4$ | 1.25 mM |
| $MgCl_2$ | 1 mM |
| $CaCl_2$ | 2 mM |
| $NaHCO_3$ | 25 mM |
| Glucose | 20 mM |

pH 7.4, 305 mOs, 100% $O_2$

Incubation Medium:

| | |
|---|---|
| $Na(CH_3SO_3)$ | 145 mM |
| (Sodium methanesulfonate) | |
| KCl | 3 mM |
| $CaCl_2$ | 0.5 mM |
| $MgCl_2$ | 1 mM |
| HEPES | 10 mM |
| Glucose | 15 mM |
| Protease type XIV | 2 mg/ml |

pH 7.4, 310 mOs, 100% $O_2$

1. Dissociated hippocampal individual neurons were prepared from 400µm thick horizontal sections according to a previously established protocal (Nagerl UV et al., 2000). Transverse hippocampal slices (400µm) were prepared with a vibrating microslicer (Leica) and transferred to a storage chamber perfused with oxygenated (95% $O_2$, 5% $CO_2$) ACSF to be maintained at room temperature. Enzymatic digestion was carried out for 10 minutes at 37°C and 5 minutes at room temperature in 5 ml of incubation medium (2 mg/ml Protease type XIV). After washing with enzyme-free incubation medium, the CA1 region was dissected and triturated with fire polished glass pipettes. The cell suspension was placed in a petri dish and superfused with ACSF. Cells were visualized and

harvested under an inverted microscope. From each animal (normal control or SE experienced), individual CA1 pyramidal neurons were harvested for later mRNA isolation by Dynabeads and subsequent real-time RT-PCR according to an absolute quantification paradigm (3.2.5.2.2).

2. Microdissected hippocampal subregions were taken from 400µm hippocampal slices with the preparation described above. Under the stereomicroscope, hippocampi were dissected as follows: dentate gyrus (DG), CA1, and CA3 subregions (Fig 2.1). Identical subregions of two adjacent slices were pooled together in a sterile microcentrifuge tube and immediately frozen in liquid nitrogen. All samples were stored at – 80°C for later mRNA or total RNA isolation in order to be used for expression microarray experiments or real-time RT-PCR.

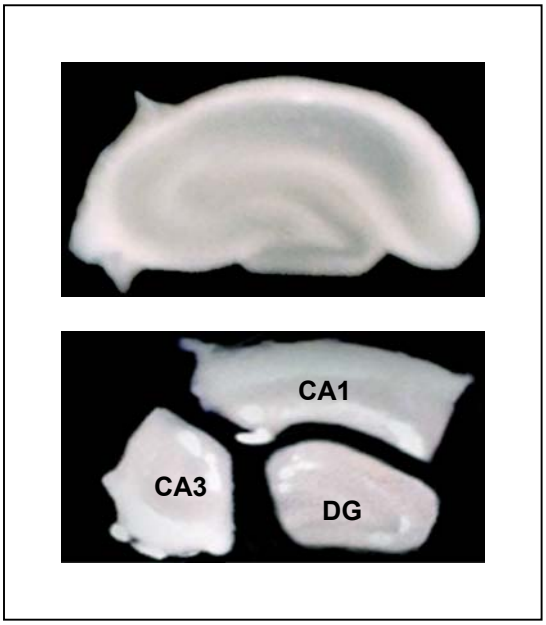


Fig 2.1: Microdissection of hippocampal subregions

3. Laser microdissected neurons were obtained using an ultraviolet laser-microdissection and harvesting system (PALM, Bernried Germany, Schütze K et al., 1998). After decapitation and brain removal, the hemispheres were coronally cut, frozen in liquid nitrogen and subsequently stored at – 80°C. 12µm

hippocampal cryosections were prepared using a Cryostat (Cryo-Star HM 560, Microm) and mounted on glass slides equipped with LPC-Membrane (PEN foil 1.35 µm). After 30 minutes air-drying, sections were stored in – 80°C for later laser-microdissection. Before laser-microdissection, cryosections were stained with haematoxylin-eosin (HE), rinsed twice in DEPC treated $H_2O$ and subsequently immersed in 70%, 90%, 100% ethanol. Neurons could be clearly identified under the microscope by cell size and morphology. Several hundreds of CA1 pyramidal neurons were laser-microdissected and pooled for later mRNA isolation and real-time RT-PCR.

#### 2.2.2.2 mRNA isolation by Dynabeads

mRNA was isolated from microdissected hippocampal subregions or harvested neurons by using the Dynabeads mRNA Direct Micro Kit (Dynal, Oslo) according to the manufacturer's protocol. After the cellular components were completely lysed in lysis/binding buffer in a RNase-free 1.5ml microcentrifuge tube, Dynabeads Oligo$(dT)_{25}$ were added. These are uniform, superparamagnetic, polystyrene beads with oligo$(dT)_{25}$ covalently bound to the surface. After mixing Dynabeads and the mRNA containing buffer thoroughly, the tube was placed on a shaker for 5 minutes at room temperature to allow the mRNA to anneal to the Dynabeads. Subsequently the tube was put in a magnetic particle concentrator. The mRNA loaded Dynabeads were fixed at the tube surface by magnetism allowing the supernatant with protein, rRNA and other debris to be removed. According to this protocol, mRNA loaded Dynabeads were washed twice by Washing Buffer A as well as twice by Washing Buffer B. Finally, mRNA was dissolved in suitable amount of DEPC treated $H_2O$ (Table 2.1 below) and stored at – 80°C for later use in real-time RT-PCR.

**Table 2.1**: volume of DEPC treated $H_2O$ applied to the isolated mRNA using the Dynabeads kit

| | DEPC treated $H_2O$ (µl) |
|---|---|
| Dissociated individual neurons | 30 |
| microdissected CA1 subregions | 60 |
| laser-microdissected neurons | 5 |

#### 2.2.2.3 Total RNA isolation by RNeasy Mini Kit

Total RNA was isolated from rat whole brain tissue or hippocampal subregions by using the Qiagen RNeasy Mini Kit (Cat Nr. 74104) for following sequencing and microarry experiments. According to the manufacture's protocol, rat brain tissue was homogenized in 350 µl Buffer RLT by rotor-stator homogenizer. After centrifugation, the supernatant was transferred to a new tube and 350 µl 70% ethanol was added and mixed well. Subsequently, samples were transferred to the mini column, centrifuged and the flowthrough was discarded. The column, which carried total RNA, was washed by Buffer RW1, then twice by Buffer RPE. Finally, the total RNA was eluted by 50 µl DEPC treated $H_2O$. The total RNA concentration was determined by use of a UV-spectrometer. Total RNA was stored at – 80°C for later use.

### 2.2.3 Partial sequence analysis of rat $Ca_V3.2$ cDNA

0.5 µg total RNA isolated from normal rat brain was applied for first-strand cDNA synthesis with oligo$(dT)_{12-18}$ by the SuperScript preamplification kit (GibcoBRL, Cat. No. 8089-11). The total reaction volume was 20.0 µl containing 2.0 µl of 10x buffer, 25ng/µl oligo$(dT)_{12-18}$, 0.5 mM dNTPs, 10 mM DTT, 2.5 mM $MgCl_2$, 10 U SuperScript II reverse transcriptase. RT-reaction was performed according to the manufacture's protocol at 42°C for 1.5h. A $Ca_V3.2$ cDNA segment was amplified by PCR with rat $Ca_V3.2$ -specific primers kindly provided by E. Perez-Reyes, (University of Virginia, Charlottesville).

forward primer: 5'-AGG AGG CTC GGC GCC GG-3'
reverse primer: 5'-GGA TAG GAG GAC GAT GGC CAA-3'

PCR was carried out in a total reaction volume of 20 µl containing 200 µM of each dNTP, 0.025 U *Taq* polymerase, 50 mM KCl, 10mM Tris-HCl pH 8.5, 1.5 mM $MgCl_2$, 0.01% gelatin and 0.2 µM of each primer. Amplification was performed in an automated thermocycler (Uno Block; Biometra, Göttingen) for 32 cycles at 94°C for 30 seconds, 57°C for 40 seconds and 72°C for 50 seconds. After purification, PCR products were sequenced on a semiautomated sequencer (373; PE Biosystems, Foster City) according to the manufacturer's protocol by a Taq cycle sequencing kit (ABI PRISM™, PE Biosystems, Foster City) using the forward and reverse primers separately.

### 2.2.4 Oligonuleotide microarrays

A well established oligonucleotide microarray system, Affymetrix GeneChip Arrays, was used for initial screening of the differential expression of a plethora of genes. Oligonucleotide microarrays can be used to profile the expression patterns of thousands of genes in parallel (Bassett DE Jr et al., 1999; Lockhart DJ et al., 2000). Further stratification allows to specifically study expression of gene groups of interest. In this study, rat U34A microarrays (Affymetrix, Santa Clara, CA) were used for large-scale gene expression profiling in CA1 areas of rats after SE vs. controls.

#### 2.2.4.1 Preparation of pilocarpine rat models and total RNA

The following five groups of animals were used in the study: controls, pilocarpine treated rats at days 3 and 14 after SE and animals in the chronic epileptic stage with low seizure frequency (<2 seizures/day, >day 20 after SE), high seizure frequency (≥10 seizures/day, >day 20 after SE). Three animals were included in each group. Hippocampal slice preparations, microdissection of CA1 and RNA isolation by the RNeasy Mini kit were carried out as described before.

#### 2.2.4.2 Sample labeling, hybridization and scanning

Sample labeling, hybridization and scanning of microarrays were carried out according to standard procedures (Wodicka L et al., 1997). Approximately 5 µg total RNA from hippocampal CA1 subfields were applied for first strand cDNA synthesis with T7-$(dT)_{24}$ primer:

5’-GGC CAG TGA ATT GTA ATA CGA CTC ACT ATA GGG AGG CGG-$(dT)_{24}$-3’

Then, the second strand cDNA was synthesized after use of RNase H, followed by normal phenol-chloroform purification. Subsequently cDNA was precipitated and washed by icy ethanol. After determination of the concentration of double-strand cDNA

(ds-cDNA) dissolved in DEPC treated $H_2O$, 2 µg ds-cDNA was *in vitro* transcribed into cRNA with biotin-labeled NTPs by use of the Bioarray *HighYield*™ RNA Transcript Labeling Kit (Enzo). The synthesized biotin-labeled antisense cRNA was purified by using the Qiagen RNeasy Mini Kit. Following determination of concentration and precipitation by icy ethanol, the cRNA pellet was dissolved in DEPC treated $H_2O$ and fragmented by fragmentation solution at 95 $^oC$ for 35 min.

15 µg fragmented biotin labeled antisense cRNA was added to a rat U34A microarray. After hybridization for 16 hours at 45 $^oC$, the microarrays were washed and stained automatically in the GeneChip fluidics station and scanned by use of the HP-GenArray™ scanner.

#### 2.2.4.3 Microarray analysis

Fifteen rat U34A microarrays have been used for gene expression profiling in CA1 subfields of SE experienced and control rats. These oligonucleotide arrays cover approximately 8000 known rat genes and a large set of unknown expressed sequence tags (ESTs). The microarray suite software version 5.0 (Affymetrix, Santa Clara, CA) was used for data analysis of the hybridized arrays. The samples were scaled to a target intensity of 1000 as suggested by the manufacturer. Genes included in the analyses had to fulfill the following criteria:

(i) perfect match/mismatch ratio to be called present or marginally present;

(ii) genes with absent calls and signal values >200 were not included in the analysis, genes with absent calls and signal values <200 as well as present calls at another stage were regarded as below the detection threshold;

(iii) $\geq$ 2 fold expression change compared to the corresponding control value had to be observed;

(iv) expression differences had to reach a p-value of $< 0.05$ (student's t-test) from three replicates for each gene and at each stage.

### 2.2.5 Real-Time RT-PCR

The combination of fluorescence techniques and RT-PCR has led to the development of the real-time RT-PCR technique which allows to precisely quantify even low amounts of mRNA by PCR. Currently, four techniques are available to detect the amplified product by a fluorescent signal generated during the PCR process: SYBR Green intercalating dyes (Schmittgen TD et al., 2000; Yin JL et al 2001), molecular beacons (Tayagi S et al., 1996), hybridization probes (Emig M, 1999; Blaschke V et al., 2000) and hydrolysis probes, also called “TaqMan” probes (Gibson UE et al., 1996, Fink L et al., 1998).

The “TaqMan” assay, in particular, integrates high sequence specificity and reaction robustness, which are mandatory for the use in single cell RT-PCR protocols. In a TaqMan assay, in addition to the normal forward and reverse primers, a third oligonucleotide probe is used, which is labeled with a reporter dye (e.g. FAM, 6-carboxyfluorescein) at the 5’ end and a quencher dye (TAMRA, 6-carboxytetramethyl-rhodamine) at the 3’ end. The fluorescence labeled oligonucleotide is designed to hybridize closely downstream of the forward primer. In the intact state of the bi-fluorescent oligonucleotide, the fluorescence energy emission of the reporter dye is absorbed by the quencher dye, based on the phenomenon of fluorescence resonance energy transfer (FRET) (Stryer L, 1978; Cardullo RA et al., 1988). During the PCR, the 5’-3’ exonuclease activity of the Taq polymerase cleaves the probe (Holland PM et al., 1991). The hydrolysis of the probe separates the reporter and quencher dyes, resulting in interruption of FRET and increase in the fluorescence of the reporter dye, which can be detected by a CCD digital video camera. Fig 2.2 shows this process of a TaqMan real-time PCR schematically. The accumulation of PCR products is directly proportional to the abundance of the fluorescence intensity to be detected.

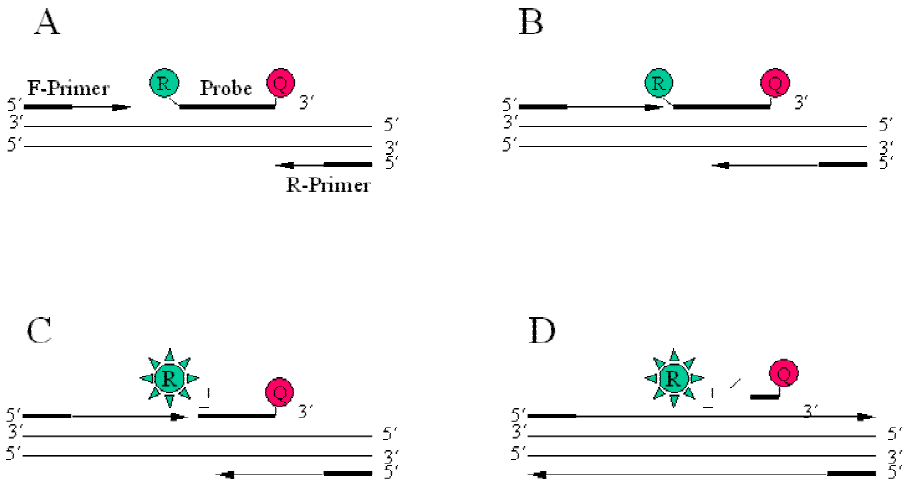


**Fig 2.2 A**, Polymerization: a fluorescent reporter dye (R) and a quencher dye (Q) are attached at the 5' and 3' ends respectively of a "TaqMan" probe; **B**, Strand displacement: during elongation, the Taq polymerase hits the bi-fluorescent labeled oligonucleotide probe; **C**, Cleavage: during each extension cycle, the DNA polymerase cleaves the reporter dye from the probe; **D**, Polymerization completed: once separated from the quencher, the reporter dye emits characteristic fluorescence.

An important issue of real-time RT-PCR is the mode of mRNA quantification. Two approaches are available: absolute and relative quantification. *Absolute* quantification relies on quantification of a gene expression level according to a standard curve. It is extremely dependent on accurate measurement of the amounts of template mRNA by optical UV spectrophotometer determination. The appliction of this protocol is limited when starting from minute amounts of mRNA. The *relative* quantification strategy is used to quantify target gene expression levels by normalization to an internal reference gene. This relative assay obviates the need of an accurate determination of initial mRNA concentrations. On the other hand, a suitable reference gene with stable expression under the experimental paradigm is essential as internal control.

In our study, absolute RT-PCR quantification was used to determine an optimal reference gene for subsequent relative RT-PCR quantification of voltage-gated ion channel subunit mRNAs in epileptic CA1 neurons. The ABI Prism Sequence Detection

System 7700 (Applied Biosystem, Foster City, CA, USA) was used for real-time RT-PCR. The reaction was performed in a MicroAmp Optical 96-Well Reaction Plate. TaqMan Easy RT-PCR Core Reagents (Part. No. 808-0236) were used for a one tube, single enzyme RT-PCR in a total reaction volume of 12.5 µl.

#### 2.2.5.1 TaqMan primer and probe design and reaction condition optimization

##### 2.2.5.1.1 TaqMan primer and probe design

Primers and hydrolysis probes for putative reference genes and voltage-gated ion channel subunits were designed with Primer Express software (Applied Biosystems, Foster City) according to the guidelines listed in the Primer Express User's Mannual. The melting temperature of all primers is predetermined at 59°C.

For optimal amplification efficiency, amplicons of approximately 70-80 base pair size were used. The amplicons should span exon / exon boundaries to ensure amplification to be mRNA specific. No significant homologies of the amplicon sequences with other previously characterized genes have been found by searching GenBank databases with BLASTN program. The sequence data of all the primers and probes are outlined in Table 2.3-2.7.

##### 2.2.5.1.2 Optimization of primer concentrations

A so called "primer matrix" experiment was carried out to determine concentrations of forward and reverse primers with optimal amplification characteristics during PCR.

Real-time RT-PCR was carried out in a total reaction volume of 12.5 µl with the TaqMan EZ RT-PCR Core reagent. Each reaction contained 1.0 ng of total RNA, 1 X EZ Buffer which includes the internal reference dye Rox, 300µM of dATP, dCTP, dGTP and 600µM of dUTP, 0.01U/µl Uracil-N-clycosylase (UNG), 100µM of TaqMan probe, 5mM $Mn(OAc)_2$, 0.01 U/µl rTth *Taq* polymerase. Nine different concentration conditions of

primers were distributed on the reaction plate according to a scheme provided in Table 2.2.

**Table 2.2**: Plate arrangement of different concentration of forward and reverse primers.

| | | Reverse Primer (nM) | | | | | |
|---|---|---|---|---|---|---|---|
| | | 50 | | 300 | | 900 | |
| **Forward Primer (nM)** | **Plate** | **1** | **2** | **3** | **4** | **5** | **6** |
| **50** | **A** | **50/50** | | **50/300** | | **50/900** | |
| **300** | **B** | **300/50** | | **300/300** | | **300/900** | |
| **900** | **C** | **900/50** | | **900/300** | | **900/900** | |
| | **D** | **NTC** | | | | | |

A one step real-time RT-PCR was performed in the ABI 7700 thermocycler. The one step RT-PCR thermal cycling conditions are given in Fig 2.3. Fluorescence data is collected only at the two-step amplification stage.

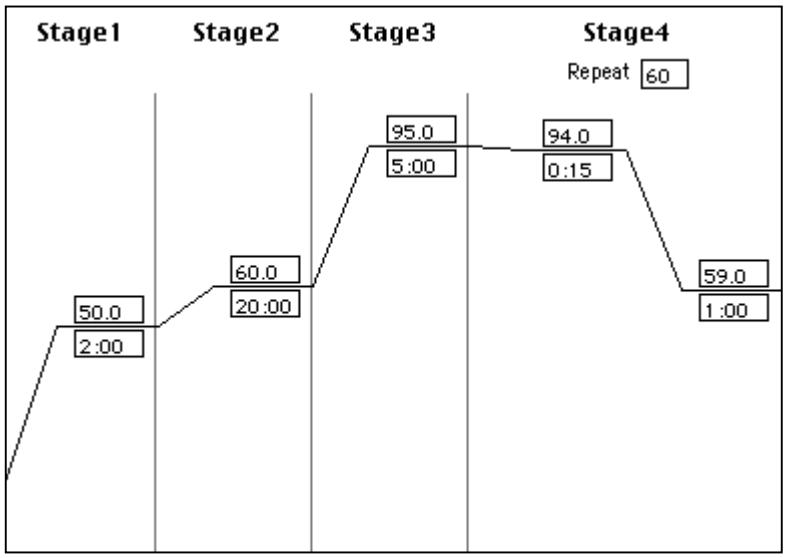


**Fig 2.3:** One step RT-PCR. Stage 1: Uracil-N-Glycosylase (UNG) incubation. "Carry over" contamination protection of PCR. PCR products which incorporated uracil are digested by UNG activity in this stage. UNG will be inactivated at temperatures higher than 55°C. Stage 2: reverse transcription with rTth *Taq* polymerase. Stage 3: complete denaturation of the cDNA. Stage 4: amplification and fluorescence data collection.

At the end of the experiment, amplification results of each well are automatically determined by the Sequence Detection System software (version 1.6.3). Optimal primer concentration combinations result in the highest amplification efficiency (Fig 2.4). Finally, the $Mn(OAc)_2$ concentration (3, 5 or 7 mM) is optimized.

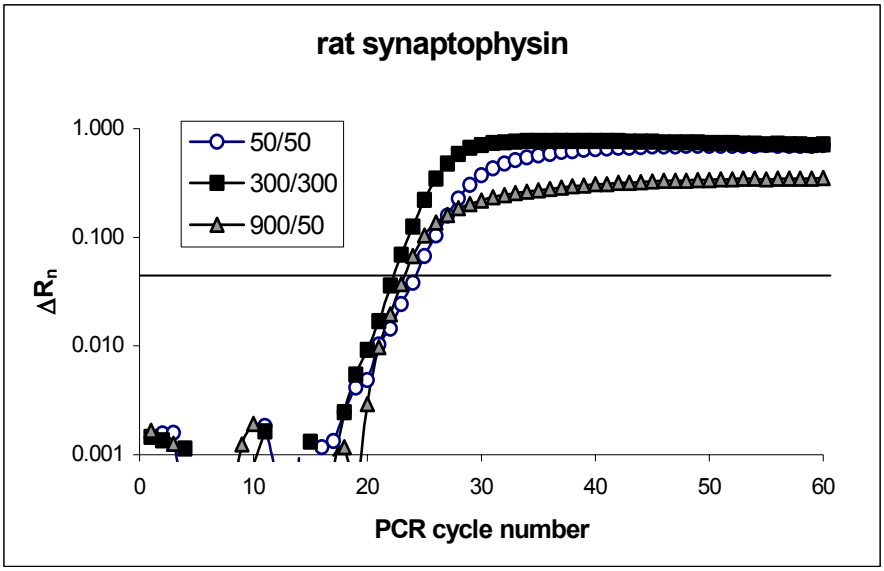


**Fig 2.4:** Amplification plot of a "primer matrix" for rat synaptophysin. Primer combination of 300nM/300nM (forward / reverse) result in optimal amplification efficiency ($\Delta R_n$: normalized reporter signal).

The optimized concentration of forward, reverse primer and $Mn(OAc)_2$ for real-time quantification RT-PCR together with the sequences are outlined in the Table 2.3-2.7.

**Table 2.3:** Sequences and concentration ratios of primers and hydrolysis probes of reference genes with labeling dyes (F for FAM as reporter dye, T for TAMRA as quencher dye) that were used for real-time RT-PCR.

| Gene | forward (f) / reverse (r) primer / hydrolysis probe | primer probe concentration (nM)(f/r/p) | $Mn(OAc)_2$ concentration (mM) | GenBank accession number |
|---|---|---|---|---|
| GAPDH | (f),5'-TGCCAAGTATGATGACATCAAGAAG-3'<br>(r), 5'-TAGCCCAGGATGCCCTTTAGT-3'<br>F5'-TGGTGAAGCAGGCGGCCGAG-3'T | 50/300/100 | 5 | NM_017008 |
| Synapto-physin | (f), 5'-TCAGGACTCAACACCTCAGTGG-3'<br>(r), 5'-AACACGAACCATAAGTTGCCAA-3'<br>F5'-TTTGGCTTCCTGAACCTGGTGCTCTG-3'T | 300/300/100 | 5 | NM_012664 |
| β-actin | (f), 5'-AGGCCCCTCTGAACCCTAAG-3'<br>(r), 5'-CCAGAGGCATACAGGGACAAC-3'<br>F5'-TTTGAGACCTTCAACACCCCAGCCA-3'T | 300/300/100 | 5 | V01217 |
| HPRT | (f), 5'-GCGAAAGTGGAAAAGCCAAGT-3'<br>(r), 5'-GCCACATCAACAGGACTCTTGTAG-3'<br>F5'-CAAAGCCTAAAAGACAGCGGCAAGTTGAA-3'T | 300/900/100 | 5 | X620085 |
| Cyclophilin | (f), 5'-CCCACCGTGTTCTTCGACAT-3'<br>(r), 5'-AAACAGCTCGAAGCAGACGC-3'<br>F5'-ACGGCTGATGGCGAGCCCTTG-3'T | 50/300/100 | 5 | M19533 |
| β-2-microglobulin | (f), 5'-CCATTCAGAAAACTCCCCAAATT-3'<br>(r), 5'-GAGGAAGTTGGGCTTCCCA-3'<br>F5'-AGTGTACTCTCGCCATCCACCGGAGA-3'T | 300/300/100 | 5 | NM_012512 |

**Table 2.4:** Sequences and concentration ratios of primers and hydrolysis probes for voltage dependent $Ca^{2+}$ channels with labeling dyes (F for FAM as reporter dye, T for TAMRA as quencher dye) that were used for real-time RT-PCR.

| Gene | forward (f) / reverse (r) primer / hydrolysis probe | primer probe concentration (nM)(f/r/p) | $Mn(OAc)_2$ concentration (mM) | GenBank accession number |
|---|---|---|---|---|
| $Ca_V2.1$ | (f), 5' - GTCGTGGTGCTAACAGGCATC -3'<br>(r), 5'- ACGAACCGCCCTCAGTGTC -3'<br>F5'- TGGCCACTGTCGGGACGGAGTT -3'T | 50/300/100 | 5 | NM_012918 |
| $Ca_V2.2$ | (f), 5'- TCATCGGCCTCGAGTTCTATATG -3'<br>(r), 5'- TCACCCACAGGCTCTGCAT -3'<br>F5'- CAAATTCCATAAGGCCTGCTTCCCCA -3'T | 300/900/200 | 3 | AF055477 |
| $Ca_V1.2$ | (f), 5'- GGAGGACTGGAATTCGGTGAT -3'<br>(r), 5'- ACTAACATCCCTGGAAAAGAGGG -3'<br>F5'- ATGATGGGATCATGGCTTATGGCGG -3'T | 200/3600/200 | 3 | M67516 |
| $Ca_V1.3$ | (f), 5'- TGCTCTTCAGGTGTGCAACAG -3'<br>(r), 5'- TCACACAGCTTCCCAGGGA -3'<br>F5'- CCTGGCAGGAGATCATGCTCGCC -3'T | 1800/1800/200 | 3 | D38101 |
| $Ca_V2.2$ | (f), 5'- TGAGGTCGTTTGGGCAATCT -3'<br>(r), 5'- TCCTTAGGAGCCGGAGAGCT -3'<br>F5'-ACCTGGCACATCTTTTGGAATCAGTGTCTTAC-3'T | 200/1200/100 | 3 | AY029412 |
| $Ca_V3.1$ | (f), 5'- ACCCTGGCAAGCTTCTCTGA -3'<br>(r), 5'- TTTCGGAGGATGTACACCAGGT -3'<br>F5'- CCAGGCAGCTGCTATGAGGAGCTACTCA -3'T | 200/1200/100 | 3 | AF203698 |
| $Ca_V3.2$ | (f), 5'- ATGTCATCACCATGTCCATGGA -3'<br>(r), 5'- ACGTAGTTGCAGTACTTGAGGGCC -3'<br>F5'- CTACAACCAGCCCAAGTCCCTGGATGA -3'T | 300/300/200 | 5 | AF290213 |
| $Ca_V3.3$ | (f), 5'- TCATCCGTATCATGCGTGTTC -3'<br>(r), 5'- GGCCCGCATTCCTGTG -3'<br>F5'- CGCCCGGGTGTTGAAGCTATTGAA -3'T | 1200/200/100 | 3 | AF290214 |
| $Ca_V\beta1$ | (f), 5'- GGCTGTGAGGTTGGTTTCATC -3'<br>(r), 5'- TGGCGCAGCGTCTGTTC -3'<br>F5'- TCAAACTGGACAGCCTTCGCCTGC -3'T | 50/300/100 | 3 | X61394 |
| $Ca_V\beta2$ | (f), 5'- CCCCAGTAAGCACGCAATAATAG -3'<br>(r),5'-AAAATCCTTTCAATTTCACTCTGAACTT-3'<br>F5'- AAGATCCAACACAAGGTCGAGCTTAGCG -3'T | 50/300/100 | 3 | M80545 |
| $Ca_V\beta3$ | (f), 5'- CAGATGCCTACCAGGACCTGTAC -3'<br>(r), 5'- TGCCCGTTAGCACTGGGT -3'<br>F5'- CTACAACCAGCCCAAGTCCCTGGATGA -3'T | 300/300/100 | 3 | NM_012828 |
| $Ca_V\alpha_2\delta$ | (f), 5'- AATGCTCAGGATGTGAGTTGTTTC -3'<br>(r), 5'- TTATTCACCGCATCCTTCAGC -3'<br>F5'- AGCCTCACCGTCAACACACCTCGG -3'T | 50/300/100 | 3 | NM_012919 |

**Table 2.5:** Sequences and concentration ratios of primers and hydrolysis probes for voltage dependent $Na^+$ channels with labeling dyes (F for FAM as reporter dye, T for TAMRA as quencher dye) that were used for RT-PCR.

| Gene | forward (f) / reverse (r) primer / hydrolysis probe | primer probe concentration (nM)(f/r/p) | $Mn(OAc)_2$ concentration (mM) | GenBank accession number |
|---|---|---|---|---|
| $Na_V1.1$ | (f), 5'- AGAAACCCTTGAGCCCGAAG -3'<br>(r), 5'- CACACTGATTTGACAGCACTTGAA -3'<br>F5'-TTGCTTCACTGAAGGCTGTGTGCAGAG-3'T | 900/900/100 | 5 | X03638 |
| $Na_V1.2$ | (f), 5'- TCGTTGATGTCTCCTTGGTTAGC -3'<br>(r), 5'- GGGACTTGATGGCACCAAGT -3'<br>F5'- AACTGCAAATGCCTTGGGCTATTCGG -3'T | 300/900/100 | 3 | X03639 |
| $Na_V1.3$ | (f), 5'- GCCGCTCCGAGCCTTATC -3'<br>(r), 5'- GATGGAGGGAATTGCACCAA -3'<br>F5'-CGCTTTGAAGGCATGAGGGTGGTTGTA-3'T | 50/300/100 | 5 | Y00766 |
| $Na_V1.5$ | (f), 5'- ATCTGGCCCTGTCCGACTT -3'<br>(r), 5'- GCTTATCTGGTTGGGTTTGGC -3'<br>F5'- ATGCCTTGTCTGAGCCGCTCCG -3'T | 50/300/100 | 3 | NM_013125 |
| $Na_V1.6$ | (f), 5'- CATCTTTGACTTTGTGGTGGTCAT -3'<br>(r), 5'- CGGATAACTCGGAATAGGGTTG -3'<br>F5'- CCATTGTGGGAATGTTCCTGGCTG -3'T | 300/300/100 | 3 | L39018 |
| $Na_V \beta1$ | (f), 5'- TGCTGCTGCCACGGAAG -3'<br>(r), 5'- TCTCGGAAGTAATGGCCAGG -3'<br>F5'- TGCTGCACAAGAGAATGCCTCGGA -3'T | 50/900/100 | 5 | NM_017288 |
| $Na_V \beta2$ | (f), 5'-TGGACTTACCAGGAGTGTAGCAATT-3'<br>(r), 5'- CTCCAAACCGCTCCAGCTT -3'<br>F5'-TCCAGTTCCGAATGAAGATCATCAACCTG-3'T | 900/900/100 | 5 | NM_012877 |

**Table 2.6:** Sequences and concentration ratios of primers and hybridization probes for voltage dependent $K^+$ channels with labeling dyes (F for FAM as reporter dye, T for TAMRA as quencher dye) that were used for real-time RT-PCR.

| Gene | forward (f) / reverse (r) primer / hydrolysis probe | primer probe concentration (nM)(f/r/p) | $Mn(OAc)_2$ concentration (mM) | GenBank accession number |
|---|---|---|---|---|
| $K_V$1.4 | (f), 5' - TTTGCAGAGGCAGATGAACCT -3'<br>(r), 5'- TGGTTACCACAGCCCACCA -3'<br>F5'- CACCCATTTCCAAAGCATTCCAGATGC -3'T | 300/900/100 | 3 | NM_012971 |
| $K_V$2.3 | (f), 5'- GCCATCTTGCCCTTCTACATAACT -3'<br>(r), 5'- CAGCTCTTGGGTGGTGTGG -3'<br>F5'- CTGGTGGAAAGCCTGAGCGGCA -3'T | 50/300/100 | 5 | NM_021697 |
| $K_V$3.3 | (f), 5'- TTCATCCACATCA GCAACAAGAC -3'<br>(r), 5'- TCCACATTGGTGATATTCTCCG -3'<br>F5'- TGACGCAGGCCTCTCCAATCCCT -3'T | 900/900/100 | 3 | M84211 |
| $K_V$3.4 | (f), 5'-GCTGCCCTGATACGTTGGA -3'<br>(r), 5'-AAGGGCAAGATGGCCACA -3'<br>F5'-TTTGTCAAGAACCTGCTCAACATCATCGACT-3'T | 300/300/100 | 5 | X62841 |
| $K_V$4.2 | (F), 5'- CTTCAGTCGGATCTACCACCAAA -3'<br>(R), 5'- CCAGCCTCGCTTTCTTCTGT -3'<br>F5'- CCAACGAGCGGACAAACGAAGGG -3'T | 50/300/100 | 5 | S64320 |
| $K_V$4.3 | (F), 5'-AGCGCTACTCCGTGGCTTT -3'<br>(R), 5'- GAGGAGGTACTCCACCGTGAAG-3'<br>F5'- TCTGCCTGGACACTGCGTGTGTCA-3'T | 50/300/100 | 5 | U42975 |
| KCNQ2 | (f), 5'- CGGCCGGACACTTGGATAT -3'<br>(r), 5'- CCCCACAATCTGGTCCACTC -3'<br>F5'- TTGTCCCGAATCAAGAGCCTGCAGTC -3'T | 50/300/100 | 3 | AF087453 |
| KCNQ3 | (f), 5'- CTCAGAAAGGGTCAGCATTTACCT-3'<br>(r), 5'- GCTGCCCTGGCTACATATGG -3'<br>F5'- CCATCCCAGCAGTCTCCAAGGAATGA -3'T | 300/900/100 | 3 | AF087454 |
| KCNQ5 | (f), 5'- GCTCAGAAGTCTCCGGTTCCT -3'<br>(r), 5'- CTTCCAGGTCCCTCCCCTT -3'<br>F5'- CAGATCCTGCGTATGGTGCGCATG -3'T | 300/300/100 | 3 | AF5259374 |

**Table 2.7:** Sequences and concentration ratios of primers and hybridization probes for HCN channels with labeling dyes (F for FAM as reporter dye, T for TAMRA as quencher dye) that were used for real-time RT-PCR.

| Gene | forward (f) / reverse (r) primer / hydrolysis probe | primer probe concentration (nM)(f/r/p) | $Mn(OAc)_2$ concentration (mM) | GenBank accession number |
|---|---|---|---|---|
| HCN1 | (f), 5'- CAGACGGCTCTTACTTTGGAGAA -3'<br>(r), 5'- GCTCGAACACTGGCAGTGC -3'<br>F5'- TATGCCTGCTGACCAAGGGCCG -3'T | 50/300/100 | 3 | AF247450 |
| HCN2 | (f), 5'- TTTGAGACCGTGGCC ATTG -3'<br>(r), 5'-AACCTTGTGTAGCAAGATGGAGTTC-3'<br>F5'- CGCCTGGACCGCATAGGCAAGA -3'T | 300/300/100 | 5 | AF247451 |
| HCN3 | (f), 5'- CGCAGGG CTTTTGAGACTGT -3'<br>(r), 5'- CGTTTCCGCTGCAATATCG -3'<br>F5'- CTTCGGCGCATCGGCAAAAAGAAT -3'T | 50/900/100 | 5 | AF247452 |
| HCN4 | (f), 5'- GTCTGGACCGCATAGGCAA -3'<br>(r), 5'- CGCCTGAGTTGAGGTCGTG -3'<br>F5'-AAGAACTCCATCCTCCTCCACAAGGTGC-3'T | 300/900/100 | 3 | AF247453 |

### 2.2.5.2 Absolute Real-Time RT-PCR Quantification of Reference Gene Transcripts

2.2.5.2.1 Preparation of the PCR products for standard curve generation

In order to determine the absolute starting copy number of the target gene, PCR products of target genes were diluted and used as template for PCR reactions to generate a standard curve (Chen J et al., 2000).

First strand cDNA was synthesized from rat brain total RNA by SuperScript First-Strand Synthesis System (Invitrogen Cat. No.11904-018). PCR was performed with the same forward and reverse primers as for the subsequent TaqMan reactions. The reaction condition was 94°C 3 min, followed by 35 cycles at 94°C 40 sec, 59°C 50 sec, 72°C 60 sec, after incubation at 72°C 10 min, stored at 4°C. The specific PCR products were cut out of the 3% agrose gel after electrophoresis. The amplicons were purified by phenol-chloroform procedure and then confirmed again by 3% agrose gel electrophoresis to monitor for contamination.

In order to determine the copy numbers of PCR products, first the concentrations of the amplicons were measured by the UV spectrophotometer at 260nm. To convert the concentration into copy number, the following calculation was used. The molecular weights of the amplicons were calculated according to average value of a single base pair (660); Avogadro's factor (1 mol = 6.022 X $10^{23}$ molecules) represents the abundance of molecules in 1 molar material.

$$\textbf{Copy Number (per µl)} = \frac{\textbf{Concentration (µg/µl) X 6.022 X } 10^{23}}{\textbf{660 X base pair number X 10 X } 10^{6}}$$

2.2.5.2.2 Real-time RT-PCR absolute quantification

mRNA samples were isolated from individual CA1 neurons from each SE experienced or control rat (30 days after SE, n=5 each). mRNAs dissolved in 30µl DEPC treated $H_2O$ were distributed for all six reference gene's absolute quantification reactions. Standard amplicons were serially diluted according to $1X10^3$, $1X10^4$, $1X10^5$, $1X10^6$ and $1X10^7$ gene copies respectively. On each RT-PCR plate, the standard dilutions and mRNA samples were run in triplicates with the optimized primer, probe, $Mn(OAc)_2$ concentrations. After real-time RT-PCR reactions, the copy numbers of the target reference genes in mRNA samples were determined by comparison with the standard curve. Data were analyzed by Sequence Detector V1.6.3 (AppliedBiosystem). With this absolute quantification method, the mRNA expression levels of five putative reference genes GAPDH (glyceraldehyde-3-phosphate dehydrogenase), β-actin, cyclophilin A, HPRT (hypoxanthine phosphoribosyl-transferase), β-2-microglobulin and the neuron-specific gene synaptophysin were compared between control and SE experienced animals. This experiment served as prerequisite to identify an optimal reference gene for later relative quantification.

### 2.2.5.3 Relative Real-time RT-PCR Quantification of Ion Channel Subunits Transcripts to Reference Gene Transcripts

The relative quantification protocol relies on the determination of starting concentration ration between target and standard transcripts (Fink L et al., 1998, User Bulletin #2). It is given by the following equation:

$$T_0/R_0=K\,(1+E)^{(Ct,R - Ct,T)}$$

$T_0$: Initial number of target gene copies;

$R_0$: Initial number of standard gene copies;

E: Efficiency of amplification;

Ct,T: Threshold cycle of target gene;

Ct,R: Threshold cycle of reference gene;

K: Constant.

The determination of PCR efficiency is an important prerequisite for the calculation. However for the TaqMan primers and fluorescence probes designed according to the above mentioned guidelines and optimized through pre-experiments, especially when the amplicons are all approximately 70-80 base pairs in size, the efficiency (E) will generally be close to one (User Bulletin #2), i.e. a complete amplification of PCR products per cycle will occurs.

As K is dependent on factors like (1) the reporter dye used in the probe, (2) sequence context effects on the fluorescence properties of the probe, (3) purity of the probe, and (4) efficiency of the probe cleavage, the exact value of K needs not be equal to one (User Bulletin #2). However, the affecting factors will vary only negligibly among single samples so that K is assumed to be equal and thus does not influence the comparison of calculated relative ratios (Fink L et al., 1998).

Therefore, the relative amount of target transcript is given by

$$X_N = 2^{-\Delta Ct}$$

$X_N$: $T_0/R_0$, the normalized amount of target;

$\Delta C_t$: $C_{t,T} - C_{t,R}$, the difference in threshold cycles of target and reference transcripts

An important prerequisite for the $\Delta C_t$ calculation is that the efficiencies of the target and the reference transcript PCR reactions are equal. The reaction efficiency is determined in the following experiments in order to determine the variation of $\Delta C_t$ between target and reference amplicons within a serial dilution of RNA.

2.2.5.3.1 PCR efficiency determination

A total RNA from rat brain was accurately diluted. The dilution values were 1 ng, 0.5 ng, 0.2 ng, 0.1 ng, 0.05 ng, 0.02 ng and 0.01 ng. These serially diluted total RNA samples were amplified for both target as well as reference genes in order to compare their $\Delta C_t$ ratio of them. In order to demonstrate that the PCR efficiencies between target and reference genes are equal, the $\Delta C_t$ of target and reference genes should be stable in the dilution series (User Bulletin #2).

2.2.5.3.2 Relative quantification with real-time RT-PCT

Relative quantification of the starting mRNA copy numbers was performed according to the $\Delta\Delta C_t$ method (Fink et al., 1998). The signal threshold was set within the exponential phase of the reaction for determination of the threshold cycle ($C_t$). Synaptophysin was used as endogenous, neuron-specific reference gene for normalization of ion channel subunit mRNAs.

Relative quantification carried out using mRNA isolated from microdissected hippocampal subregions or laser-microdissected neurons according to the cycling conditions described before.

In all experiments, statistical significance was tested with a two-tailed Student's t-test with the level of significance set to $p<0.05$.

### 2.2.6 *In situ* hybridization

In order to confirm the real-time RT-PCR results for the reference genes GAPDH and synaptophysin, *in situ* hybridization was performed for both genes with a digoxigenin (DIG) labeled *in vitro* transcription product (cRNA probe) according to a previously described protocol (Hans VH et al., 1999) on 12 µm cryosections of pilocarpine and control brains (n=3 each).

#### 2.2.6.1 Preparation of the cRNA probe

Hybridization probes were specific for GAPDH and synaptophysin cDNAs covering nucleotides 204-581 of the rat GAPDH (GenBank accession Nr. NM_017008) and 389-753 of the rat synaptophysin (GenBank accession Nr. NM_012664) cDNAs. Both fragments were generated by RT-PCR using primers specific to GAPDH and synaptophysin starting from rat brain total RNA.

| | | |
|---|---|---|
| rat GAPDH | Forward Primer | 5'-CAAGGCTGAGAATGGGAAG-3' |
| | Reverse Primer | 5'-TTCTGAGTGGCAGTGATGG-3' |
| rat synaptophysin | Forward Primer | 5'-TCTTCCTGCAGAACAAGTACCG-3' |
| | Reverse Primer | 5'-GCCAGGTGCTGGTTGCT-3' |

The RT reaction was carried out as described earlier with GilboBRL kits. PCR amplification was performed in a total reaction volume of 100 µl containing 200 µM of each dNTP, 0.05 U/µl Taq polymerase, 50 mM KCl, 10mM Tris-HCl pH 8.5, 1.5 mM $MgCl_2$, 0.01% gelatin and 0.2 µM of each primer in an automated thermocycler (Uno Block, Biometra) for 36 cycles at 94°C for 30 seconds, 59°C for 40 seconds, and 72°C for 40 seconds.

By using the DIG RNA labeling Kit (Roche), cRNA probes were transcribed from RT-PCR fragments generated previously with the primer carrying a T7 RNA polymerase

recognition site sequence ( 5'-AAACGACGGCCAGTGAATTGTAATACGACTCACTAT AGGCGC-3' ). After ethanol precipitation, the cRNA probe was resuspended in DEPC treated $H_2O$.

### 2.2.6.2 *in situ* hybridization

All solutions were prepared with of DEPC treated $H_2O$

| 4% PFA / pH7.4 | |
|---|---|
| 4% (w/v) | Paraformaldehyde in 1 x PBS |

| 0.1% Triton / pH7.4 | |
|---|---|
| 0.1% (v/v) | TritonX-100 in 1 x PBS |

| 0.1M TEA solution / pH 8.0 | |
|---|---|
| 100 mM | Triethalnolamine |
| 0.15 mM | NaCl |
| 0.5% (v/v) | Acetic anhydride |

| 50 x Dehnhardt's | |
|---|---|
| 1%(w/v) | Ficoll |
| 1%(w/v) | Polyvinyl- pyrolidone 40 |
| 1%(w/v) | BSA |

| 20 x SSC / pH 7.0 | |
|---|---|
| 3 M | NaCl |
| 0.3 M | Sodium citrate |

| 0.1M Maleic acid / pH7.5 | |
|---|---|
| 100 mM | Maleic acid |
| 0.15 mM | NaCl |

| Pre-hybridization buffer | |
|---|---|
| 50%(v/v) | Formamide |
| 5 x | SSC |
| 5 x | Denhardt's |
| 500ug/ml | Sheared salmon testes DNA |

| Blocking buffer | |
|---|---|
| 100 mM | Phosphate buffer |
| 50% | Glycerin |
| 1 mg/ml | Sodium azid |
| 75 mg/ml | Gelatine |

| Substrate buffer / pH9.5 | |
|---|---|
| 100 mM | Tris-HCl |
| 100 mM | NaCl |
| 50 mM | $MgCl_2$ |

| Stop buffer / pH 8.0 | |
|---|---|
| 10 mM | Tris-HCl |
| 1 mM | EDTA |

| NBT | | BCIP | |
|---|---|---|---|
| 75mg in 1ml | Nitro blue tetrazolium Dimethylformamide | 50mg | 5-Bromo-4-chloro-3-indoly phosphate in 1ml Dimethylformamide |

The 12µm cryosections were fixed by 4% PFA (4°C). Then, they were incubated with 0.1M TEA solution, followed by 0.1% Triton X solution.

After blocking with pre-hybridization buffer, the probe was resuspended in pre-hybridization buffer. Slides were hybridized overnight at 60°C in a wet box. Following hybridization, slides were washed with 5 x SSC 5 min and 2 x SSC 60 min at 60°C, followed by washing in 0.2 x SSC for 5 min at room temperature.

Visualization of DIG-labeled probes was carried out with alkaline phosphatase-conjugated anti-DIG antibodies (Boehringer Mannheim), NBT and BCIP. The method for visualization was performed according to the manufacturer's specification (Boehringer Mannheim). NBT yields a blue product. In control experiments, sections were hybridized with sense probes. No specific signals were detected in these preparations.

#### 2.2.6.3 Data analysis

The optical density of hybridization signals was captured and quantified by digital image analysis (MetaView 4.5r5). Neuronal signal intensities in CA1, CA3 and DG subfields were compared between pilocarpine treated and normal rats (n=3 each). Statistical significance was determined with a two-tailed Student’s t-test with the level of significance set to $p<0.05$.

# 3 Results

Rats subjected to pilocarpine induced status epilepticus (SE) develop recurrent epileptic seizures after a latency period of approximately 15 days (Cavalheiro EA et al., 1996). Histopathologically, the hippocampi of pilocarpine treated rats exhibit a lesion pattern resembling human Ammon's horn sclerosis (AHS), i.e. neuronal degeneration in CA1 and CA3/4 whereas the CA2 and DG areas appear more resistant to excitotoxic damage. In addition, substantial astrogliosis can be observed in areas with prominent neuronal cell loss. A variety of neurotransmitter receptors and ion channel subunits exhibit alterations in distribution and expression in TLE hippocampi. In order to gain a comprehensive view on expression alterations of voltage-gated ion channel subunits in the development of chronic TLE, we have used oligonucleotide microarrays that allow parallel expression monitoring of numerous genes (Barlow C et al., 2002; Becker AJ, et al., 2003).

## 3.1 Array analysis of ion channel expression patterns in hippocampal CA1 sub-region of rats following pilocarpine induced status epilepticus

Expression profiles were determined by Affymetrix rat U34A microarrays with RNA from CA1 subregions at the acute stage day 3 after SE (n=3 each), within the latency period at day 14 after SE (n=3) and at the chronic stage after day 20 following SE in rats. The rats in the chronic stage with spontaneous seizure activity were further grouped according to low (<2 seizures/day) or high (≥10 seizures/day; n=3 each) seizure activity (Becker AJ et al., 2003). Among the 8799 genes on rat U34A microarray, 48 voltage-gated ion channels are represented. Those include 41 pore forming- and 7 accessory subunit genes. 13 genes are represented by more than one target sequence on the array. Table 3.1 summarizes mRNA expression profiles of the voltage-gated ion channels.

**Table 3.1** mRNA expressions of voltage-gated ion channels in hippocampal CA1 areas at different stages of the pilocarpine TLE model using Affymetrix U34A microarrays (red: genes expressed > 2-fold compared to controls; green: genes expressed <0.5 compared to controls; A: absent expression).

| | | CA1 | | | |
|---|---|---|---|---|---|
| Ion channel | GenBank accession number | Day03 | Day14 | Chronic stage (high freq.) | Chronic stage (low freq.) |
| $Na_V1.1$ | M22253 | 0,67 | 3,1 | 4,2 | 5,8 |
| $Na_V1.2$ | M22254 | 0,67 | 0,91 | 1,2 | 1,9 |
| $Na_V1.3$ | Y00766 | 0,83 | 0,63 | 0,63 | 0,91 |
| $Na_V1.4$ | M26643 | A | A | A | A |
| $Na_V1.6$ | M27223 | A | A | 2,3 | 1,5 |
| $Na_V1.6$ | L39018 | A | 0,77 | 0,67 | 0,91 |
| $Na_V1.7$ | U79568 | A | A | A | A |
| $Na_V1.7$ | AF000368 | A | A | A | -1 |
| Nax | S75991 | A | 0,83 | 0,63 | 0,91 |
| $\beta_1$ | M91808 | 0,53 | 0,67 | 0,83 | 0,59 |
| $Ca_V1.2$ | U31815 | A | A | A | A |
| $Ca_V2.1$ | AF051526 | A | A | 2 | A |
| $Ca_V2.1$ | AF051527 | A | A | 8,2 | A |
| $Ca_V2.1$ | M99222 | A | A | A | A |
| $Ca_V2.2$ | AF055477 | 0,71 | 0,77 | 0,91 | 1,4 |
| $Ca_V3.1$ | AF027984 | 1,1 | 0,83 | 0,91 | 1 |
| $\alpha_2\delta$ | M86621 | 0,56 | 0,67 | 0,91 | 1,4 |
| $\beta_2$ | M80545 | 1 | 1,5 | 2,5 | 2,2 |
| $\beta_3$ | M88751 | 0,63 | 0,45 | 0,45 | 0,77 |
| gamma | Y09453 | 1,1 | 1,5 | A | A |
| VDAC1 | AF048828 | 0,77 | 1,4 | 1,2 | 1,7 |
| VDAC1 | AF048828 | 1,1 | 3,4 | 2,9 | 4,9 |
| CLC-1 | D13985 | 1,2 | 2 | 1,5 | 2,2 |
| CLC-1 | D13985 | 1,0 | 1,4 | 1,3 | 1,8 |
| CLC-2 | AF005720 | 0,27 | -1,8 | -1,7 | 0,43 |
| Clcn4-2 | Z36944 | A | 1,5 | 1,5 | 1,8 |
| CLC-5 | Z56277 | 2,8 | 1,9 | A | 1,5 |

| | | CA1 | | | |
|---|---|---|---|---|---|
| Ion channel | GenBank accession number | Day03 | Day14 | Chronic stage (high freq.) | Chronic stage (low freq.) |
| $K_V1.1$ | M26161 | 1,1 | 0,56 | 0,71 | 1,3 |
| $K_V1.1$ | X12589 | 1,1 | 0,91 | 1,1 | 1,7 |
| $K_V1.2$ | J04731 | A | 1,9 | A | A |
| $K_V1.4$ | M32867 | 1,2 | 1,3 | 2,1 | 3,7 |
| $K_V1.4$ | X16002 | A | -1,5 | A | A |
| $K_V2.1$ | X16476 | 0,32 | 0,42 | 0,77 | 0,77 |
| $K_V3.1$ | X62840 | 0,32 | 0,83 | 0,83 | 1,2 |
| $K_V3.2$ | X62839 | 0,63 | 0,91 | 1,2 | 1,9 |
| $K_V3.2b$ | M59211 | 2,4 | A | 4,1 | 2,7 |
| $K_V3.2c$ | M59313 | A | A | A | A |
| $K_V3.4$ | X62841 | A | 1,7 | 1,4 | 3,5 |
| $K_V4.2$ | S64320 | 0,63 | 0,33 | 0,45 | 0,53 |
| $K_V4.2$ | M59980 | 0,56 | 0,29 | 0,67 | 0,37 |
| $K_V5.1$ | Z34264 | 0,71 | 1,2 | 2,1 | 2,9 |
| $K_V6.1$ | M81784 | A | 1,6 | 1,6 | A |
| $K_V8.1$ | X98564 | A | 0,67 | 1 | 1,4 |
| $K_V9.3$ | Y17607 | A | 1,2 | 1,7 | 2,4 |
| KCNQ2 | AF087453 | 1 | A | A | 0,77 |
| KCNQ3 | AF091247 | 0,71 | 0,77 | 0,83 | 1,1 |
| SK1 | AF000973 | A | 4,9 | A | A |
| SK2 | U69882 | A | 4,7 | 4,1 | 4,6 |
| slo1 | AF083341 | A | 0,42 | A | A |
| Kir2.3 | X87635 | A | A | A | A |
| Kir2.4 | AJ003065 | A | 2,8 | 2,6 | A |
| Kir3.1 | U09243 | A | A | A | 3,5 |
| Kir3.1 | U72410 | A | A | A | 0,83 |
| Kir3.4 | L35771 | 1,2 | 2,1 | 1,4 | 2,1 |
| Kir5.1 | X83581 | A | 1 | 0,91 | 1,5 |
| Kir6.2 | D86039 | A | A | 5,3 | A |
| Kir6.2 | D86039 | A | 0,77 | 1,8 | 1,5 |
| ERG | U75210 | A | 0,63 | 0,63 | 0,2 |
| TWIK | AF022819 | 1 | 1,1 | 1,3 | 4,2 |
| $\beta_1$ | X70662 | A | A | 5,7 | 2,7 |
| $\beta_1$ | AF020712 | 0,83 | A | 0,71 | 1,2 |

Within these voltage-gated pore forming and accessory ion channel transcripts, 10 sequences target $Na^+$ channels, 34 sequences represent $K^+$ channels, 8 $Ca^{2+}$ channel subunits are found as well as 1 anion- and 4 $Cl^-$ channels. 29 sequences were found to be differentially expressed in pilocarpine treated versus control animals ($\geq$ 2-fold expression change).

With respect to the $Na^+$ channels, only $Na_V1.1$ showed a strong up-regulation at day 14 and chronic stages. $Na_V1.6$ was found to be induced at the chronic stage. $Na_V1.4$ and $Na_V1.7$ were not expressed in the brain.

For $K^+$ channels a variety of expression alterations were observed. Distinct A-type $K^+$ channels, $K_V1.4$ and $K_V3.4$ were induced in expression, particularly in the chronic stage, whereas $K_V4.2$ expression was reduced. Also $K_V3.2b$ and $K_V5.1$ revealed increased mRNA levels at different TLE stages. Both of the M-channel genes (KCNQ2 and KCNQ3) did not show significant expression changes on the arrays.

With respect to $Ca^{2+}$ channels, differential expression could be observed for distinct pore forming as well as accessory subunits including $Ca_V2.1$, $\beta_2$ and $\beta_3$. However, distinct recently cloned members of the voltage-gated calcium channel family were not represented on the array. In addition, substantial sequence homologies existed particularly between the pore forming subunits that rendered the subunit specificity of sequences on the array rather problematic.

Gene expression profiling allowed an overview on expression alterations in experimental TLE. The data shown above revealed expression alterations in several voltage-gated ion channel subfamilies. It had to be taken into account that mRNA isolates from microdissected hippocampal subfields after pilocarpine treatment compared to control specimen contained net effects of different cell types. In consequence, differences in cellular composition may contribute to expression differences. Therefore, in order to study differential gene expression patterns of entire families of voltage-gated ion channels in detail with cellular resolution level,

highly dynamic molecular biological techniques that allow strong amplification of mRNAs such as real-time RT-PCR have to be applied.

## 3.2 Identification of reference genes for relative quantification by real-time RT-PCR in epileptic hippocampal CA1 neurons

In order to apply a relative quantification protocol for real-time RT-PCR, it was necessary to initially identify appropriate reference genes lacking mRNA expression changes in epileptic animals. The absolute mRNA expression levels of five putative reference genes GAPDH (glyceraldehyde-3-phosphate dehydrogenase), β-actin, cyclophilin A, HPRT (hypoxanthine phosphoribosyltransferase), β-2-microglobulin and the neuron-specific gene synaptophysin were compared between SE experienced and control animals.

### 3.2.1. Establishment of standard DNA fragments and dilutions for the potential reference genes

First, standard PCR products of all six genes were amplified using conventional RT-PCR. The forward and reverse primers were identical to those used in the TaqMan real-time RT-PCR (Table 2.3). The amplicons were purified by standard phenol-chloroform procedure and appropriate sizes were successfully assessed by 3% agrose gel electrophoresis (Fig 3.2).

The OD values of the different PCR products were determined by a UV-spectrophotometer at 260 nm. The concentrations (DNA copy number/µl) were calculated according to the equations described in table 3.2.

Based on these calculations, standard PCR products were serially (10-fold steps) diluted in a range from 1.000.000 to 1.000 PCR product copies respectively for the later standard curves.

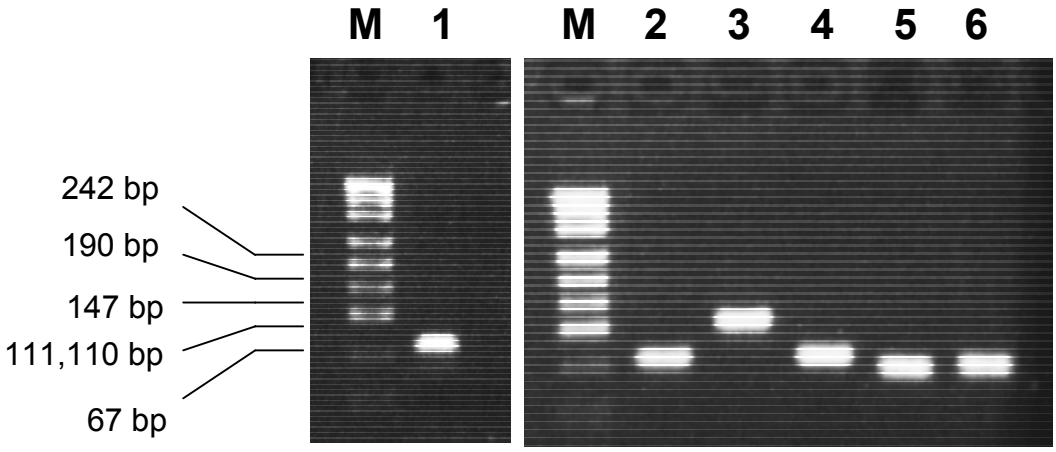


**Fig 3.2 Electrophoresis of PCR products derived from the following six potential reference genes in a 3% agrose gel.** lane M: pUC19 DNA / MspI marker; lane 1: GAPDH; lane 2: Synaptophysin; lane 3: β-actin; lane 4: HPRT lane 5: cyclophilin A; lane 6: β-2-microglobulin.

**Table 3.2** Results and calculation of six reference genes' copy numbers for standard fragments in real-time absolute quantification RT-PCR.

| Gene | amplicon size (bp) | OD value (260nm) | concentration (μg/μl) [a] | copy number per μl [b] |
|---|---|---|---|---|
| GAPDH | 72 | 0.355 | 0.355 | $4.501 \times 10^{12}$ |
| Synaptophysin | 74 | 0.048 | 0.096 | $1.1837 \times 10^{12}$ |
| β-actin | 118 | 0.126 | 0.252 | $1.9486 \times 10^{12}$ |
| Cyclophilin | 66 | 0.136 | 0.272 | $3.7603 \times 10^{12}$ |
| HPRT | 76 | 0.147 | 0.294 | $3.5296 \times 10^{12}$ |
| β-2-microglobulin | 71 | 0.145 | 0.290 | $3.7286 \times 10^{12}$ |

a **concentration (μg/μl) = OD value X 50 X dilution folder / 1000** dilution folder of GAPDH was 20 and others were 40.

b **Copy Number (per μl) =** $\dfrac{\text{Concentration (μg/μl) X } 6.022 \times 10^{23}}{\text{660 X base pair number X 10 X } 10^{6}}$

### 3.2.2. Expression of reference genes analyzed by real-time absolute quantification RT-PCR in status epilepticus experienced and control neurons

Exact 45 CA1 neurons from each animal were harvested for real-time RT-PCR mRNA determination of the six reference genes using an absolute quantification protocol (n=5 in SE experienced and control groups). The copy numbers in mRNA samples from individual SE experienced (filled circles) and control rat neurons (empty squares) were determined by comparison to the standard curve (Fig. 3.3 A, B, filled squares). This analysis revealed a significant expression increase of GAPDH in SE experienced vs. control animals (1.77 fold; *t-test* $p<0.005$). Expression differences of β-actin (1.28 fold), cyclophilin (1.16 fold), and HPRT (1.14 fold) between SE experienced and controls did not reach statistical significance. Expression of β-2-microglobulin was below the detection threshold by real-time RT-PCR in CA1 neurons. Quantitatively, the difference in synaptophysin expression was smallest amongst the reference genes tested (1.01 fold) (Fig. 3.3 C).

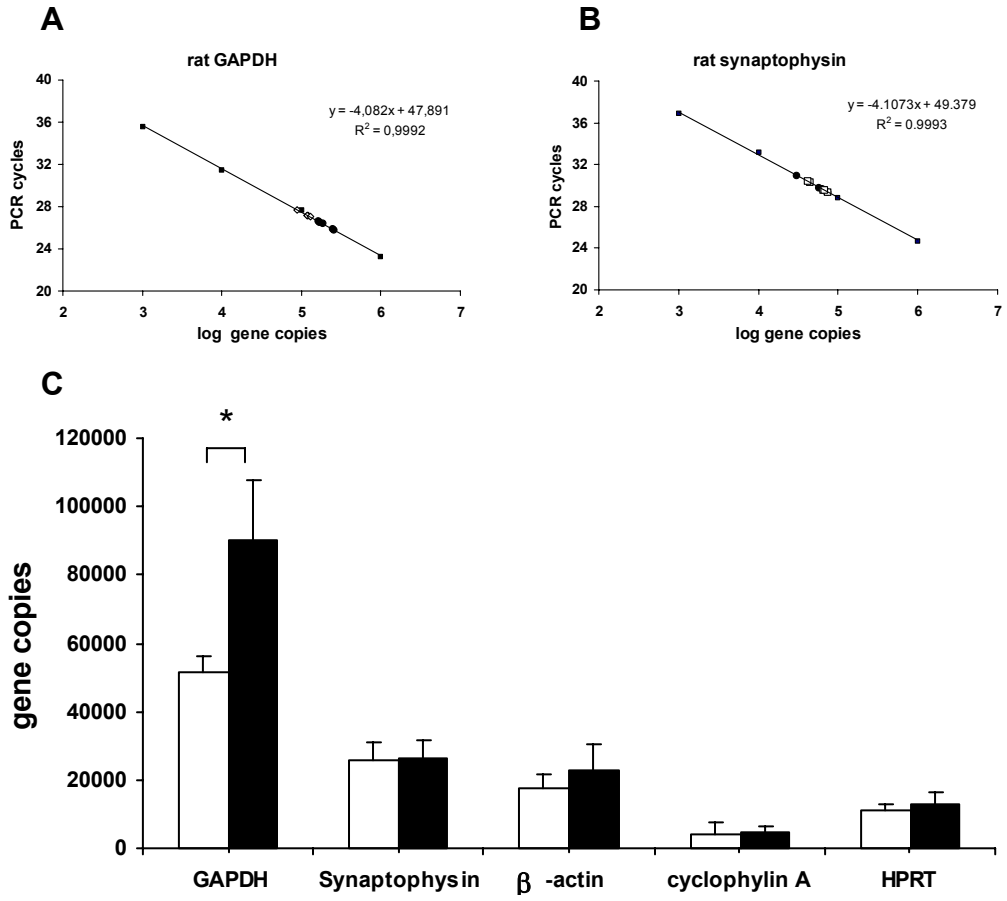


**Fig 4.3 Absolute real-time RT-PCR quantification of common reference genes.** GAPDH, synaptophysin, β-actin, cyclophilin A and HPRT mRNA expression levels were analyzed in individual CA1 pyramidal neurons from SE experienced rats versus controls. **A:** Representative standard curve for GAPDH absolute mRNA quantification. Control (open square) and SE experienced animals (closed circles) exhibit two expression clusters indicating different mRNA expression levels. **B:** Synaptophysin expression is not significantly altered between control (open square) and SE experienced animals (closed circles). Standards are given as closed squares. **C:** Quantification of the five reference genes in control vs SE experienced groups (white: controls, black: SE experienced). The strongest and significant differential expression was observed for GAPDH.

### 3.2.3. Determination of synaptophysin mRNA expression in CA1 neurons at acute and chronic stages after pilocarpine induced status epilepticus

Real-time absolute quantification RT-PCR did not reveal significant differences in mRNA expression of synaptophysin in CA1 neurons of control and chronic epileptic rats ≥30 days after pilocarpine induced SE. In order to assess potential expression alterations for two putative reference genes during epileptogenesis, relative gene expression was determined for synaptophysin and HPRT at days 1, 3, 5, 10 and 30 after pilocarpine induced SE. No significant differences in mRNA expression for synaptophysin and HPRT were observed in this time course experiment ($\Delta C_t$ = 1.72 ± 0.06, n=5, Fig 3.4).

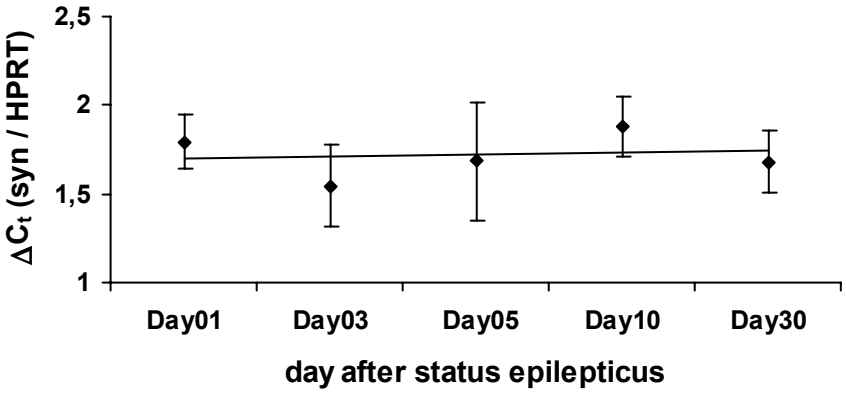


**Fig 3.4: Real-time RT-PCR analysis.** mRNA of Synaptophysin and HPRT were determined at different stages in hippocampal CA1 pyramidal neurons from SE experienced rats. No significant alterations in mRNA expression were observed between the two genes.

### 3.2.4. Analysis of hippocampal GAPDH and synaptophysin mRNA expression in rats after pilocarpine induced status epilepticus by *in situ* hybridization

In order to confirm mRNA expression data of GAPDH and synaptophysin in hippocampal CA1 neurons of SE experienced rats determined by real-time RT-PCR, *in situ* hybridization analyses were carried out for both genes using digoxigenin (DIG)-labeled in vitro transcription products (cRNA). Hybridizations were performed according to standard procedures as described in detail before (Hans VH et al., 1999). The optical densities of the hybridization signals were determined by digital image analysis (n = 10 neurons / subregion, 3 animals per group, MetaView 4.5r5). *In situ* hybridization revealed significantly increased GAPDH expression in SE experienced (day 30 after SE) versus control rats in hippocampal CA1, CA3 and DG areas (CA1: 2.2 fold; *t-test* $p<0.01$, CA3: 1.6 fold; *t-test* $p<0.04$, DG: 2.1 fold; *t-test* $p<0.04$) (Fig. 3.5 a, b, A). In contrast, no significant differences in hippocampal mRNA expression were observed for synaptophysin (Fig. 3.5 c, d, B). For control purposes, adjacent hippcampal sections were hybridized to sense oligonucleotides. No specific signals were detected (data not shown).

*In situ* hybridization as well as real-time RT-PCR absolute quantification data reveal substantial mRNA expression differences in hippocampi of rats subjected to pilocarpine induced SE. Due to these expression alterations, GAPDH appears not as appropriate reference gene for real-time RT-PCR in epileptic CA1 neurons using a relative quantification protocol. Our results also suggest synaptophysin not to exhibit significant mRNA expression differences in CA1 neurons of the pilocarpine TLE model at the stages under study. Therefore, in the subsequent real-time RT-PCR experiments in order to determine expression levels of certain ion channel subunits under epileptic conditions, synaptophysin was used as reference gene.

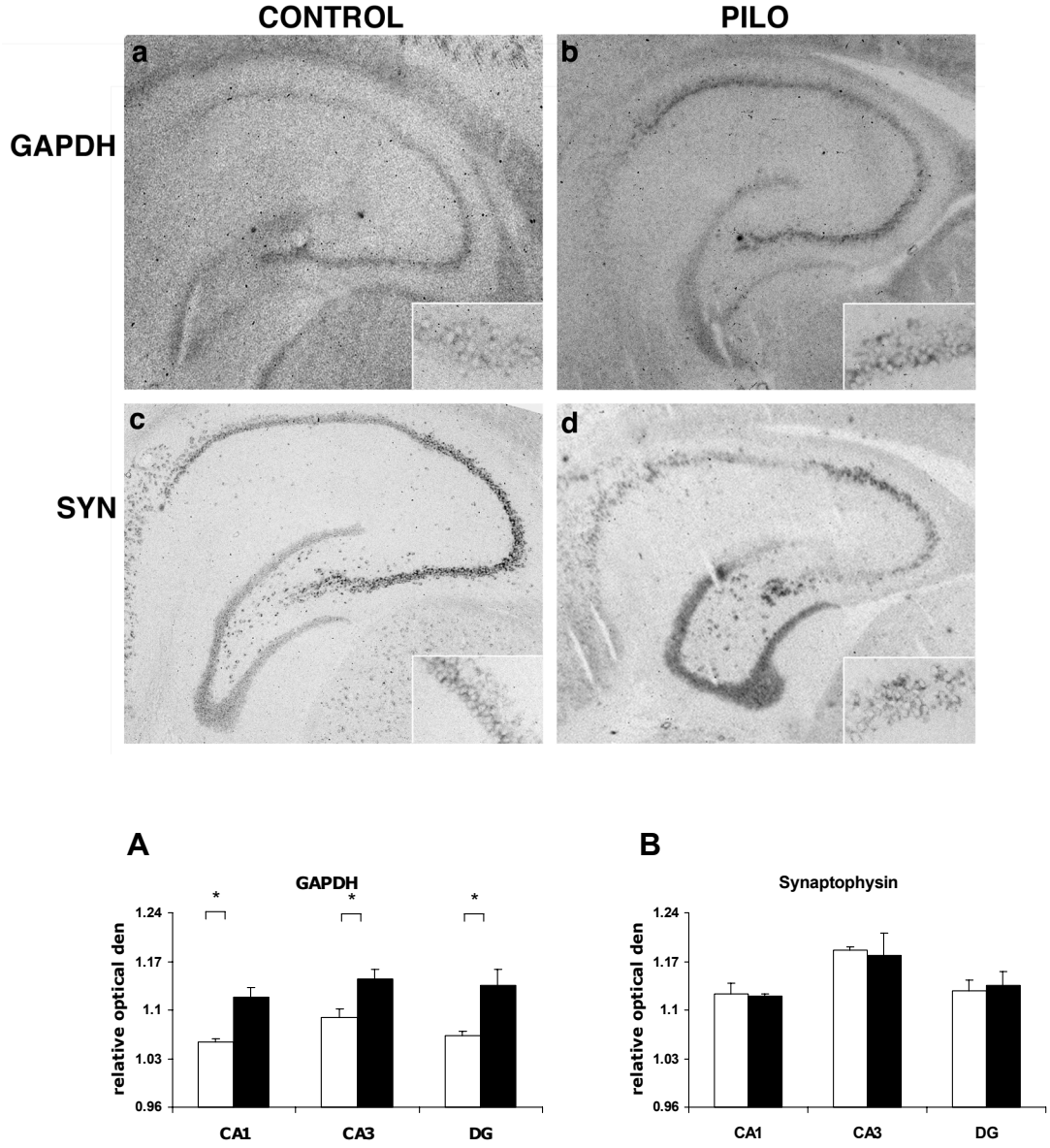


**Fig.3.5** ***In situ*** **hybridization analysis of GAPDH and synaptophysin mRNA expression. a,b:** Control and SE experienced hippocampal sections were hybridized by GAPDH cRNA probes (x4; insert shows corresponding CA1 neurons x10), **c,d:** Control and SE experienced sections hybridized with synaptophysin cRNA probes (x4; insert shows corresponding CA1 neurons x10), **A:** Relative optical densities of synaptophysin between SE experienced rats and normal control were no significant difference. **B:** Relative optical densities of GAPDH of SE experienced rats were significantly higher than those of normal controls. (10 neurons were normalized by background in each region CA1, CA3 and DG, n=3 animals each; white: controls, black: SE experienced).

## 3.3 Expression analysis of voltage-gated calcium channels in CA1 neurons of rats after pilocarpine induced status epilepticus

### 3.3.1. Partial sequence analysis of rat $Ca_V3.2$

When we initiated the real-time RT-PCR experiments for voltage-gated $Ca^{2+}$ channels, sequence data on the rat $Ca_V3.2$ subunit in order to design primers and the bi-fluorescent oligonucleotide for real-time RT-PCR was not available in GenBank. Preliminary information on $Ca_V3.2$ sequence fragments was kindly provided by E. Perez-Reyes (University of Virginia, Charlottesville). Using a corresponding PCR primer pair, a 356bp-amplicon based on $Ca_V3.2$ cDNA from rat brain was amplified by RT-PCR and subsequently sequenced:

```
5′-AGGAGGCTCG  GCGCCGGGAG  GAGAAACGGC  TGCGGCGCCT  GGAGAGGAGG
   CGCAGGAAGG  CCCAGCGCCG  GCCCTACTAC  GCAGACTATT  CACACACTCG
   CCGCTCCATC  CATTCGCTGT  GCACCAGCCA  CTACCTGGAC  CTCTTCATCA
   CCTTCATCAT  CTGCCTCAAT  GTCATCACCA  TGTCCATGGA  GCACTACAAC
   CAGCCCAAGT  CCCTGGATGA  GGCCCTCAAG  TACTGCAACT  ACGTCTTTAC
   CATCGTCTTC  GTCTTTGAGG  CTGCACTGAA  GCTGGTGGCC  TTTGGGTTCC
   GGAGGTTCTT  CAAGGACAGG  TGGAACCAGC  TGGACTTGGC  CATCGTCCTC
   CTATCC-3′
```

This amplicon corresponds to the nucleotide sequence of AF290213 (from 4768 to 5123), which was later published in GenBank. Based on this sequence data, primers and the bifluorescent oligonucleotide for $Ca_V3.2$ real-time RT-PCR were designed by Primer Express Software.

### 3.3.2. Expression analysis of voltage-gated calcium channels in status epilepticus experienced CA1 neurons

mRNA expression levels of voltage-gated calcium channel subunits, i.e. $\alpha$- as well as accessory subunits were quantified by real-time RT-PCR using a relative quantification protocol with synaptophysin as reference gene (Fig. 3.6) in SE experienced rats at different time points after pilocarpine induced SE as well as in controls. Previous functional studies had shown a $Ca^{2+}$ dependent mechanism for burst discharges as well as an increase of T-type currents in SE experienced CA1 neurons (Su H et al., 2002).

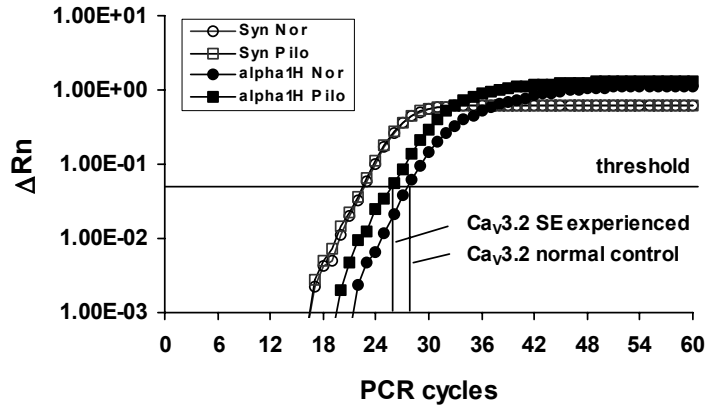


**Fig.3.6 Changes in $Ca_V3.2$ subunit expression. A:** Quantitative determination of $Ca^{2+}$ channel subunit mRNAs was carried out using the TaqMan real-time RT-PCR. The increase of fluorescence intensity per PCR cycle reflecting the specific amplification is shown in an exemplary fashion for the amplification of $Ca_V3.2$ and the reference synaptophysin mRNA in SE experienced and control animals. For data analysis the fluorescent signals are normalized to an internal, passive reference dye ($R_n$), yielding a normalized value $\Delta R_n$. Dashed lines indicate the threshold cycle ($C_t$) for $Ca_V3.2$. Note that synaptophysin expression is virtually identical in SE experienced and control animals, but mRNA levels for $Ca_V3.2$ are considerably augmented in SE experienced animals.

Considering these functional alterations in SE experienced CA1 neurons, we have tested the hypothesis that a selective transcriptional up-regulation of $Ca^{2+}$ channel subunit(s) underlies the observed T-type $Ca^{2+}$ channel increase by analyzing expression changes in $Ca^{2+}$ channel subunits ($Ca_v1.2$, $Ca_v1.3$, $Ca_v2.1$ - $Ca_v2.3$, $Ca_v3.1$ - $Ca_v3.3$, $\beta_1$, $\beta_2$, $\beta_3$, $\alpha_2\delta$) in CA1 neurons at different stages after pilocarpine induced SE. mRNA was isolated from CA1 neurons microdissected from acute hippocampal slices as well as laser captured CA1 neurons. The most striking finding was a significant increase in $Ca_v3.2$, but not other T-type $Ca^{2+}$ channel $\alpha_1$ subunit mRNAs at day 3 after SE. These data support the notion that transcriptional up-regulation of $Ca_v3.2$ subunits contributes to the appearance of low-threshold bursting in CA1 pyramidal cells. Other $Ca^{2+}$ channel subunits, notably the accessory subunit mRNAs $\beta_1$, $\beta_3$, $\alpha_2\delta$ and the L-type subunit $Ca_v1.2$ also revealed a significant up-regulation with a similar temporal pattern after SE, while other high-threshold $Ca^{2+}$ channel mRNAs did not exhibit significant changes, or down-regulation (Figs. 3.7-3.9).

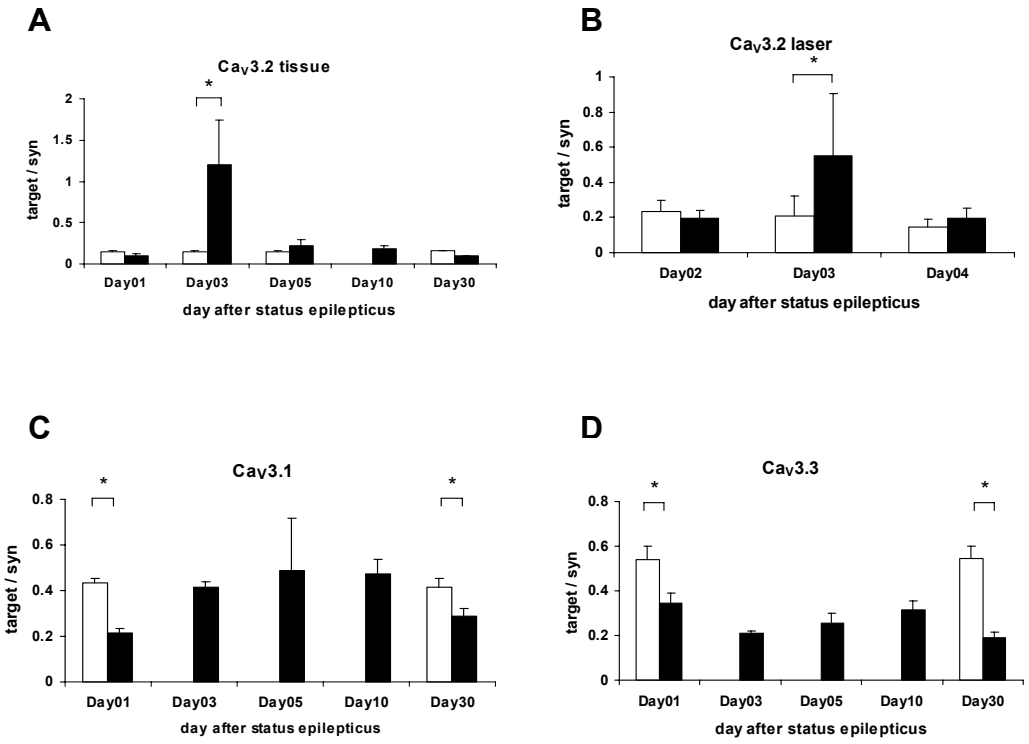


**Fig.3.7 Changes in low voltage activated T-type $Ca^{2+}$ channel subunit expression.** **A:** The mRNA levels for $Ca_V3.2$ in SE experienced and control animals were determined 1-30 days following SE (see materials and methods). A striking increase of $Ca_V3.2$ mRNA levels was observed at day 3 after SE (8.16-fold increase, $p<0.05$, asterisk) from microdissected CA1 region. **B:** The increase of $Ca_V3.2$ mRNA expression level at day 3 was confirmed in laser microdissected CA1 pyramidal neurons (2.64-fold increase, $p<0.04$). **C:** $Ca_V3.1$ mRNAs were only reduced in expression at day 1 and day 30 (50.5% $p<0.0005$ and 67.9% $p<0.005$). **D:** $Ca_V3.3$ mRNAs were persistently reduced after SE (47.8% $p<1E-07$; white: controls, black: SE experienced).

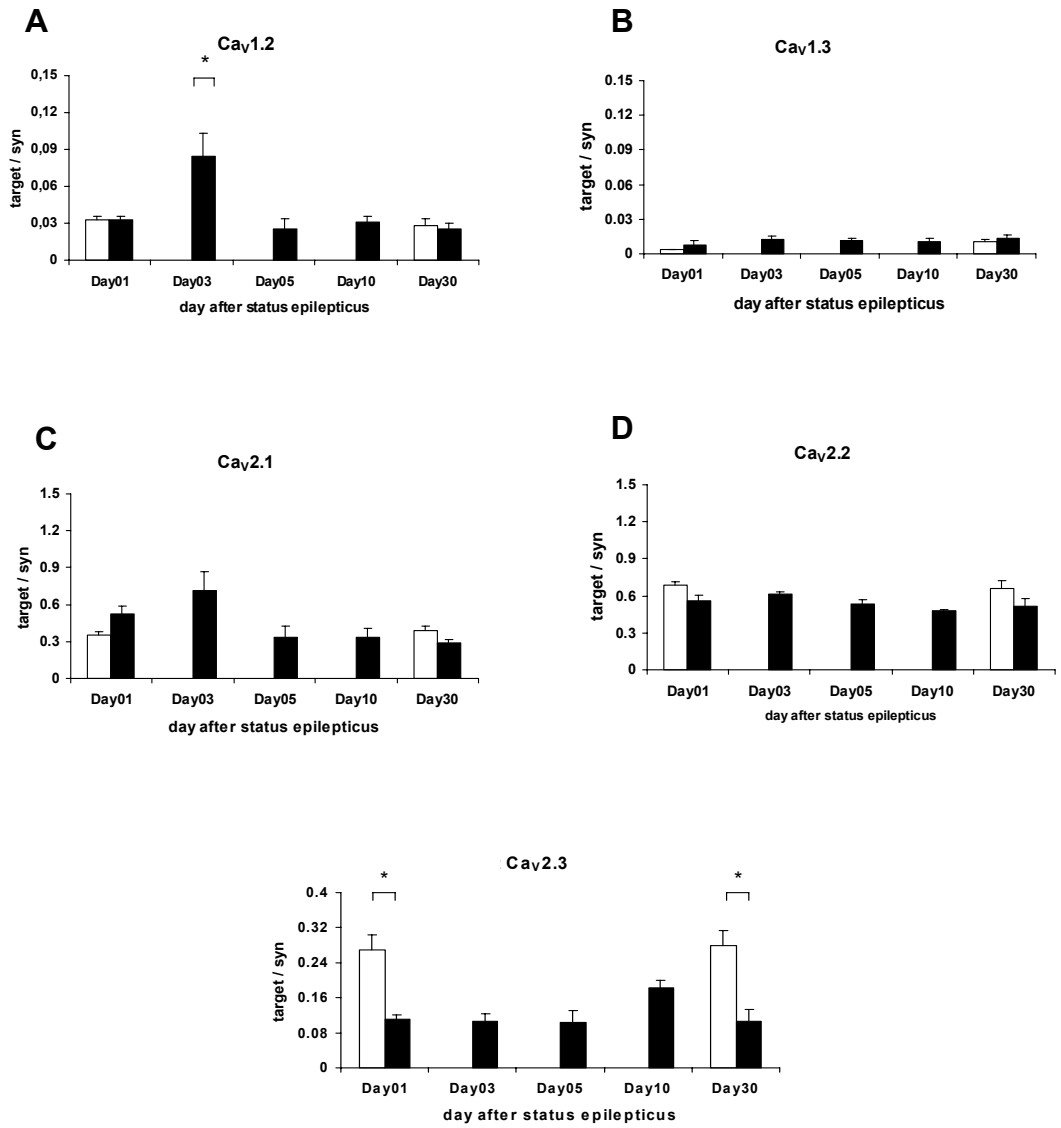


**Fig 3.8 Changes in high voltage activated $Ca^{2+}$ channel subunits expression.** Analysis of the mRNA levels of the high voltage activated $Ca^{2+}$ channel $\alpha_1$ subunit using real-time relative quantification RT-PCR 1-30 days following SE. **A:** $Ca_V1.2$ mRNAs were increased (2.78-fold, $p<0.03$) at day 3, showing a similar expression patten as $Ca_V3.2$. **B:** $Ca_V1.3$ mRNA levels were unchanged. **C:** $Ca_V2.1$ mRNA levels were only transiently increased (1.41-fold, $p<0.02$) at day 1. **D:** $Ca_V2.2$ mRNA levels were decreased after day 5 ($Ca_V2.2$, 74.8%). **E:** mRNA expression levels for $Ca_V2.3$ were persistently reduced in SE experienced rat models (44.7% $p<1E-06$; white: controls, black: SE experienced).

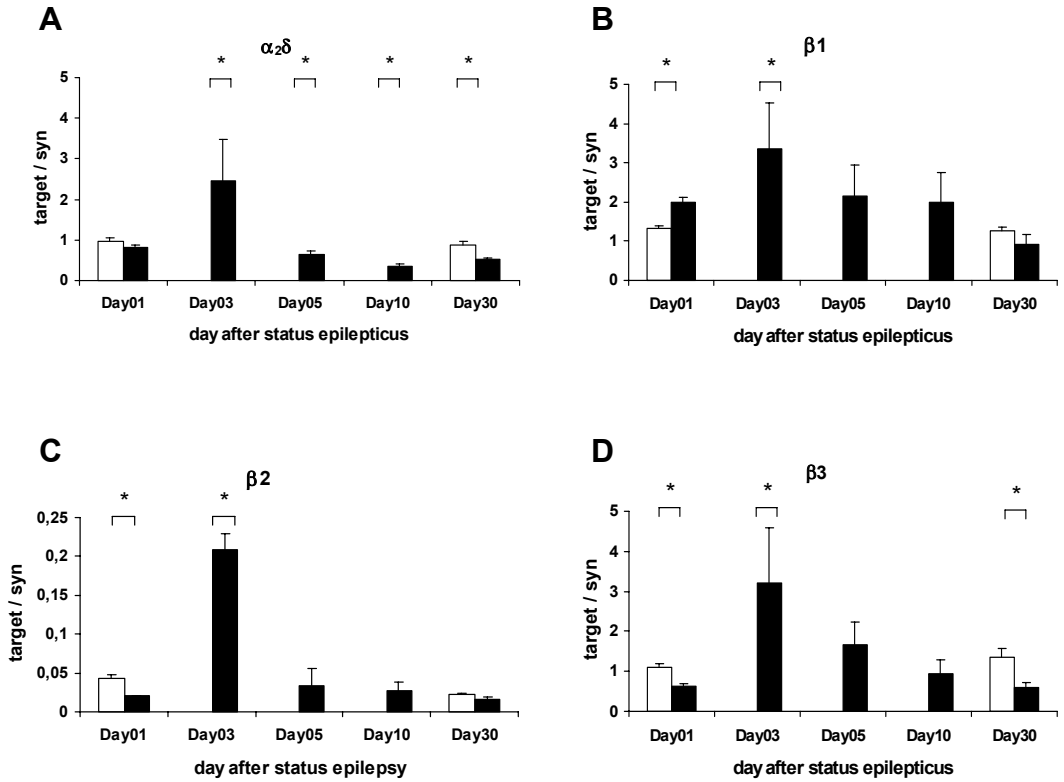


**Fig 3.9: Changes in accessory $Ca^{2+}$ channel subunit expression.** Analysis of the mRNA levels of the accessory $Ca^{2+}$ channel subunits using real-time RT-PCR 1-30 days following SE. All subunits exhibit similar showed the same expression patterns as $Ca_V3.2$, transiently increased at day 3 in SE experienced rat models. Except that $\beta_3$ did not show a significant increase, for the remaining accessory subunits, a transient increase in mRNA expression levels at day 3 were observed ($\alpha_2\delta$ 2,67-fold, $p<0.05$; $\beta_1$ 2,60-fold, $p<0.03$; $\beta_2$ 6.45-fold, $p<0.0001$), with subsequently decreased ($\alpha_2\delta$ and $\beta_3$) or unchanged ($\beta_1$ and $\beta_2$) mRNA (white: controls, black: SE experienced).

## 3.4 Expression analysis of voltage-gated sodium channels in CA1 neurons of rats after pilocarpine induced status epilepticus

It had been recently shown that voltage-gated $Na^+$ channels are subjected to molecular and functional alterations in DG after pilocarpine induced SE (Ellerkmann RK et al., 2003). In order to address whether expression alterations can be also found in CA1 neurons after pilocarpine induced SE, the mRNA expression levels of all CNS expressed voltage-gated $Na^+$ channel $\alpha$ subunits ($Na_V1.1$, $Na_V1.2$, $Na_V1.3$, $Na_V1.5$ and $Na_V1.6$), as well as accessory subunits ($\beta_1$ and $\beta_2$) were quantified by real-time relative quantification RT-PCR in SE experienced vs. control rats (n=3 at day 1 and n=4 at day 10 in SE experienced group, n=5 in SE experienced animals at other stages and control groups, Fig 3.10). One of the most prominent expression alterations found was the sustained lower expression of $Na_V1.2$ and $Na_V1.6$ subunits after pilocarpine induced SE. Reduced expression of $Na_V1.2$ and $Na_V1.6$ was also described in DG following pilocarpine induced status epilepticus (Ellerkmann RK et al. 2003). Further expression alterations were $Na_V1.5$ induction at days 1 and 30 after SE as well as reduced expression of $Na_V1.1$ at day 1 after SE and $Na_V1.3$ at day 30 after SE.

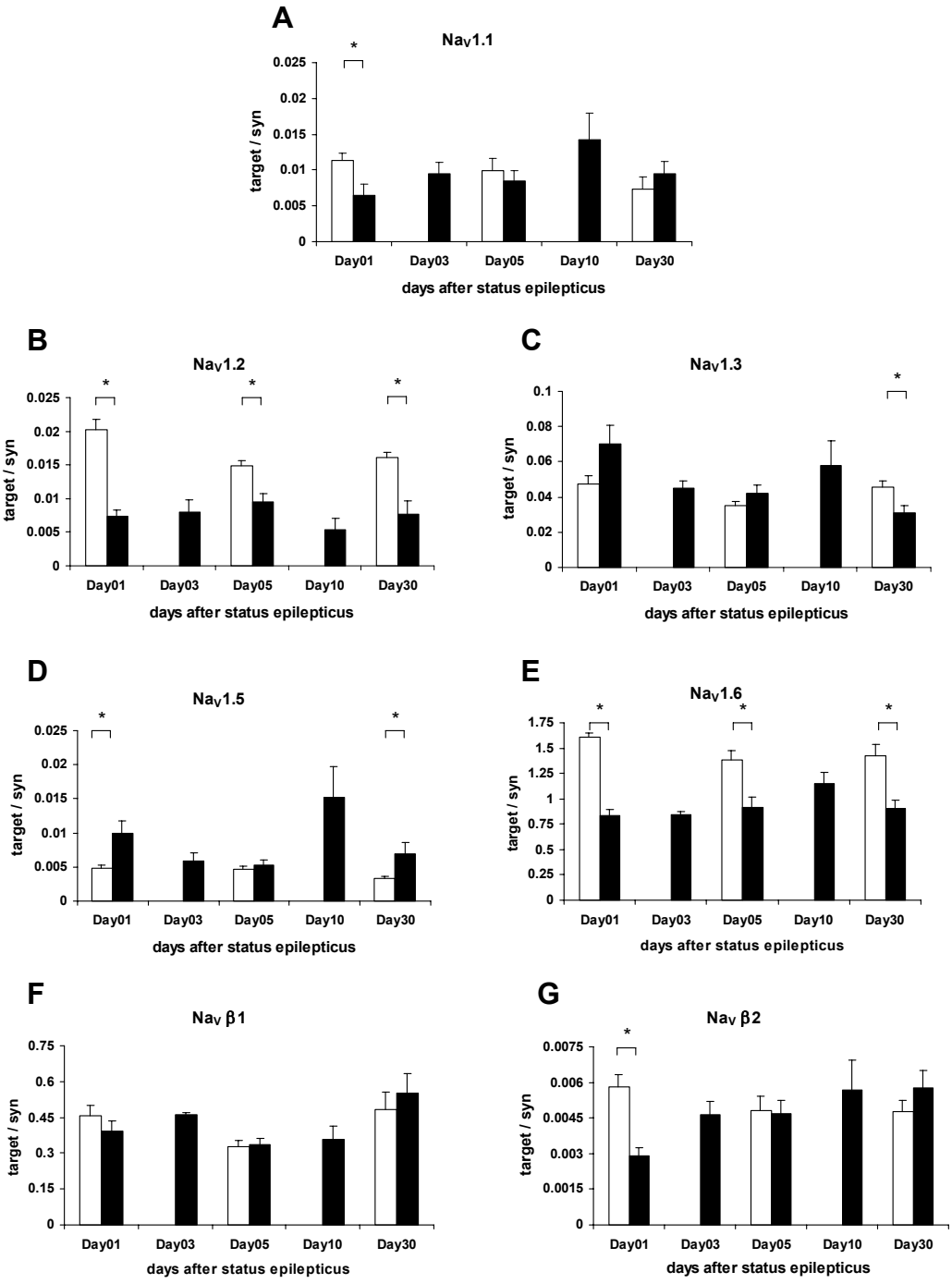


**Fig 3.10: Changes in voltage-gated $Na^+$ channel subunit expression.** Expression analysis of the voltage-gated $Na^+$ channel $\alpha_1$ subunit by real-time relative quantification RT-PCR 1-30 days following SE. **A:** $Na_V1.1$mRNA decreased at day 1 after SE (56.8%, p<0.05), **B:** $Na_V1.2$ mRNA were persistently reduced after SE (46.2%, p< 3E-9), **C:** $Na_V1.3$ wasonly reduced at day 30 (67.8%, p<0.03), **D:** $Na_V1.5$ was up-regulated at day 1 and day 30 after SE (2.05 fold, p<0.03 and 3.31 fold, p<0.02), **E:** mRNA of $Na_V1.6$ was persistently reduced after SE (63.6%, p<2E-9), **F:** $Na_V\beta_1$ remained unchanged, **G:** $Na_V\beta_2$ was only reduced at day 1 (50.3%, p<0.01; white: controls, black: SE experienced).

## 3.5 Expression analysis of KCNQ channels in CA1 neurons after pilocarpine induced status epilepticus.

In addition to analyzing expression of genes that relate to depolarizing inward currents, we have determined the transcript patterns of genes that underlie repolarizing outward currents including potassium channel subunits. mRNA abundance of the KCNQ2, KCNQ3 and KCNQ5 subunits known to be expressed in CNS were determined by real-time relative quantification RT-PCR (Fig 3.11). The most prominent finding was a sustained decreased expression of KCNQ2 (58.4%, $p<0.001$, Fig 3.11 A) in SE experienced CA1 neurons. KCNQ3 was also down-regulated at days 1 and 30 after SE (Fig 3.11 B). The expression level of KCNQ5 was only slightly reduced at day 5 (Fig 3.11 C).

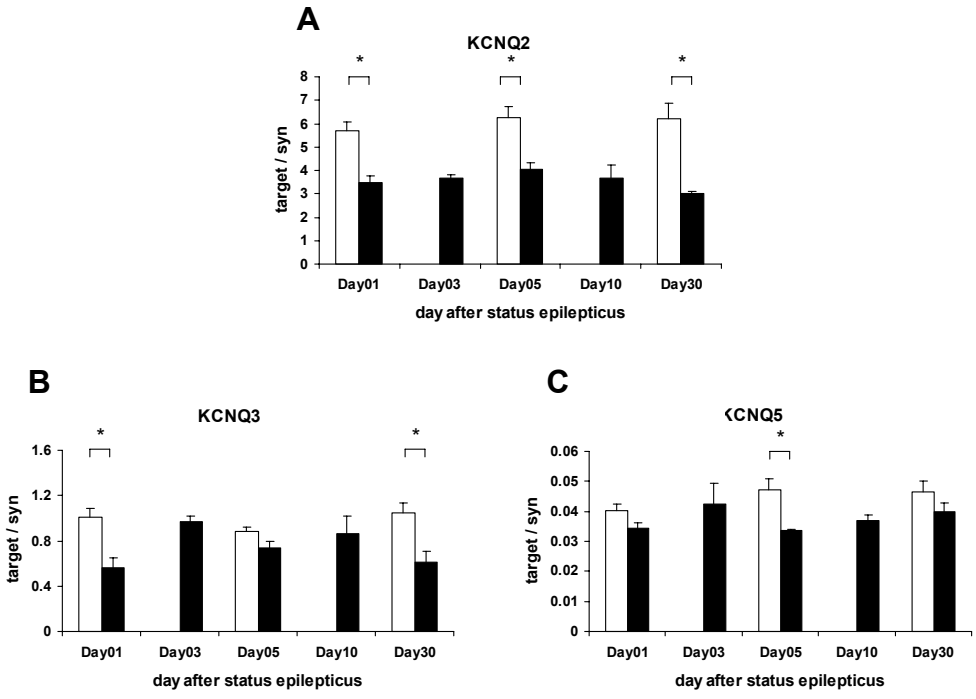


**Fig 3.11 Changes in voltage-gated M-channel subunit expression.** Analysis of the mRNA levels of the KCNQ subunits using real-time relative quantification RT-PCR 1-30 days following SE. **A:** mRNA of KCNQ2 was persistently reduced in SE experienced rat models (58.4%, $p<0.001$), **B:** KCNQ3 was reduced at day1 and day 30 (56.0%, $p<0.02$ and 58.4%, $p<0.02$ Fig 4.11 B), **C:** KCNQ5 was reduced at day 5. (71.3%, $p<0.03$; white: controls, black: SE experienced).

## 3.6 Expression analysis of A-type potassium channels in CA1 neurons after pilocarpine induced status epilepticus.

We have also analyzed the expression of genes that give raise to transient $K^+$ channels. These particular channels are subjected to rapid activation and inactivation after depolarization. Changes of mRNA expression levels of the A-type channel subunits ($K_V$1.4, $K_V$2.3, $K_V$3.3 and 3.4, as well as $K_V$4.2 and 4.3) in microdissected CA1 areas were determined at days 3 and 30 after SE induced by pilocarpine (n=5 animals per group). $K_V$2.3 was reduced in expression at day 3 after SE, while $K_V$1.4 and $K_V$4.2 were significantly lower at day 30 after SE compared to controls. No significant alterations in expression of other A-type $K^+$ channels ($K_V$3.3, $K_V$3.4 and $K_V$4.3) were found in epileptic CA1 neurons (Fig 3.12).

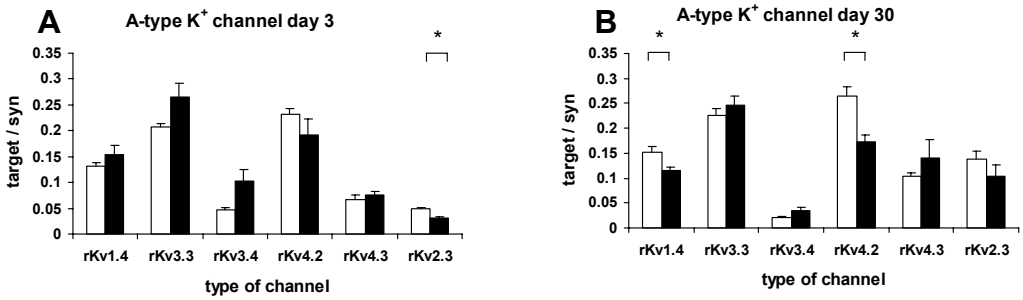


**Fig 3.12 Changes in A-type $K^+$ channel subunit expression in CA1 neurons.** Analysis of the mRNA levels of the A-type $K^+$ channel subunits using real-time relative quantification RT-PCR at day 3 and day 30 days following SE. **A:** $K_V$2.3 was reduced at day 3 after SE (64.5%, $p<0.004$). B: $K_V$1.4 and $K_V$4.2 were lower in expression at day 30 (75.6%, $p<0.03$ and 65.7%, $p<0.003$; white: controls, black: SE experienced).

## 3.7 Expression analysis of HCN channels in epileptic CA1 neurons

HCN subunits underlie H-currents ($I_H$) in native neurons. Different HCN channel subunits are expressed (HCN1-4) in the CNS. Expression alterations of the different HCN channels were analyzed by real-time relative quantification RT-PCR (n=3 at day 1, n=4 at day 10 after SE, n=5 in all other SE experienced/control groups, Fig 3.13). Significant and sustained reduced expression after day 3 was observed for HCN1 after SE, and HCN2 was reduced at days 1, 3 and 30. In contrast, the slow gating HCN3 and HCN4 subunits revealed a transient increase at day 1 after SE and subsequently returned to control levels. These data indicate distinct expression alterations of different HCN subunits in CA1 neurons following SE.

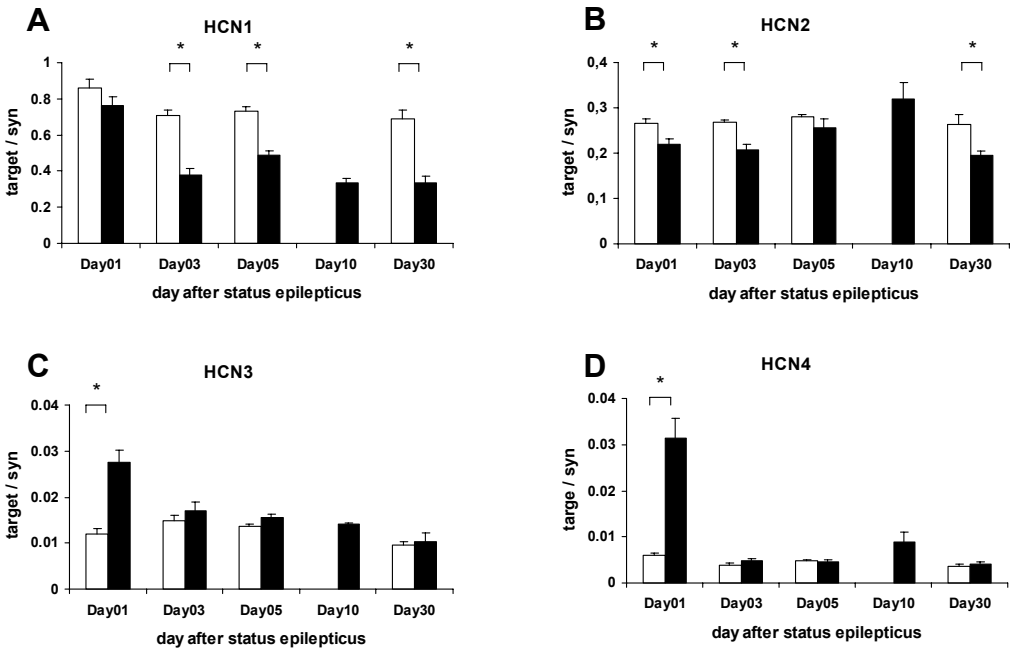


**Fig 3.13 Changes in H-channel subunit expression.** Analysis of the mRNA levels of the HCN subunits using real-time relative quantification RT-PCR 1-30 days following SE. **A:** mRNA of KCNQ1 was persistently reduced after day 3 in SE experienced rat models (54.3%, p<4.6E-12), **B:** HCN2 was reduced at days 1, 3 and 30 (82.1%, p<0.04, 77.9%, p<0.002 and 74.1%, p<0.02), **C,D:** HCN3 and HCN4 were transiently increased at day1 and then returned back to the control levels (2.3-fold, p<0.002 and 5.2-fold, p<0.001; white: controls, black: SE experienced).

# 4 Discussion

Pilocarpine induced status epilepticus has been shown to promote multiple long-term changes in neuronal networks similar to human TLE (McNamara JO. 1986, Blümcke I et al., 2002; Ben-Ari, Y. 2001). As briefly outlined in the introduction, multiple changes in synaptic communication between neurons have been described, both on the pre- and on the postsynaptic level. In contrast, fairly little is known about changes in the intrinsic membrane properties of neurons during epileptogenesis, even though these may be extremely important in determining neuronal input-output relation. Indeed, one seminal study has demonstrated that dramatic changes in the intrinsic discharge behavior of neurons occur in the pilocarpine model of epilepsy (Sanabria et al., 2001), consisting of a conversion of most CA1 neurons from a regular firing to a burst-firing mode. As stated in the introduction, the intrinsic discharge behavior is determined by the types of different voltage-gated ion channels in the neuronal membrane. Therefore, we set out to determine changes in the expression of different families of voltage-gated ion channels in chronic epilepsy. We have used different molecular biological techniques to examine coordinated changes in gene expression after seizures.

## 4.1 Expression profiling: comprehensive expression changes of voltage-gated ion channels and neurotransmitter receptors in epileptogenesis

So far, analyses of the molecular correlates of epilepsy-induced hippocampal plasticity have largely focused on individual candidate genes, with particular emphasis on genes with known functions for specific pathogenetic aspects (Coulter DA, 2001). DNA microarrays provide the opportunity to monitor gene expression in a comprehensive, genome-wide fashion (Bassett DE Jr, 1999). To this end, we have used high-density oligonucleotide microarray assays in the present experiments. Using this method, we found 29 genes amongst 61 voltage-gated ion channels that were differentially expressed after pilocarpine induced SE. In contrast to stress related genes, which were

differentially regulated in the early stage after SE, most of the significant changes in voltage-gated ion channel expression were found in the chronic epileptic stage. The changes observed were found in various families of ion channel subunits. In addition to voltage-gated ion channels, altered expression was found for several neurotransmitter receptor genes, most prominently an up-regulation of the $GABA_A$ receptor $\beta_1$ subunit, or an induction of D1A dopamine receptors (Becker AJ et al., 2003). Thus, the expression profiling results derived from oligonucleotide microarrays point to distinct changes in multiple ion channel- and neurotransmitter receptor subunits.

However, we had to note that a substantial number of expression changes detected in array experiments were not reflected in subsequent determinations of mRNA abundance with other techniques such as quantitative real-time RT-PCR. A major limitation of microarray assays is the relatively large amount of template RNA needed. And furthermore, the pilocarpine induced SE experienced rats, in contrast to controls, severe segmental neuronal cell loss and gliosis is found in the hippocampal CA1, CA3 and CA4 regions (Blümcke I et al., 1999b). The expression data from hippocampal tissue reflect altered composition of the tissue in addition to changes in gene expression on the cellular level (Becker AJ et al., 2002). Real-time RT-PCR provides a tool to accurately, specifically and sensitively profile gene expression in quantitative terms even on a single cell level (Chen J et al., 2001). These will be discussed in detail later. The present data underline the necessity to employ such techniques in order to complement and verify microarray analyses (Becker AJ et al, 2002).

## 4.2 Real-time RT-PCR analysis of voltage-gated ion channel expression

Based on functional studies, certain voltage-gated ion channels appear as particular interesting candidates to underlie functional alterations related to intrinsic neuronal plasticity in the course of epileptogenesis. These are T-type $Ca^{2+}$ currents (Sanabria ER et al., 2001; Su H et al., 2002), persistent $Na^{+}$ currents (Azouz R et al., 1996; Jensen MS et al., 1996; Su H et al., 2001), M-type $K^{+}$ currents (Jentsch TJ, 2000), A-type $K^{+}$ currents (Kang J et al., 2000; Kanold PO et al., 1999) and hyperpolarization activated cation currents (Magee JC. 1999a; 1999b; Beaumont V et al., 2000). The expression of these ion channels in epileptic CA1 neurons is therefore discussed below in correlation to functional alterations.

### 4.2.1 Molecular changes of voltage-gated $Ca^{2+}$ channels in TLE rats

*T- and R-type $Ca^{2+}$ channels*

Voltage-gated $Ca^{2+}$ channels are formed by one of a number of pore-forming subunits $Ca_V1$-3, as outlined in introduction (Ertel EA et al. 2000). The pore-forming subunits underlying T-type $Ca^{2+}$ currents are the $Ca_V3$ subunits, including $Ca_V3.1$, $Ca_V3.2$ and $Ca_V3.3$ (Perez-Reyes E, 2003). The currents generated by some T-type $Ca^{2+}$ channels ($Ca_V3.2$), as well as the R-type $Ca_V2.3$ $Ca^{2+}$ channels, are blocked by low concentrations of $Ni^{2+}$ (< 50 µM).

Using real-time RT-PCR, we found that the mRNA levels for the $Ca_V3.2$ subunit were transiently increased in CA1 neurons with a sharp peak on day 3 following SE, while other $Ni^{2+}$ sensitive T- or R-type subunits ($Ca_V3.1$, $Ca_V3.3$ or $Ca_V2.3$) were down-regulated or not significantly changed. This transient increase of $Ca_V3.2$ transcripts was observed both in microdissected CA1 tissue and in laser-microdissected CA1 pyramid

neurons. In addition, transient up-regulation of accessory subunits ($\beta_{1-3}$ and $\alpha_2\delta$) on day 3 after SE was observed.

Is this up-regulation reflected in changes on the functional level? In a partner study, the density of different $Ca^{2+}$ channel components was quantified in hippocampal CA1 neurons in the same animal model. Interestingly, the density of T-type $Ca^{2+}$ current considerably (2.2 to 3.3-fold) increased in CA1 pyramidal cells after status epilepticus, while the density of all other types of $Ca^{2+}$ current (including the R-type) was either unaltered or decreased (Su H et al., 2002). Furthermore, the augmented T-type $Ca^{2+}$ current in the seizure-experienced group was highly sensitive to $Ni^{2+}$, consistent with increased expression of $Ca_V3.2$ subunits. As both $Ca_V3.1$ and $Ca_V3.3$ subunits are much less sensitive to $Ni^{2+}$, it is improbable that these subunits contribute much to T-type currents in epileptic CA1 neurons. Thus, the analysis of our expression and electrophysiological data suggested that among the three low threshold T-type $Ca^{2+}$ channel pore forming $\alpha_1$ subunit ($Ca_V3.1$, $Ca_V3.2$ and $Ca_V3.3$), the up-regulation of $Ca_V3.2$ expression most probably underlies the augmented this subunit of T-type $Ca^{2+}$ channel and leads to T-type $Ca^{2+}$ current increase.

The same partner study (Su H et al., 2002) has also addressed the role of increased T-type currents in the increased intrinsic burst firing observed in the pilocarpine model. Pharmacological experiments demonstrated that aberrant intrinsic burst firing in pilocarpine-treated animals was suppressed by low concentrations of $Ni^{2+}$ (30-100 µM) that selectively block T-type and R-type $Ca^{2+}$ channels, but was not suppressed by other organic $Ca^{2+}$ channel blockers that affect L-, N-, P- and Q-type $Ca^{2+}$ channels (Sanabria ER et al., 2001; Su H et al., 2002). These data indicated that the pathological bursting relies on up-regulation of the T-type $Ca^{2+}$ channels mediated by $Ca_V3.2$ subunits.

The time course of appearance of $Ni^{2+}$-sensitive intrinsic burst firing is consistent with a role of $Ca_V3.2$, since peak $Ca_V3.2$ mRNA levels preceded the maximal incidence of intrinsic burst firing by 1-2 days. Compared to the transient increase in $Ca_V3.2$ mRNA levels, however, $Ni^{2+}$-sensitive intrinsic burst firing declines more slowly, and is still

substantially increased 30-40 days following status epilepticus. Likewise, a substantial fraction of neurons still exhibits increased T-type $Ca^{2+}$ channel densities 30-40 days after seizures (Su H et al., 2002). These findings may indicate that the turnover of the involved channel proteins is slow, as was shown for the wild-type glycosylated Shaker $K^+$ channels which were stable up to at least 48 hours (Khanna R et al., 2001). Another possibility might be that spontaneous seizures occurring at late stages in SE experienced animals might induce intermittent increases in $Ca_V3.2$ mRNA. This increase of $Ca_V3.2$ mRNA would sustain the T-type $Ca^{2+}$ current elevation in some of the CA1 neurons. But such mRNA up-regulations following spontaneous seizures may have remained undetected when averaging across many animals because these seizure events would not be expected to occur synchronously in the chronically epileptic cohort of animals.

From the knowledge of T-type $Ca^{2+}$ channel biophysics, it appears as if these channels are particularly suited to mediate burst discharges (Huguenard JR 1996). The main properties responsible for this functional specialization are that T-type $Ca^{2+}$ channels are activated at hyperpolarized potentials (around –65 mV, Fishman MC et al., 1981; Nowycky MC et al. 1985), and that they display a slow rate of deactivation (time constants in the order of several milliseconds) at potentials close to the neuronal resting potential (Randall A et al., 1997; Kozlov AS et al., 1999). Thus, T-type $Ca^{2+}$ currents are potently activated by both action potentials, and the prior subthreshold depolarization, and are capable of mediating slow inward tail currents that outlast the duration of action potentials (Sochivko D et al., 2002; Su H et al., 2002). Consequently, these tail currents generate depolarizing spike afterpotentials. If these are large enough, they reach threshold for generation of a second and perhaps third spike, thus giving rise to a burst of action potentials.

*High-threshold and accessory $Ca^{2+}$ channel subunits*

Sustained down-regulation of $Ca_V2.2$ mRNA was observed after day 5 in SE experienced rats. Furthermore, transient up-regulation of $Ca_V1.2$ and accessory

subunits ($\beta_{1-3}$ and $\alpha_2\delta$) in day 3 after SE was observed. These subunits showed the same expression time course pattern as $Ca_V3.2$.

The down-regulation of $Ca_V2.2$ mRNA was in good agreement with the down-regulation of N-type $Ca^{2+}$ currents reported in CA1 neurons in the pilocarpine model (Su H et al., 2002). Since $Ca_V2.2$ are found on presynaptic region of neurons (Ino M et al. 2001) and play a prominent role in GABA and glutamate release (Luebke JI et al. 1993; Woodward JJ et al. 1988; Ino M et al. 2001), this down-regulation might also impact synaptic function, a topic that was not further explored so far. In contrast to these congruent molecular and functional findings, the transient up-regulation of $Ca_V1.2$ mRNA on day 3 was not parallelled by a up-regulation of L-type $Ca^{2+}$ currents (Su H et al., 2002). This could conceivably be due to the late stage (30 days) at which functional measurements were carried out.

A striking finding was the up-regulation of accessory $Ca^{2+}$ channel subunits in a transient fashion, similar to the $Ca_V3.2$ subunit. It is possible, that up-regulation of the accessory subunits due to the transient increase of the mRNA expression also contributes to the augmentation of the T-type $Ca^{2+}$ current in CA1 neurons from SE experienced animals. It is currently a matter of debate in how far T-type currents are modulated by coexpression of accessory subunits. Accessory $\beta$ subunits do not appear to contribute to T-type currents in cultured neurons (Lambert RC et al., 1997). However, specific splice variants of the $\alpha_2\delta$ subunit act to increase functional expression of $Ca_V3.1$ $Ca^{2+}$ channel subunits, and also shift the voltage-gated inactivation in a depolarizing direction, consistent with increased availability of these channels (Hobom M et al., 2000). Thus, increased expression of accessory subunits may well contribute to increased availability of T-type $Ca^{2+}$ channels during burst discharges.

### 4.2.2 Molecular changes of voltage-gated $Na^+$ channels in TLE rats

Real-time RT-PCR was also used to analyze the expression changes of voltage-gated $Na^+$ channels in SE experienced CA1 neurons of the hippocampus. One of the most striking findings was the long-term down-regulation of $Na_V1.2$ and $Na_V1.6$ mRNA. A similar down-regulation of $Na_V1.2$ and $Na_V1.6$ was also found in the dentate gyrus following pilocarpine induced status epilepticus (Ellerkmann RK et al. 2003). Down-regulation of $Na_V1.2$ is also consistent with previous reports showing the same down-regulation in the CA1-CA3 subregion in chronic human epilepsy with *in situ* hybridization (Whitaker WR et al., 2001). In contrast, a down-regulation of $Na_V1.2$ in CA1 neurons was not detected in the kainate model of epilepsy in CA1 (Gastaldi M et al., 1997; Bartolomei F et al. 1997). In these studies, the major alteration reported was an up-regulation of neonatal isoforms of $Na_V1.2$ and 1.3 which arise via alternative splicing (Gastaldi M et al., 1997; Aronica E et al., 2001). Our techniques did not allow us to detect different splice variants. Although several groups have examined how $Na^+$ channels are altered on the functional level in experimental models of epilepsy (Vreugdenhil M et al., 1998; Ketelaars SO et al., 2001; Ellerkmann RK et al., 2003), correlation to molecular findings has been difficult, primarily because of the lack of subunit-selective blockers that can be used in physiological experiments.

### 4.2.3 Molecular changes of KCNQ channels in TLE rats

Besides changes in channel families that mediate depolarizing inward currents, we also analyzed different families of potassium channels. Our analyses of those members of the KCNQ family that are expressed in brain (KCNQ2, 3 and 5) revealed that KCNQ2 expression was significantly down regulated during the entire time course after pilocarpine induced SE. KCNQ3 was also down-regulated on day 1 and day 30 and KCNQ5 only slightly reduced on day 5.

The down-regulation of KCNQ channels is interesting because inhibiting M-currents with high doses of the selective KCNQ channel blocker linopirdine induces epileptic seizures

in experimental animals (Aiken SP et al., 1996). Secondly, the selective KCNQ channel agonist retigabine is an effective antiepileptic agent in both experimental and human epilepsy (Rostock A et al., 1996). Thirdly, loss of function mutations in KCNQ2 and 3 are associated with BFNC (Jentsch TJ, 2000). Interestingly, these mutations result only in a reduction of M-current through KCNQ2/KCNQ3 channels by about 25%, indicating that only a partial loss of M-current function is sufficient to cause increased susceptibility to seizures. A similar phenomenon is also seen in a genetic mouse model. While knockout mice lacking KCNQ2 die at birth, the heterozygous mice displaying decreased expression of KCNQ2 show increased seizure susceptibility (Watanabe H et al., 2000).

The expression patterns of KCNQ2, KCNQ3 and KCNQ5 in the brain overlap extensively (Bievert C et al., 1998; Schroeder BC et al., 1998; Tinel N et al., 1998; Cooper EC et al., 2000; Schroeder BC et al., 2000). In hippocampus, CA1 pyramidal neurons express all three subunits, that most probably combine to form both hetero- and homomeric channels (Wang HS et al., 1998; Schoeder BC et al., 1998). It is unclear whether the changes we have observed here are paralleled by a different subunit stochiometry of KCNQ channels.

Regardless of these issues – are the molecular changes we have described paralleled by a reduction in M-current density? Unpublished electrophysiological data indicates that this is the case, and that M-current density obtained by normalizing to cell capacitance is reduced by around 50% in the chronic stage (~60-90) days following status epilepticus (Sochivko D, unpublished data). Interestingly, this M-current density decrease could only be found in the chronic stage, but not in the acute stage (~15 days after status epilepticus). These findings may indicate a slow turnover of the relevant channel proteins. Taken together, these data suggest that reduction of M-currents is not only a mechanism underlying some forms of genetic epilepsies, but is also a feature of chronic acquired epilepsy.

### 4.2.4 Molecular changes of A-type $K^+$ channels in TLE rats

Transient $K^+$ currents are a subgroup of voltage-gated $K^+$ currents. They are characterized by their rapid activation and inactivation upon depolarization (Hille B, 1992; Coetzee WA et al., 1999). The presence of such currents profoundly affects membrane excitability. The rapid kinetics of transient $K^+$ currents make them well suited to contribute to action potential repolarization (Kang J et al., 2000). In addition, the activation of transient $K^+$ currents during action potentials provides transient hyperpolarizing drive that prolongs the interspike interval and may permit some neurons to discharge at slow rates (Connor JA et al,. 1971a; Connor JA et al,. 1971b; Kang J et al., 2000; Kanold PO et al., 1999).

Among the five genes that encode transient $K^+$ channels, we found that the expression of $K_V1.4$ and $K_V4.2$ was down-regulated in the chronic stage (day 30 after status epilepticus). The expression of all other transient $K^+$ channel subunits was remarkably stable. Expression level of $K_V2.3$ was also down-regulated in the acute stage day 3. This subunit is a silent $K^+$ channel $\alpha$ subunit, but it is capable of forming heterotetramers with other pore-forming subunits to form transient $K^+$ currents (Chiara MD et al., 1999).

What is the role of $K_V4.2$ in CA1 neurons? A large body of literature indicates that this subunit underlies the dendritic A-type $K^+$ channel in CA1 neurons (Hoffman D et al., 1997). In this cellular compartment, this current limits EPSP propagation to the soma, as well as inhibiting the back-propagation of action potentials into the distal dendritic tree (Hoffman D et al., 1997). Interestingly, this current is target of modulation not only by PKA and PKC (Hoffmann D et al., 1998), but also by the mitogen-activated protein kinase pathway (MAPK pathway, Yuan LL et al., 2002). The modulation of dendritic $K_V4.2$ channels by the latter cascade appears to underlie postsynaptic increases in dendritic excitability associated with induction of long-term potentiation (Frick A et al., 2004). Collectively, these data indicate that down-regulation of $K_V4.2$ might profoundly increase dendritic excitability in CA1 neurons in a manner comparable with down-regulation during induction of synaptic long-term potentiation.

In the pilocarpine model of epilepsy, action potential back-propagation is augmented in CA1 neurons (Bernard C, unpublished data). Pharmacologically blocking A-type currents facilitates action potential back-propagation to similar levels in control and epileptic animals, indicative of down-regulation of dendritic A-type currents in epilepsy. Regarding the $K_V1.4$ channel, this channel subunit is expressed in axons and perhaps presynaptic terminals. It is as yet unclear what consequences down-regulation of such channels might have.

### 4.2.5 Molecular changes of HCN channels in TLE rats

We also observed changes in the expression of HCN subunits, which underlie H-currents ($I_H$) in native neurons. We observed a potent and chronic down-regulation of the fast-gating HCN1 subunit expression. The HCN2 subunit, which underlies $I_H$ currents with slower kinetics, showed only a slight down-regulation at various timepoints. In contrast, the slow gating HCN3 and HCN4 subunits showed only transient up-regulation on the first day after SE and then returned to control levels. These data indicate differential regulation of different HCN subunits.

The expression of HCN subunits has been examined following febrile seizures and kainate-induced convulsions in immature rats using semiquantitative in situ hybridization (Brewster A et al., 2002). In this study, both types of seizures caused a down-regulation of HCN1 mRNA levels in CA1 neurons. This down-regulation proved to last into adulthood following febrile seizures. Thus, seizures appear to down-regulate HCN1 not only in our adult epilepsy model, but also in the immature brain. In contrast to our data, HCN2 subunit mRNA was up-regulated following febrile seizures, but this up-regulation was transient and not detected 3 months after febrile seizures.

What might the functional consequences of rather selective changes in HCN1 subunits be? One of the consequences could be that the proportion of heteromultimers containing HCN1 subunits is decreased in the various seizure models. This would be expected to influence both the kinetics and the cAMP sensitivity of $I_H$ (Brewster A et al.,

2002). It is not clear how these molecular data are related to functional data showing that $I_H$ is augmented following febrile seizures (Chen K et al., 2001).

The generation of mice lacking either the HCN1 or the HCN2 subunit has allowed to address the consequences of reduced $I_H$ in intact animals. HCN2 knockout mice exhibit a reduction of hippocampal $I_H$ or about one third. In addition, they display spontaneous absence seizures (Ludwig A et al., 2003). HCN knockout animals show deficits in motor learning and certain integrative properties of Purkinje neurons (Nolan MF et al., 2003). However, susceptibility to hippocampal seizures has not been tested in both these mouse strains.

## 4.3 Methodical considerations: expression profiling vs. real-time RT-PCR analyses

The use of microarray technology to monitor expression levels of genes has one major advantage: it allows profiling the expression patterns of thousands of genes in parallel. We have used Affymetrix GeneChips to examine changes in a large number of genes in the CA1 region following pilocarpine induced status epilepticus. Surprisingly, a large number of expression changes found in the microarray experiments were not replicated in the real-time RT-PCR experiments. These discrepancies may be derived from problems inherent in the former technology.

Even though microarrays allow monitoring expression of large numbers of genes, interpretation of the data is frequently difficult, for the following reasons. Firstly, relatively high amounts of mRNA are required for such an analysis, normally at least 0.5–3.0 µg of total RNA (Duggan DJ et al., 1999). For this reason, most studies have used tissue samples comprising different CNS nuclei or subfields. In this study, we have avoided contamination by regulation processes occurring in other hippocampal subfields by dissecting the hippcampal CA1 region from slices. Nevertheless, pilocarpine induced status epilepticus causes quite dramatic shifts in the numbers of various cell types within the tissue. CA1 pyramidal neurons and some types of interneurons undergo severe cell loss, while other interneuron types are conserved. Furthermore, a proliferation of glial cells is observed. Thus, expression changes observed in array studies might either reflect a veritable change in mRNA abundancy in one of the major cell categories, or a change in the size of the cell population (Becker AJ, et al., 2003). This confounding factor may explain part of the observed discrepancies and highlights the importance of using molecular techniques with cellular resolution for complex neurological disorders.

Real-time RT-PCR is a highly appropriate technique for this purpose, since it offers a high sensitivity, high specificity, and highly accurate quantification. Thus, it can be used for small amounts of tissue and single cell analyses. Furthermore, deriving gene

expression data from harvested neurons allows absolute quantification of transcript abundance per neuron, which avoids balancing artifacts. Effects of altered tissue composition can also be avoided by quantifying the gene of interest relative to neuron-specific reference genes, i.e. synaptophysin. Hitherto, glyceraldehyde-3-phosphate dehydrogenase (GAPDH) and β-actin have been commonly used as reference genes in relative quantification. However, these two reference genes exhibit considerable changes in expression under disease condition (Suzuki T et al. 2000), especially wide criticism on GAPDH. In our pilocarpine induced status epilepticus rat model, both real-time RT-PCR and *in situ* hybridization revealed a striking up-regulation for GAPDH. This change in expression would introduce a large error into mRNA quantification based on normalization to GAPDH. Surprisingly, when comparing SE experienced and control animals, the most stable expression was synaptophysin. It is an integral membrane protein in presynaptic small translucent vesicles, and also present in dispersed neuroendocrine cells. The 5' upstream region of synaptophysin is devoid of any TATA or CAAT boxes, but shows typical features of 'housekeeping' genes, i.e., G + C-rich islands and four Sp1-binding motifs (Bargou RC et al., 1991). The structure of the synaptophysin gene promoter indicates that this gene also might belong to a class of 'house-keeping' genes and our data also showed its stable expression between the SE experienced and normal rats. In addition, the use of synaptophysin as reference gene for mRNA expression studies bears a second advantage: the expression of synaptophysin, same as the most voltage-gated ion channels, is restricted to neurons, mRNA expression levels of these target voltage-gated ion channels will not be affected by changes in the populations of neuronal and nonneuronal cells in our SE experienced rats. This approach can be particularly helpful for experiments in microdissected tissue samples.

Finally, real-time RT-PCR bears the advantage of allowing reliable analysis of genes that are not strongly expressed, such as many of the ion channel genes. Such analyses of low-abundancy transcripts have also encountered problems when microarray technology was used.

## 4.4 Temporal patterns of transcriptional regulation: Implications for coordinate regulation of ion channel genes?

Our data do not allow us to speculate on the mechanisms underlying transcriptional control of ion channel subunits. However, the analysis of expression changes in the same seizure model for a large number of ion channel subunits revealed that subgroups of ion channels exist that may be concurrently regulated. Thus, seizure may cause coordinated changes in certain subsets of ion channel mRNAs. Such a scenario has been proposed for GABA-A receptors following pilocarpine induced status epilepticus. In a combined functional and molecular study, all GABA-A receptor subunit mRNAs were analyzed simultaneously from single hippocampal neurons using aRNA amplification techniques. Correlation analyses revealed that only certain subunits appeared to be expressed in a highly coordinated manner (Brooks-Kayal AR et al., 1998). Such data may indicate that concurrently regulated genes may share promoter motifs that govern their expression.

The transcriptional regulation processes that underlie distinct cell-type and tissue-specific expression patterns of voltage-gated ion channels genes have been elucidated for only a few genes. Neuron-specific expression of the rat $Na_V1.2$ is regulated by a silencer located in the 5'-upstream region of the gene (Maue RA et al., 1990; Kraner SD et al., 1992). A 397 bp stretch of the 5'- upstream region of human $Na_V1.2$ can promote luciferase expression in neuroblastoma cells, but not in non-neuronal cells (Schade SD et al., 2000). The transcription of $K_V1.5$ is regulated by glucocorticoids and camp in both GH3 cells and cardiac myocytes (Takimoto K et al., 1993; 1994; Mori Y et al., 1993). An enhancer that consists of an $(ATG)_7$ trinucleotide repeat sequence is identified in $Ca_V1.3$ and the transcription is increased during differentiation in the presence of prostaglandin E1 or retinoic acid in NG 108-15 cells (Kamp TJ et al., 1995). A 2.5 kb upstream region of the human $Ca_V1.3$ shows high CAT activity when transfected to NG108-15 cells (Kim HL et al., 1998). Neuron-specific elements of mouse $Ca_V2.1$ were located in the distal region (-6273 to -3021) of the 5'-upstream sequence (Takahashi E, et al., 1999), the

similar results of human $Ca_V2.2$ showed the distal upstream region (-3992 to -1788) may be important for neuron-specific expression (Kim DS et al., 1997).

Even less is known about the mechanisms underlying the activity-induced plasticity after seizures. Following induced seizures, a number of transcription factors have been shown to be altered, for instance Sp-1 in hippocampus (Feng Z et al., 1999) or ΔFosB, a splice variant of fosB gene. Some of these factors were demonstrated to regulate downstream gene transcription, such as the NR1 subunit of NMDA receptors (Hiroi N et al., 1998) and cyclin-dependent kinase 5 (cdc5) (Chen J et al., 2000), which were identified as targets of delta FosB. Data on coordinate cellular or temporal gene expression changes similar to that presented here may allow us to derive candidate transcription factors that contribute to generating such regulation patterns.

# 5 Conclusion

Status epilepticus (SE) is known to cause numerous structural and functional alterations in brain. The changes observed in chronic epilepsy have been grouped into one of two categories: changes on the synaptic or changes on the intrinsic level. Some investigators have advanced the idea that changes on the synaptic level are most important in mediating neuronal synchronization and hyperexcitability (the 'epileptic network' hypothesis). Far fewer studies have addressed the possibility that intrinsic properties of neurons might be altered (the 'epileptic neuron' hypothesis). It now appears clear that a multitude of changes occur, both on the synaptic and intrinsic level. In fact, the epileptic network and epileptic neuron hypotheses are quite obviously not mutually exclusive. In fact, the input-output relationship of neuronal networks depends both on their synaptic connectivity and on the intrinsic properties of their neuronal elements. Long-term changes in this relationship can thus be achieved by changes in synaptic and/or intrinsic neuronal properties.

In this study, expression of various voltage-gated ion channels in rat hippocampal CA1 neurons at different time points after an episode of SE induced by pilocarpine. The data presented here clearly demonstrates that abnormal brain activity can modulate the molecular characteristics of voltage-gated ion channels, possibly leading to persistent changes in neuronal discharge behavior. Our data also suggest that changes in transcription of ion channels can be highly coordinated, and result in tightly controlled alterations of specific voltage-gated and transmitter-gated ionic currents in neurons.

How important is intrinsic plasticity, and the conversion of neurons from a nonbursting to a bursting mode in the generation of seizures (Sanabria ER et al., 2001; Su H et al., 2002)? Evidence that bursting may be important is derived from several main lines of evidence. Firstly, spontaneously bursting neurons, which do not occur in the normal CA1 region, are the initiators of epileptiform discharges in this region (Sanabria ER et al., 2001). Secondly, increased bursting is up-regulated in various acute models of seizures, while synaptic transmission is affected in different ways, indicating that bursting may be an important determinant of seizures generated in-vitro. Finally, modeling studies have shown that bursting neurons can be extremely

important for neuronal synchronization in the context of seizures (Miles R et al., 1983; Traub RD et al., 1982). We thus suggest that intrinsic plasticity is a potent mechanism that, in conjunction with synaptic plasticity, can fundamentally alter the input-output properties of neuronal networks in the mammalian brain.

# 6 References


Aiken SP, Zaczek R, Brown BS. Pharmacology of the neurotransmitter release enhancer linopirdine (DuP 996), and insights into its mechanism of action. Adv Pharmacol 1996;35:349-84

Alkadhi KA, Tian LM. Veratridine-enhanced persistent sodium current induces bursting in CA1 pyramidal neurons. Neuroscience 1996;71(3):625-32

Altomare C, Bucchi A, Camatini E, Baruscotti M, Viscomi C, Moroni A, DiFrancesco D. Integrated allosteric model of voltage gating of HCN channels. J Gen Physiol 2001;117(6):519-32

Alzheimer C**,** Schwindt PC, and Crill WE. Modal gating of $Na^+$ channels as a mechanism of persistent $Na^+$ current in pyramidal neurons from rat and cat sensorimotor cortex. J Neurosci 1993; 13: 660 - 673

Amaral DG, Dolorfo C, Alvarez-Royo P. Organization of CA1 projections to the subiculum: a PHA-L analysis in the rat. Hippocampus 1991;1(4):415-35

Amaya F, Decosterd I, Samad TA, Plumpton C, Tate S, Mannion RJ, Costigan M, Woolf CJ. Diversity of expression of the sensory neuron-specific TTX-resistant voltage-gated sodium ion channels SNS and SNS2. Mol Cell Neurosci 2000;15(4):331-42

Andersen P, Holmqvist B, Voorhoeve PE. Entorhinal activation of dentate granule cells. Acta Physiol Scand 1966;66(4):448-60

Antonucci DE, Lim ST, Vassanelli S, Trimmer JS. Dynamic localization and clustering of dendritic $K_v2.1$ voltage-dependent potassium channels in developing hippocampal neurons. Neuroscience 2001;108(1):69-81

Armstrong CM, Matteson DR. Two distinct populations of calcium channels in a clonal line of pituitary cells. Science 1985;227(4682):65-7

Aronica E, Yankaya B, Troost D, van Vliet EA, Lopes da Silva FH, Gorter JA. Induction of neonatal sodium channel II and III alpha-isoform mRNAs in neurons and microglia after status epilepticus in the rat hippocampus. Eur J Neurosci 2001;13(6):1261-6

Azouz R, Jensen MS, Yaari Y. Ionic basis of spike after-depolarization and burst generation in adult rat hippocampal CA1 pyramidal cells. J Physiol 1996;492 (Pt 1):211-23

Azouz R, Alroy G, Yaari Y. Modulation of endogenous firing patterns by osmolarity in rat hippocampal neurones. J Physiol 1997;502 (Pt 1):175-87

Bargou RC, Leube RE. The synaptophysin-encoding gene in rat and man is specifically transcribed in neuroendocrine cells. Gene 1991;99(2):197-204

Barlow C, Lockhart DJ. DNA arrays and neurobiology--what's new and what's next? Curr Opin Neurobiol 2002;12(5):554-61

Bartolomei F, Gastaldi M, Massacrier A, Planells R, Nicolas S, Cau P. Changes in the mRNAs encoding subtypes I, II and III sodium channel alpha subunits following kainate-induced seizures in rat brain. J Neurocytol 1997;26(10):667-78

Bassett DE Jr, Eisen MB, Boguski MS. Gene expression informatics--it's all in your mine. Nat Genet 1999;21(1 Suppl):51-5

Beaumont V, Zucker RS. Enhancement of synaptic transmission by cyclic AMP modulation of presynaptic Ih channels. Nat Neurosci 2000;3(2):133-41

Becker AJ, Chen J, Paus S, Normann S, Beck H, Elger CE, Wiestler OD, Blumcke I. Transcriptional profiling in human epilepsy: expression array and single cell real-time qRT-PCR analysis reveal distinct cellular gene regulation. Neuroreport 2002;13(10):1327-33

Becker AJ, Chen J, Zien A, Sochivko D, Normann S, Schramm J, Elger CE, Wiestler OD, Blumcke I. Correlated stage- and subfield-associated hippocampal gene expression patterns in experimental and human temporal lobe epilepsy. Eur J Neurosci 2003;18(10):2792-802

Becker AJ, Wiestler OD, Blumcke I. Functional genomics in experimental and human temporal lobe epilepsy: powerful new tools to identify molecular disease mechanisms of hippocampal damage. Prog Brain Res 2002;135:161-73

Ben-Ari Y. Cell death and synaptic reorganizations produced by seizures. Epilepsia 2001;42 Suppl 3:5-7

Bers DM, Perez-Reyes E. $Ca^{2+}$ channels in cardiac myocytes: structure and function in $Ca^{2+}$ influx and intracellular $Ca^{2+}$ release. Cardiovasc Res 1999;42(2):339-60

Biervert C, Schroeder BC, Kubisch C, Berkovic SF, Propping P, Jentsch TJ, Steinlein OK. A potassium channel mutation in neonatal human epilepsy. Science 1998;279(5349): 403-6

Biervert C, Steinlein OK. Structural and mutational analysis of KCNQ2, the major gene locus for benign familial neonatal convulsions. Hum Genet 1999;104(3):234-40

Bischofberger J, Geiger JR, Jonas P. Timing and efficacy of $Ca^{2+}$ channel activation in hippocampal mossy fiber boutons. J Neurosci 2002;22(24):10593-602

Blackstad TW, Brink K, Hem J, Jeune B. Distribution of hippocampal mossy fibers in the rat. An experimental study with silver impregnation methods. J Comp Neurol 1970;138(4):433-49

Blaschke V, Reich K, Blaschke S, Zipprich S, Neumann C. Rapid quantitation of proinflammatory and chemoattractant cytokine expression in small tissue samples and monocyte-derived dendritic cells: validation of a new real-time RT-PCR technology. J Immunol Methods 2000;246(1-2):79-90

Blümcke I, Beck H, Lie AA, Wiestler OD. Molecular neuropathology of human mesial temporal lobe epilepsy. Epilepsy Res 1999a;36(2-3):205-23

Blümcke I, Zuschratter W, Schewe JC, Suter B, Lie AA, Riederer BM, Meyer B, Schramm J, Elger CE, Wiestler OD. Cellular pathology of hilar neurons in Ammon's horn sclerosis. J Comp Neurol 1999b;414(4):437-53

Blümcke I, Thom M, Wiestler OD. Ammon's horn sclerosis: a maldevelopmental disorder associated with temporal lobe epilepsy. Brain Pathol 2002;12(2):199-211

Bourinet E, Soong TW, Sutton K, Slaymaker S, Mathews E, Monteil A, Zamponi GW, Nargeot J, Snutch TP. Splicing of alpha 1A subunit gene generates phenotypic variants of P- and Q-type calcium channels. Nat Neurosci 1999;2(5):407-15

Brahmajothi MV, Morales MJ, Liu S, Rasmusson RL, Campbell DL, Strauss HC. In situ hybridization reveals extensive diversity of $K^+$ channel mRNA in isolated ferret cardiac myocytes. Circ Res 1996;78(6):1083-9

Brewster A, Bender RA, Chen Y, Dube C, Eghbal-Ahmadi M, Baram TZ. Developmental febrile seizures modulate hippocampal gene expression of hyperpolarization-activated channels in an isoform- and cell-specific manner. J Neurosci 2002;22(11):4591-9

Brown DA, Adams PR. Muscarinic suppression of a novel voltage-sensitive $K^+$ current in a vertebrate neurone. Nature 1980; 283(5748):673-6

Carbone E, Lux HD. A low voltage-activated calcium conductance in embryonic chick sensory nerons. Biophys J 1984;46(3):413-8

Cardullo RA, Agrawal S, Flores C, Zamecnik PC, Wolf DE. Detection of nucleic acid hybridization by nonradiative fluorescence energy transfer. Proc Natl Acad Sci USA 1988;85(23):8790-4

Catterral WA Structure and regulation of voltage-gated $Ca^{2+}$ channels. Annu Rev Cell Dev Biol 2000;16:521-55

Cavalheiro EA, Santos NF, Priel MR. The pilocarpine model of epilepsy in mice. Epilepsia 1996;37(10):1015-9

Charlier C, Singh NA, Ryan SG, Lewis TB, Reus BE, Leach RJ, Leppert M. A pore mutation in a novel KQT-like potassium channel gene in an idiopathic epilepsy family. Nat Genet 1998;18(1):53-5

Chen H, Kurennyi DE, Smith PA. Modulation of M-channel conductance by adenosine 5' triphosphate in bullfrog sympathetic B-neurones. J Auton Pharmacol 2001;21(1):57-62

Chen J, Piper DR, Sanguinetti MC. Voltage sensing and activation gating of HCN pacemaker channels. Trends Cardiovasc Med 2002 Jan;12(1):42-5

Chen J, Sochivko D, Beck H, Marechal D, Wiestler OD, Becker AJ. Activity-induced expression of common reference genes in individual CNS neurons. Lab Invest 2001;81(6):913-6

Chen J, Zhang Y, Kelz MB, Steffen C, Ang ES, Zeng L, Nestler EJ. Induction of cyclin-dependent kinase 5 in the hippocampus by chronic electroconvulsive seizures: role of [Delta]FosB. J Neurosci 2000;20(24):8965-71

Chen K, Aradi I, Thon N, Eghbal-Ahmadi M, Baram TZ, Soltesz I. Persistently modified h-channels after complex febrile seizures convert the seizure-induced enhancement of inhibition to hyperexcitability. Nat Med 2001;7(3):331-7

Chen S, Wang J, Siegelbaum SA. Properties of hyperpolarization-activated pacemaker current defined by coassembly of HCN1 and HCN2 subunits and basal modulation by cyclic nucleotide. J Gen Physiol 2001;117(5):491-504

Chiara MD, Monje F, Castellano A, Lopez-Barneo J. A small domain in the N terminus of the regulatory alpha-subunit $K_v2$. 3 modulates $K_v2.1$ potassium channel gating. J Neurosci 1999;19(16): 6865-73

Coetzee WA, Amarillo Y, Chiu J, Chow A, Lau D, McCormack T, Moreno H, Nadal MS, Ozaita A, Pountney D, Saganich M, Vega-Saenz de Miera E, Rudy B. Molecular diversity of $K^+$ channels. Ann N Y Acad Sci 1999;868:233-85

Connor JA, Stevens CF. Prediction of repetitive firing behaviour from voltage clamp data on an isolated neurone soma. J Physiol 1971a;213(1):31-53

Connor JA, Stevens CF. Voltage clamp studies of a transient outward membrane current in gastropod neural somata. J Physiol 1971b;213(1):21-30

Cooper EC, Aldape KD, Abosch A, Barbaro NM, Berger MS, Peacock WS, Jan YN, Jan LY. Colocalization and coassembly of two human brain M-type potassium channel subunits that are mutated in epilepsy. Proc Natl Acad Sci USA 2000;97(9):4914-9

Cooper EC, Harrington E, Jan YN, Jan LY. M channel KCNQ2 subunits are localized to key sites for control of neuronal network oscillations and synchronization in mouse brain. J Neurosci 2001;21(24):9529-40

Coulter DA. Chronic epileptogenic cellular alterations in the limbic system after status epilepticus. Epilepsia 1999; 40 Suppl 1:S23-33

Coulter DA. Epilepsy-associated plasticity in gamma-aminobutyric acid receptor expression, function, and inhibitory synaptic properties. Int Rev Neurobiol 2001;45:237-52

Crill WE. Persistent sodium current in mammalian central neurons. Annu Rev Physiol 1996;58:349-62

Cummins TR, Xia Y, Haddad GG. Functional properties of rat and human neocortical voltage-sensitive sodium currents. J Neurophysiol 1994;71(3):1052-64

Debanne D, Guerineau NC, Gahwiler BH, Thompson SM. Action-potential propagation gated by an axonal I(A)-like $K^+$ conductance in hippocampus. Nature 1997;389(6648):286-9

DiFrancesco D. Pacemaker mechanisms in cardiac tissue. Annu Rev Physiol 1993;55:455-72

Duggan, D.J., Bittner, M., Chen, Y., Meltzer, P. and Trent, J.M. Expression profiling using cDNA microarrays. Nat. Genet 1999;21 (1):10-14

Elger, C.E. and Schramm, J. The surgical treatment of epilepsy. Radiologe 1993;33 (4):165-171

Ellerkmann RK, Remy S, Chen J, Sochivko D, Elger CE, Urban BW, Becker A, Beck H. Molecular and functional changes in voltage-dependent $Na^+$ channels following pilocarpine-induced status epilepticus in rat dentate granule cells. Neuroscience 2003;119(2):323-33

Emig M, Saussele S, Wittor H, Weisser A, Reiter A, Willer A, Berger U, Hehlmann R, Cross NC, Hochhaus A. Accurate and rapid analysis of residual disease in patients with CML using specific fluorescent hybridization probes for real time quantitative RT-PCR. Leukemia 1999;13(11):1825-32

Ertel EA, Campbell KP, Harpold MM, Hofmann F, Mori Y, Perez-Reyes E, Schwartz A,Snutch TP, Tanabe T, Birnbaumer L, Tsien RW, Catterall WA. Nomenclature of voltage-gated calcium channels. Neuron 2000;25(3):533-5

Escayg A, MacDonald BT, Meisler MH, Baulac S, Huberfeld G, An-Gourfinkel I, Brice A, LeGuern E, Moulard B, Chaigne D, Buresi C, Malafosse A. Mutations of SCN1A, encoding a neuronal sodium channel, in two families with GEFS+2. Nat Genet 2000;24(4):343-5

Escayg A, Heils A, MacDonald BT, Haug K, Sander T, Meisler MH. A novel SCN1A mutation associated with generalized epilepsy with febrile seizures plus--and prevalence of variants in patients with epilepsy. Am J Hum Genet 2001;68(4):866-73

Feng Z, Chang RC, Bing G, Hudson P, Tiao N, Jin L, Hong JS. Long-term increase of Sp-1 transcription factors in the hippocampus after kainic acid treatment. Brain Res Mol Brain Res 1999;69(1):144-8

Finch DM, Nowlin NL, Babb TL. Demonstration of axonal projections of neurons in the rat hippocampus and subiculum by intracellular injection of HRP. Brain Res 1983;271(2):201-16

Fink L, Seeger W, Ermert L, Hanze J, Stahl U, Grimminger F, Kummer W, Bohle RM. Real-time quantitative RT-PCR after laser-assisted cell picking. Nat Med 1998;4(11):1329-33

Fishman MC, Spector I. Potassium current suppression by quinidine reveals additional calcium currents in neuroblastoma cells. Proc Natl Acad Sci USA 1981;78(8):5245-9

Frick A, Magee J, Johnston D. LTP is accompanied by an enhanced local excitability of pyramidal neuron dendrites. Nat Neurosci 2004;7(2):126-35

Gaarskjaer FB. Organization of the mossy fiber system of the rat studied in extended hippocampi. I. Terminal area related to number of granule and pyramidal cells. J Comp Neurol 1978;178(1):49-78

Gastaldi M, Bartolomei F, Massacrier A, Planells R, Robaglia-Schlupp A, Cau P. Increase in mRNAs encoding neonatal II and III sodium channel alpha-isoforms during kainate-induced seizures in adult rat hippocampus. Mol Brain Res 1997;44(2):179-90

Geiger JR, Jonas P. Dynamic control of presynaptic $Ca^{2+}$ inflow by fast-inactivating $K^{+}$ channels in hippocampal mossy fiber boutons. Neuron 2000;28(3):927-39

Gibson UE, Heid CA, Williams PM. A novel method for real time quantitative RT-PCR. Genome Res 1996;6(10):995-1001

Goldin AL, Barchi RL, Caldwell JH, Hofmann F, Howe JR, Hunter JC, Kallen RG, Mandel G, Meisler MH, Netter YB, Noda M, Tamkun MM, Waxman SG, Wood JN, Catterall WA. Nomenclature of voltage-gated sodium channels. Neuron 2000;28(2):365-8

Goldin AL. Resurgence of sodium channel research. Annu Rev Physiol 2001;63:871-94

Goldstein SAN, Wang KW, Han Nitza, Pausch MH. Sequence and function of the two P domain potassium channels: implications of an emerging superfamily. J Mol Med 1998;76:13-20

Halliwell JV. M-current in human neocortical neurones. Neurosci Lett 1986;67(1):1-6

Hans VH, Kossmann T, Lenzlinger PM, Probstmeier R, Imhof HG, Trentz O, Morganti-Kossmann MC. Experimental axonal injury triggers interleukin-6 mRNA, protein synthesis and release into cerebrospinal fluid. J Cereb Blood Flow Metab 1999;19(2):184-94

Hille B. ionic channels of exciatable membranes, 1992 2 ed. Sinauer Ass. Sunderland

Hiroi N, Marek GJ, Brown JR, Ye H, Saudou F, Vaidya VA, Duman RS, Greenberg ME, Nestler EJ. Essential role of the fosB gene in molecular, cellular, and behavioral actions of chronic electroconvulsive seizures. J Neurosci 1998;18(17):6952-62

Hirose S, Zenri F, Akiyoshi H, Fukuma G, Iwata H, Inoue T, Yonetani M, Tsutsumi M, Muranaka H, Kurokawa T, Hanai T, Wada K, Kaneko S, Mitsudome A. A novel mutation of KCNQ3 (c.925T→C) in a Japanese family with benign familial neonatal convulsions. Ann Neurol 2000;47(6):822-6

Hobom M, Dai S, Marais E, Lacinova L, Hofmann F, and Klugbauer N. Neuronal distribution and functional characterization of the $Ca^{2+}$ channel $\alpha_2\delta$-2 subunit. Europ J Neurosci 2000;12, 1217-1226

Hodgkin AL, Huxley AF. A quantitative description of membrane current and its application to conduction and excitation in nerve. J Physiol 1952;117(4):500-44

Hoffman DA, Johnston D. Downregulation of transient $K^+$ channels in dendrites of hippocampal CA1 pyramidal neurons by activation of PKA and PKC. J Neurosci 1998;18(10):3521-8

Hoffman DA, Magee JC, Colbert CM, Johnston D. $K^+$ channel regulation of signal propagation in dendrites of hippocampal pyramidal neurons. Nature 1997;387(6636): 869-75

Hofmann F, Lacinova L, Klugbauer N. Voltage-dependent calcium channels: from structure to function. Rev Physiol Biochem Pharmacol 1999;139:33-87

Holland PM, Abramson RD, Watson R, Gelfand DH. Detection of specific polymerase chain reaction product by utilizing the 5'→3' exonuclease activity of Thermus aquaticus DNA polymerase. Proc Natl Acad Sci USA 1991;88(16):7276-80

Hobom M, Dai S, Marais E, Lacinova L, Hofmann F, Klugbauer N. Neuronal distribution and functional characterization of the calcium channel alpha2delta-2 subunit. Eur J Neurosci 2000;12(4):1217-26

Huguenard JR Low-threshold calcium currents in central nervous system neurons. Annu Rev Physiol 1996;58:329-48

Ino M, Yoshinaga T, Wakamori M, Miyamoto N, Takahashi E, Sonoda J, Kagaya T, Oki T, Nagasu T, Nishizawa Y, Tanaka I, Imoto K, Aizawa S, Koch S, Schwartz A, Niidome T, Sawada K, Mori Y. Functional disorders of the sympathetic nervous system in mice lacking the alpha 1B subunit (Cav 2.2) of N-type calcium channels. Proc Natl Acad Sci USA 2001;98(9):5323-8

Ishizuka N, Weber J, Amaral DG. Organization of intrahippocampal projections originating from CA3 pyramidal cells in the rat. J Comp Neurol 1990;295(4):580-623

Isom LL, De Jongh KS, Patton DE, Reber BF, Offord J, Charbonneau H, Walsh K, Goldin AL, Catterall WA. Primary structure and functional expression of the beta 1 subunit of the rat brain sodium channel. Science 1992;256(5058):839-42

Isom LL, Scheuer T, Brownstein AB, Ragsdale DS, Murphy BJ, Catterall WA. Functional co-expression of the beta 1 and type IIA alpha subunits of sodium channels in a mammalian cell line. J Biol Chem 1995;270(7):3306-12

Isom LL, Ragsdale DS, De Jongh KS, Westenbroek RE, Reber BF, Scheuer T, Catterall WA. Structure and function of the beta 2 subunit of brain sodium channels, a transmembrane glycoprotein with a CAM motif. Cell 1995;83(3):433-42

Jackson GD, McIntosh AM, Briellmann RS, Berkovic SF. Hippocampal sclerosis studied in identical twins. Neurology 1998;51(1):78-84

Jensen MS, Azouz R, Yaari Y. Spike after-depolarization and burst generation in adult rat hippocampal CA1 pyramidal cells. J Physiol 1996;492 ( Pt 1):199-210

Jentsch TJ. Neuronal KCNQ potassium channels: physiology and role in disease. Nat Rev Neurosci 2000;1(1):21-30

Kamp TJ, Mitas M, Fields KL, Asoh S, Chin H, Marban E, Nirenberg M. Transcriptional regulation of the neuronal L-type calcium channel alpha 1D subunit gene. Cell Mol Neurobiol 1995;15(3):307-26

Kang J, Huguenard JR, Prince DA. Voltage-gated potassium channels activated during action potentials in layer V neocortical pyramidal neurons. J Neurophysiol 2000;83(1):70-80

Kanold PO, Manis PB. Transient potassium currents regulate the discharge patterns of dorsal cochlear nucleus pyramidal cells. J Neurosci 1999;19(6):2195-208

Kaupp UB, Seifert R. Molecular diversity of pacemaker ion channels. Annu Rev Physiol 2001;63:235-57

Ketelaars SO, Gorter JA, van Vliet EA, Lopes da Silva FH, Wadman WJ. Sodium currents in isolated rat CA1 pyramidal and dentate granule neurones in the post-status epilepticus model of epilepsy. Neuroscience 2001;105(1):109-20

Khanna R, Myers MP, Laine M, Papazian DM. Glycosylation increases potassium channel stability and surface expression in mammalian cells. J Biol Chem 2001;276(36):34028-34

Kharkovets T, Hardelin JP, Safieddine S, Schweizer M, El-Amraoui A, Petit C, Jentsch TJ. KCNQ4, a $K^+$ channel mutated in a form of dominant deafness, is expressed in the inner ear and the central auditory pathway. Proc Natl Acad Sci USA 2000;97(8):4333-8

Kim DS, Jung HH, Park SH, Chin H. Isolation and characterization of the 5'-upstream region of the human N-type calcium channel alpha1B subunit gene. Chromosomal localization and promoter analysis. J Biol Chem 1997;272(8):5098-104

Kim HL, Chang YJ, Lee SM, Hong YS. Genomic structure of the regulatory region of the voltage-gated calcium channel alpha 1D. Exp Mol Med 1998;30(4):246-51

Kohler C. Intrinsic projections of the retrohippocampal region in the rat brain. I. The subicular complex. J Comp Neurol 1985;236(4):504-22

Kozlov AS, McKenna F, Lee JH, Cribbs LL, Perez-Reyes E, Feltz A, Lambert RC. Distinct kinetics of cloned T-type $Ca^{2+}$ channels lead to differential $Ca^{2+}$ entry and frequency-dependence during mock action potentials. Eur J Neurosci 1999;11(12):4149-58

Kraner SD, Chong JA, Tsay HJ, Mandel G. Silencing the type II sodium channel gene: a model for neural-specific gene regulation. Neuron 1992;9(1):37-44

Lambert RC, Maulet Y, Mouton J, Beattie R, Volsen S, De Waard M, Feltz A. T-type $Ca^{2+}$ current properties are not modified by $Ca^{2+}$ channel beta subunit depletion in nodosus ganglion neurons. J Neurosci 1997;17(17):6621-8

Lerche H, Biervert C, Alekov AK, Schleithoff L, Lindner M, Klinger W, Bretschneider F, Mitrovic N, Jurkat-Rott K, Bode H, Lehmann-Horn F, Steinlein OK. A reduced $K^+$ current due to a novel mutation in KCNQ2 causes neonatal convulsions. Ann Neurol 1999;46(3):305-12

Llinas R, Ribary U, Jeanmonod D, Cancro A, Kronberg E, Schulman J, Zonenshayn M, Magnin M, Morel A and Sigmund M. Thalamocortical dysrhythmia. I. Functional and imaging aspects. Thalamus Related Syst 2001 1:237-244

Lockhart DJ, Winzeler EA. Genomics, gene expression and DNA arrays. Nature 2000;405(6788):827-36

Loscher W. Animal models of epilepsy for the development of antiepileptogenic and disease-modifying drugs. A comparison of the pharmacology of kindling and post-status epilepticus models of temporal lobe epilepsy. Epilepsy Res 2002;50(1-2):105-23

Ludwig A, Budde T, Stieber J, Moosmang S, Wahl C, Holthoff K, Langebartels A, Wotjak C, Munsch T, Zong X, Feil S, Feil R, Lancel M, Chien KR, Konnerth A, Pape HC, Biel M, Hofmann F. Absence epilepsy and sinus dysrhythmia in mice lacking the pacemaker channel HCN2. EMBO J 2003;22(2):216-24

Ludwig A, Zong X, Jeglitsch M, Hofmann F, Biel M. A family of hyperpolarization-activated mammalian cation channels. Nature 1998;393(6685):587-91

Luebke JI, Dunlap K, Turner TJ. Multiple calcium channel types control glutamatergic synaptic transmission in the hippocampus. Neuron 1993;11(5):895-902

Luthi A, McCormick DA. H-current: properties of a neuronal and network pacemaker. Neuron 1998;21(1):9-12

Magee JC. Dendritic Ih normalizes temporal summation in hippocampal CA1 neurons. Nat Neurosci 1999a;2(6):508-14

Magee JC, Carruth M. Dendritic voltage-gated ion channels regulate the action potential firing mode of hippocampal CA1 pyramidal neurons. J Neurophysiol 1999b;82(4):1895-901

Maue RA, Kraner SD, Goodman RH, Mandel G. Neuron-specific expression of the rat brain type II sodium channel gene is directed by upstream regulatory elements. Neuron 1990;4(2):223-31

McCormick DA, Bal T. Sleep and arousal: thalamocortical mechanisms. Annu Rev Neurosci 1997;20:185-215

McCormick DA, Contreras D. On the cellular and network bases of epileptic seizures. Annu Rev Physiol 2001;63:815-46

McNamara JO. Kindling model of epilepsy. Adv Neurol 1986;44:303-18

McNamara JO. Emerging insights into the genesis of epilepsy. Nature 1999;399 (6738 Suppl):A15-22

Mello LE, Cavalheiro EA, Tan AM, Kupfer WR, Pretorius JK, Babb TL, Finch DM. Circuit mechanisms of seizures in the pilocarpine model of chronic epilepsy: cell loss and mossy fiber sprouting. Epilepsia 1993;34(6):985-95

Miles R, Wong RK. Single neurones can initiate synchronized population discharge in the hippocampus. Nature 1983;306(5941):371-3

Mintz IM, Adams ME, Bean BP. P-type calcium channels in rat central and peripheral neurons. Neuron 1992;9(1):85-95

Mintz IM, Venema VJ, Swiderek KM, Lee TD, Bean BP, Adams ME. P-type calcium channels blocked by the spider toxin omega-Aga-IVA. Nature 1992;355(6363):827-9

Miraglia del Giudice E, Coppola G, Scuccimarra G, Cirillo G, Bellini G, Pascotto A. Benign familial neonatal convulsions (BFNC) resulting from mutation of the KCNQ2 voltage sensor. Eur J Hum Genet 2000;8(12):994-7

Morgan K, Stevens EB, Shah B, Cox PJ, Dixon AK, Lee K, Pinnock RD, Hughes J, Richardson PJ, Mizuguchi K, Jackson AP. beta 3: an additional auxiliary subunit of the voltage-sensitive sodium channel that modulates channel gating with distinct kinetics. Proc Natl Acad Sci USA 2000;97(5):2308-13

Morgans CW, Gaughwin P, Maleszka R. Expression of the alpha1F calcium channel subunit by photoreceptors in the rat retina. Mol Vis 2001;7:202-9

Mori Y, Matsubara H, Folco E, Siegel A, Koren G. The transcription of a mammalian voltage-gated potassium channel is regulated by cAMP in a cell-specific manner. J Biol Chem 1993;268(35):26482-93.

Nagerl UV, Mody I, Jeub M, Lie AA, Elger CE, Beck H. Surviving granule cells of the sclerotic human hippocampus have reduced $Ca^{2+}$ influx because of a loss of calbindin-D(28k) in temporal lobe epilepsy. J Neurosci 2000;20(5):1831-6

Newcomb R, Szoke B, Palma A, Wang G, Chen X, Hopkins W, Cong R, Miller J, Urge L, Tarczy-Hornoch K, Loo JA, Dooley DJ, Nadasdi L, Tsien RW, Lemos J, Miljanich G. Selective peptide antagonist of the class E calcium channel from the venom of the tarantula Hysterocrates gigas. Biochemistry 1998;37(44):15353-62

Noda M, Shimizu S, Tanabe T, Takai T, Kayano T, Ikeda T, Takahashi H, Nakayama H, Kanaoka Y, Minamino N, et al. Primary structure of Electrophorus electricus sodium channel deduced from cDNA sequence. Nature 1984;312(5990):121-7

Nolan MF, Malleret G, Lee KH, Gibbs E, Dudman JT, Santoro B, Yin D, Thompson RF, Siegelbaum SA, Kandel ER, Morozov A. The hyperpolarization-activated HCN1 channel is important for motor learning and neuronal integration by cerebellar Purkinje cells. Cell 2003;115(5):551-64.

Nowycky MC, Fox AP, Tsien RW. Three types of neuronal calcium channel with different calcium agonist sensitivity. Nature 1985;316(6027):440-3

Numa S, Noda M. Molecular structure of sodium channels. Ann N Y Acad Sci 1986;479:338-55

Ottschytsch N, Raes A, Van Hoorick D, Snyders DJ. Obligatory heterotetramerization of three previously uncharacterized Kv channel alpha-subunits identified in the human genome. Proc Natl Acad Sci USA 2002;99(12):7986-91

Pape HC. Queer current and pacemaker: the hyperpolarization-activated cation current in neurons. Annu Rev Physiol 1996;58:299-327

Perez-Reyes E. Molecular physiology of low-voltage-activated t-type calcium channels. Physiol Rev 2003;83(1):117-61

Qian J, Saggau P. Modulation of transmitter release by action potential duration at the hippocampal CA3-CA1 synapse. J Neurophysiol 1999;81(1):288-98

Raman IM, Sprunger LK, Meisler MH, Bean BP. Altered subthreshold sodium currents and disrupted firing patterns in Purkinje neurons of Scn8a mutant mice. Neuron 1997;19(4):881-91

Randall A, Tsien RW. Pharmacological dissection of multiple types of $Ca^{2+}$ channel currents in rat cerebellar granule neurons. J Neurosci 1995;15(4):2995-3012

Rettig J, Wunder F, Stocker M, Lichtinghagen R, Mastiaux F, Beckh S, Kues W, Pedarzani P, Schroter KH, Ruppersberg JP, et al. Characterization of a Shaw-related potassium channel family in rat brain. EMBO J 1992;11(7):2473-86

Rios E, Pizarro G. Voltage sensor of excitation-contraction coupling in skeletal muscle. Physiol Rev 1991;71(3):849-908

Robbins J. KCNQ potassium channels: physiology, pathophysiology, and pharmacology. Pharmacol Ther 2001;90(1):1-19

Rostock A, Tober C, Rundfeldt C, Bartsch R, Engel J, Polymeropoulos EE, Kutscher B, Loscher W, Honack D, White HS, Wolf HH. D-23129: a new anticonvulsant with a broad spectrum activity in animal models of epileptic seizures. Epilepsy Res 1996;23(3):211-23

Rudy B, Chow A, Lau D, Amarillo Y, Ozaita A, Saganich M, Moreno H, Nadal MS, Hernandez-Pineda R, Hernandez-Cruz A, Erisir A, Leonard C, Vega-Saenz de Miera E. Contributions of $K_v3$ channels to neuronal excitability. Ann N Y Acad Sci 1999;868:304-43

Ruppersberg JP, Frank R, Pongs O, Stocker M. Cloned neuronal $IK_A$ channels reopen during recovery from inactivation. Nature 1991;353(6345):657-60

Sanabria ER, Su H, Yaari Y. Initiation of network bursts by $Ca^{2+}$-dependent intrinsic bursting in the rat pilocarpine model of temporal lobe epilepsy. J Physiol 2001;532(Pt 1):205-16

Sano Y, Mochizuki S, Miyake A, Kitada C, Inamura K, Yokoi H, Nozawa K, Matsushime H, Furuichi K. Molecular cloning and characterization of Kv6.3, a novel modulatory subunit for voltage-gated $K^+$ channel $K_v2.1$. FEBS Lett 2002;512(1-3):230-4

Santoro B, Liu DT, Yao H, Bartsch D, Kandel ER, Siegelbaum SA, Tibbs GR. Identification of a gene encoding a hyperpolarization-activated pacemaker channel of brain. Cell 1998;93(5):717-29

Santoro B, Chen S, Luthi A, Pavlidis P, Shumyatsky GP, Tibbs GR, Siegelbaum SA. Molecular and functional heterogeneity of hyperpolarization-activated pacemaker channels in the mouse CNS. J Neurosci 2000;20(14):5264-75

Schade SD, Brown GB. Identifying the promoter region of the human brain sodium channel subtype II gene (SCN2A). Brain Res Mol Brain Res 2000;81(1-2):187-90

Schmittgen TD, Zakrajsek BA, Mills AG, Gorn V, Singer MJ, Reed MW. Quantitative reverse transcription-polymerase chain reaction to study mRNA decay: comparison of endpoint and real-time methods. Anal Biochem 2000;285(2):194-204

Schroeder BC, Kubisch C, Stein V, Jentsch TJ. Moderate loss of function of cyclic-AMP-modulated KCNQ2/KCNQ3 K+ channels causes epilepsy. Nature 1998;396 (6712):687-90

Schroeder BC, Hechenberger M, Weinreich F, Kubisch C, Jentsch TJ. KCNQ5, a novel potassium channel broadly expressed in brain, mediates M-type currents. J Biol Chem 2000;275(31):24089-95

Schütze K, Lahr G. Identification of expressed genes by laser-mediated manipulation of single cells. Nat Biotechnol 1998;16(8):737-42

Shah MM, Mistry M, Marsh SJ, Brown DA, Delmas P. Molecular correlates of the M-current in cultured rat hippocampal neurons. J Physiol 2002;544(Pt 1):29-37

Sheng M, Tsaur ML, Jan YN, Jan LY. Subcellular segregation of two A-type $K^+$ channel proteins in rat central neurons. Neuron 1992;9(2):271-84

Simmons MA, Becker JB, Mather RJ. Desensitization of the inhibition of the M-current in sympathetic neurons: effects of ATP analogs, polyanions, and multiple agonist applications. Neuron 1990;4(4):557-62

Singh NA, Charlier C, Stauffer D, DuPont BR, Leach RJ, Melis R, Ronen GM, Bjerre I, Quattlebaum T, Murphy JV, McHarg ML, Gagnon D, Rosales TO, Peiffer A, Anderson VE, Leppert M. A novel potassium channel gene, KCNQ2, is mutated in an inherited epilepsy of newborns. Nat Genet 1998;18(1):25-9

Sloviter RS. Status epilepticus-induced neuronal injury and network reorganization. Epilepsia 1999;40 Suppl 1:S34-9

Sochivko D, Pereverzev A, Smyth N, Gissel C, Schneider T, Beck H. The $Ca_V2.3$ $Ca^{2+}$ channel subunit contributes to R-type $Ca^{2+}$ currents in murine hippocampal and neocortical neurones. J Physiol 2002;542(Pt 3):699-710

Stryer L. Fluorescence energy transfer as a spectroscopic ruler. Annu Rev Biochem 1978;47:819-46

Su H, Alroy G, Kirson ED, Yaari Y. Extracellular calcium modulates persistent sodium current-dependent burst-firing in hippocampal pyramidal neurons. J Neurosci 2001;21(12):4173-82

Su H, Sochivko D, Becker A, Chen J, Jiang Y, Yaari Y, Beck H. Upregulation of a T-type $Ca^{2+}$ channel causes a long-lasting modification of neuronal firing mode after status epilepticus. J Neurosci 2002;22(9):3645-55

Suzuki T, Higgins PJ, Crawford DR. Control selection for RNA quantitation. Biotechniques. 2000;29(2):332-7

Takahashi T, Momiyama A. Different types of calcium channels mediate central synaptic transmission. Nature 1993;366(6451):156-8

Takahashi E, Murata Y, Oki T, Miyamoto N, Mori Y, Takada N, Wanifuchi H, Wanifuchi N, Yagami K, Niidome T, Tanaka I, Katayama K. Isolation and functional characterization of the 5'-upstream region of mouse P/Q-type $Ca^{2+}$ channel alpha1A subunit gene. Biochem Biophys Res Commun 1999;260(1):54-9

Takimoto K, Fomina AF, Gealy R, Trimmer JS, Levitan ES. Dexamethasone rapidly induces $K_v1.5$ $K^+$ channel gene transcription and expression in clonal pituitary cells. Neuron 1993;11(2):359-69.

Takimoto K, Levitan ES. Glucocorticoid induction of Kv1.5 $K^+$ channel gene expression in ventricle of rat heart. Circ Res 1994;75(6):1006-13

Traub RD, Wong RK. Cellular mechanism of neuronal synchronization in epilepsy. Science 1982;216(4547):745-7

Tinel N, Lauritzen I, Chouabe C, Lazdunski M, Borsotto M. The KCNQ2 potassium channel: splice variants, functional and developmental expression. Brain localization and comparison with KCNQ3. FEBS Lett 1998;438(3):171-6

Trimmer JS. Immunological identification and characterization of a delayed rectifier $K^+$ channel polypeptide in rat brain. Proc Natl Acad Sci USA 1991;88(23):10764-8

Turski WA, Cavalheiro EA, Schwarz M, Czuczwar SJ, Kleinrok Z, Turski L. Limbic seizures produced by pilocarpine in rats: behavioural, electroencephalographic and neuropathological study. Behav Brain Res 1983;9(3):315-35.

Tyagi S, Kramer FR. Molecular beacons: probes that fluoresce upon hybridization. Nat Biotechnol 1996;14(3):303-8

Van Roost, D., Solymosi, L., Schramm, J., van Oosterwyck, B. and Elger, C.E. Depth electrode implantation in the length axis of the hippocampus for the presurgical evaluation of medial temporal lobe epilepsy: a computed tomography-based stereotactic insertion technique and its accuracy. Neurosurgery 1998;43(4):819-826

Veh RW, Lichtinghagen R, Sewing S, Wunder F, Grumbach IM, Pongs O. Immunohistochemical localization of five members of the $K_v1$ channel subunits: contrasting subcellular locations and neuron-specific co-localizations in rat brain. Eur J Neurosci 1995;7(11):2189-205

Vreugdenhil M, Faas GC, Wadman WJ. Sodium currents in isolated rat CA1 neurons after kindling epileptogenesis. Neuroscience. 1998;86(1):99-107

Wallace RH, Wang DW, Singh R, Scheffer IE, George AL Jr, Phillips HA, Saar K, Reis A, Johnson EW, Sutherland GR, Berkovic SF, Mulley JC. Febrile seizures and generalized epilepsy associated with a mutation in the $Na^+$-channel beta1 subunit gene SCN1B. Nat Genet 1998;19(4):366-70

Wallace RH, Scheffer IE, Barnett S, Richards M, Dibbens L, Desai RR, Lerman-Sagie T, Lev D, Mazarib A, Brand N, Ben-Zeev B, Goikhman I, Singh R, Kremmidiotis G, Gardner A, Sutherland GR, George AL Jr, Mulley JC, Berkovic SF. Neuronal sodium-channel alpha1-subunit mutations in generalized epilepsy with febrile seizures plus. Am J Hum Genet 2001;68(4):859-65

Wang HS, McKinnon D. Potassium currents in rat prevertebral and paravertebral sympathetic neurones: control of firing properties. J Physiol 1995;485 ( Pt 2):319-35

Wang HS, Pan Z, Shi W, Brown BS, Wymore RS, Cohen IS, Dixon JE, McKinnon D. KCNQ2 and KCNQ3 potassium channel subunits: molecular correlates of the M-channel. Science 1998;282(5395):1890-3

Watanabe H, Nagata E, Kosakai A, Nakamura M, Yokoyama M, Tanaka K, Sasai H. Disruption of the epilepsy KCNQ2 gene results in neural hyperexcitability. J Neurochem 2000;75(1):28-33

Waxman SG, Dib-Hajj S, Cummins TR, Black JA. Sodium channels and pain. Proc Natl Acad Sci USA 1999;96(14):7635-9

Wheeler DB, Randall A, Tsien RW. Roles of N-type and Q-type $Ca^{2+}$ channels in supporting hippocampal synaptic transmission. Science 1994;264(5155):107-11

Whitaker WR, Faull RL, Dragunow M, Mee EW, Emson PC, Clare JJ. Changes in the mRNAs encoding voltage-gated sodium channel types II and III in human epileptic hippocampus. Neuroscience 2001;106(2):275-85

Witter MP, Groenewegen HJ, Lopes da Silva FH, Lohman AH. Functional organization of the extrinsic and intrinsic circuitry of the parahippocampal region. Prog Neurobiol 1989;33(3):161-253

Wodicka L, Dong H, Mittmann M, Ho MH, Lockhart DJ. Genome-wide expression monitoring in Saccharomyces cerevisiae. Nat Biotechnol 1997;15(13):1359-67

Woodward JJ, Rezazadeh SM, Leslie SW. Differential sensitivity of synaptosomal calcium entry and endogenous dopamine release to omega-conotoxin. Brain Res 1988;475 (1):141-5

Wu RL, Barish ME. Two pharmacologically and kinetically distinct transient potassium currents in cultured embryonic mouse hippocampal neurons. J Neurosci 1992;12(6): 2235-46

Yaari Y, Hamon B, Lux HD. Development of two types of calcium channels in cultured mammalian hippocampal neurons. Science 1987;235(4789):680-2

Yin JL, Shackel NA, Zekry A, McGuinness PH, Richards C, Putten KV, McCaughan GW, Eris JM, Bishop GA. Real-time reverse transcriptase-polymerase chain reaction (RT-PCR) for measurement of cytokine and growth factor mRNA expression with fluorogenic probes or SYBR Green I. Immunol Cell Biol 2001;79(3):213-21

Yuan LL, Adams JP, Swank M, Sweatt JD, Johnston D. Protein kinase modulation of dendritic $K^+$ channels in hippocampus involves a mitogen-activated protein kinase pathway. J Neurosci 2002;22(12):4860-8

Zentner J, Hufnagel A, Wolf HK, Ostertun B, Behrens E, Campos MG, Solymosi L, Elger CE, Wiestler OD, Schramm J. Surgical treatment of temporal lobe epilepsy: clinical, radiological, and histopathological findings in 178 patients. J Neurol Neurosurg Psychiatry 1995;58(6):666-73

# 7 Appendix:

## Publication


1. **Chen J**, Liu WP, Chen MJ et al. The molecular basis of β-thalassemia Intermedia-the Conjunction of defects in both α-and β-globingene Loci. Blood 1995;86(10 Supplement 1): 645a(2566)

2. **Chen J**, Liu WP, Sheng M et al. Molecular diagnosis of a β-thalassemia intermedia Family--the conjunction of abnormalities in both α-and β-globin gene loci. Chin J Hematol, 1996;17(8):402-405

3. **Chen J**, Liu WP, Sheng M et al. A β-fhalassemia intermedia family with the conjunction of β IVS II-654 splicing mutation and α-globin gene abnormalities (triplication or deletion). J Genet Mol Biol 1996;7(3): 49-53.

4. **Chen J**, Liu WP, Chen MJ et al. Molecular diagnosis of β-thalassemia intermedia. Natl Med J China 1997;77(8): 575-578

5. Chen MJ, **Chen J**, Huang SZ et al. Identification of α-globin gene organization using long PCR. Chin J Hematol 1997;18:529-531

6. **Chen J**, Liu WP, Chen MJ et al. A study of α-globin gene organization in 250 cord blood specimens. Acta Acdemiae Medicinae Shanghai 1997,24:Suppl: 6-8

7. Lu H, **Chen J**, Jiang DS et al. A study of preparation the monoepitopic yntibody against the C-terminal of human erythrocyte membrane band 3 protein. Journal of East China Normal University (Natural Science) 1997;12:55-59

8. **Chen J**, Sun Q, Chen MJ et al. An analysis of α-globin genes in 124 cases with HbH disease. Shanghai Medical Journal, 1999, 22(2): 83-86.

9. Lu H, Zhao S, **Chen J** et al. Study on the membrane protein composition of several hematopathies. Journal of East China Normal University (Natural Science), 1999,2:95

10. **Chen J**, Sochivko D, Beck H, Marechal D, Wiestler OD, Becker AJ. Activity-induced expression of common reference genes in individual CNS neurons. Lab Invest 2001 Jun;81(6):913-6

11. Riazanski V, Becker AJ, **Chen J**, Sochivko D, Lie A, Wiestler OD, Elger CE, Beck H. Functional and molecular analysis of transient voltage-dependent $K^+$ currents in rat hippocampal granule cells. J Physiol 2001;537(Pt2):391-406

12. Su H, Sochivko D, Becker A, **Chen J**, Jiang Y, Yaari Y, Beck H. Upregulation of a T-type $Ca^{2+}$ channel causes a long-lasting modification of neuronal firing mode after status epilepticus. J Neurosci 2002;22(9):3645-55

13. Becker AJ, **Chen J**, Paus S, Normann S, Beck H, Elger CE, Wiestler OD, Blumcke I. Transcriptional profiling in human epilepsy: expression array and

single cell real-time qRT-PCR analysis reveal distinct cellular gene regulation. Neuroreport 2002;13(10):1327-33

14. Sochivko D, **Chen J**, Becker AJ, Beck H. Blocker-Resistant $Ca^{2+}$ currents in rat CA1 hippocampal pyramidal neurons. Neuroscience 2003;116:629-638

15. Ellerkmann R, Remy S, **Chen J**, Sochivko D, Elger CE, Urban BW, Becker AJ, Beck H. Molecular and functional changes in voltage-dependent $Na^{+}$ channels following pilocarpine-induced status epilepticus in rat dentate granule cells. Neuroscience 2003;119(2) :323-33.

16. Becker AJ, **Chen J**, Zien A, Sochivko D, Normann S, Schramm J, Elger CE, Wiestler OD, Blumcke I. Correlated stage- and subfield-associated hippocampal gene expression patterns in experimental and human temporal lobe epilepsy. Eur J Neurosci 2003;18(10):2792-802

17. Volk HA, Burkhardt K, Potschka H, **Chen J**, Becker A, Loscher W. Neuronal expression of the drug efflux transporter P-glycoprotein in the rat hippocampus after limbic seizures. Neuroscience 2004;123(3):751-9.

18. Kam R, **Chen J**, Blumcke I, Normann S, Fassunke J, Elger CE, Schramm J, Wiestler OD, Becker AJ. The reelin pathway components disabled-1 and p35 in gangliogliomas - a mutation and expression analysis. Neuropathol Appl Neurobiol 2004;30(3):225-32.

19. **Chen J**, Larionov S, Hoerold N, Ullmann C, Elger CE, Schramm J, Becker AJ. Expression analysis of metabotropic glutamate receptors I and III in mouse strains with different susceptibility to experimental temporal lobe epilepsy. Neuroscience Letters (in review)

## Poster

1. J. Chen, D. Sochivko, H. Beck, O. D. Wiestler, A. J. Becker. Activity-induced expression alterations of voltage dependent ion channels in CNS neurons. Joint Meeting of the Belgian, Dutch and German Societies of Neuropathology (Also 47th Annual Meeting of the Deutsche Gesellschaft für Neuropathologie und Neuroanatomie e.V.) 8 - 12 October 2002, Aachen, Germany.

2. A.J. Becker, J. Chen, D. Sochivko, S. Normann, O.D. Wiestler, I. Blümcke. Expression array analysis of regional hippocampal epileptogenesis. Neuroscience Meeting, Orlando FL, 2-7 November 2002

3. J. Chen, A. J. Becker, D. Sochivko, O. D. Wiestler, H. Beck. Activity-induced expression alterations of voltage dependent ion channels in epileptic neurons. American Epilepsy Society Annual Meeting, Boston, MA, 5-9 December 2003

4. S. Larionov, J. Chen, D. Dietrich, N. Hoerold, C. Ulmann, O. D. Wiestler, A.J. Becke[1] Up-regulation of the metabotropic glutamate receptor mGluR4 relates to strain-dependent susceptibility to pilocarpine-induced limbic epilepsy. American Epilepsy Society Annual Meeting, Boston, MA, 5-9 December 2003

## Awards

Award for unusual scientific achievements in the project A6 in the SFB400 in the year 2002.

## Acknowledgements:

I take this opportunity to sincerely thank the following people who helped me during my PhD study.

Prof. Dr. Heinz Beck and Dr. Albert Becker who accepted me to do my PhD study in their groups and gave me direct, detail advice and active discussion on my research work as well as thesis. Besides that, I particularly appreciate that they gave me a lot kind help on my private life in Germany.

Prof. Dr. Thomas Magin who friendly agreed to be my supervisor in the Faculty of Mathematics and Natural Sciences.

Prof. Dr. Christian E Elger who always encouraged me to work hard by asking me “Where is your nature paper?”

Mr. Dmitry Sochivko who had a lot of scientific discussion with me and made the pilocarpine rats and dissected brain together with me at beginning when I start to work.

Miss Sabine Normann and Ms Margit Reitze who always gave me technical supports and helped me fulfil the managements in the labs.

All the colleagues and friends around me gave me supports and provided a happy working environment.

At last, I would like to thank my wife Hong Lu especially for her constructive comments on my research work and selfless supports to my family.

# Curriculum Vitae


**Name:** **Jian Chen** **Sex:** **Male**

**Address:** **Heinrich-Blömer-Weg 22, 53127 Bonn, Germany**

**Tel:** **++49-228-9289805**

**Email:** **jianluchen@yahoo.co.uk**


**Personal Details:**

**Date of Birth:** **Dec. 27th 1967**

**Marital Status:** **Married** **Wife:** **Hong Lu (Jan. 1st 1969)**

**Daughter:** **Sijia Chen (Sep. 18th 1996)**

**Citizenship:** **P. R. China**

**Educational and Working Background:**

**03.1975 - 07.1980** Primary school study at Jianxian Primary School, Shanghai, China.

**09.1980 - 07.1986** High school study at Weiyu High School, Shanghai, China.

**09.1986 - 07.1991** Undergraduate study at East China Normal University (ECNU), Shanghai, China; major in Molecular Biology, received B.Sc.

Thesis: Ultrastructure study on the effects of 4-fluoro-DL-Phenylalanine on the *Plasmodium Yoelii* (supervised by Prof. Dr. Hanming Cao in Dept. Biology, ECNU)

**09.1991- 07.1994** Graduate study at East China Normal University, Shanghai, China; major in Biochemistry, received M.Sc.

Thesis: A study of preparation the monoepitopic Antibody against the C-terminal of human erythrocyte membrane band 3 protein (supervised by Prof. Dr. Peichang Fan in Dept. Biology, ECNU)

**08.1994 - 03.1999** Shanghai Institute of Medical Genetics, Shanghai Children's Hospital, Shanghai, China.

Research on the molecular abnormalities of globin genes, especially the $\alpha$, $\beta$, $\gamma$ goblin gene abnormalities in $\beta$-thalassemia intermedia patients related to their clinical phenotype; research on the alteration of globin gene expression in $\beta$-thalassemia carriers and related cell lines; construction and identification of the foreign genes in transgenic mice and goats (led by Prof. Dr. Yitao Zeng, academician of Chinese Academy of Engineering)

**04.1999 - 09.1999** Department of Pediatrics, Nara Medical University, Kashihara City, Nara, Japan.

Research on the gene structure and protein function of human factor VIII and IX and gene diagnoses of hemophilia A (led by Prof. Dr. Akira Yoshioka in Dept. Pediatrics, Nara Medical University, Japan)

**10.1999 - 04.2004** PhD study in Laboratory of Experimental Epileptology, Dept. of Epileptology and Instit. of Neuropathology, University of Bonn Medical Center, Bonn, Germany

PhD study on the regulation of voltage-gated ion channel ($Ca^{2+}$, $Na^{+}$, A-type $K^{+}$, KCNQ, HCN) expression during epileptogenesis in the rat models with real-time RT-PCR and microarray (supervised by Prof. Dr Heinz Beck and Dr. Albert Becker)